

UNCLASSIFIED

AD NUMBER

ADB017742

LIMITATION CHANGES

TO:

Approved for public release; distribution is unlimited.

FROM:

Distribution authorized to U.S. Gov't. agencies only; Test and Evaluation; FEB 1997. Other requests shall be referred to Rome Air Development Center, Griffiss AFB, NY.

AUTHORITY

RADC ltr 23 May 1978

THIS PAGE IS UNCLASSIFIED

THIS REPORT HAS BEEN DELIMITED  
AND CLEARED FOR PUBLIC RELEASE  
UNDER DOD DIRECTIVE 5200.20 AND  
NO RESTRICTIONS ARE IMPOSED UPON  
ITS USE AND DISCLOSURE.

DISTRIBUTION STATEMENT A

APPROVED FOR PUBLIC RELEASE;  
DISTRIBUTION UNLIMITED.

AD BO 17742

RADC-TR-76-321  
In-house Report  
February 1977



FL

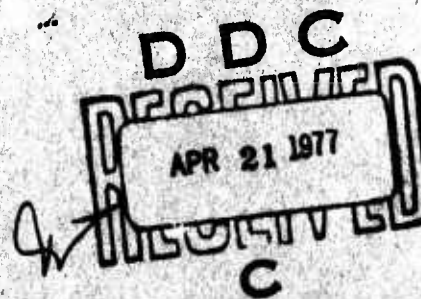
PERFORMANCE COMPARISON OF BIPOLAR ALTERNATE MARK INVERSION AND  
CONDITIONED DIPHAASE WAVEFORMS OVER WIRELINE MEDIA

Captain Guy E. Eller, USAF  
Captain Steven S. Russell, USAF

Distribution limited to U. S. Government Agencies  
only; test and evaluation; February 1977. Other  
requests for this document must be referred to  
RADC (DCLF), Griffiss AFB NY 13441.

AD No. \_\_\_\_\_  
DDC FILE COPY

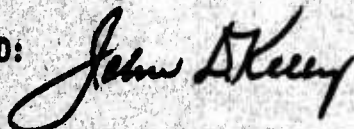
ROME AIR DEVELOPMENT CENTER  
AIR FORCE SYSTEMS COMMAND  
GRIFFISS AIR FORCE BASE, NEW YORK 13441



This evaluation was performed in-house for the Defense Communications Agency under Job Order Number R2110101 at RADC's Digital Communications Experimental Facility. Data was taken from October 1975 to March 1976.

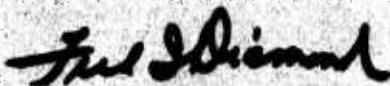
This report has been reviewed and is approved for publication.

APPROVED:



JOHN D. KELLY  
Chief, Telecommunications Branch  
Communications and Control Division

APPROVED:



FRED I. DIAMOND  
Technical Director  
Communications and Control Division

FOR THE COMMANDER:



JOHN P. HUSS  
Acting Chief  
Plans Office

APPROVED FOR	DATE	BY	REMARKS
17/10	10/10/76	John D. Kelly	
17/10	10/10/76	Fred I. Diamond	
17/10	10/10/76	John P. Huss	

Do not return this copy. Retain or destroy.



UNCLASSIFIED

SECURITY CLASSIFICATION OF THIS PAGE (When Data Entered)

REPORT DOCUMENTATION PAGE		READ INSTRUCTIONS BEFORE COMPLETING FORM
1. REPORT NUMBER RADC-TR-76-321	2. GOVT ACCESSION NO.	3. RECIPIENT'S CATALOG NUMBER
4. TITLE (AND SUBTITLE) Performance Comparison of Bipolar Alternate Mark Inversion and Conditioned Diphase Waveforms Over Wireline Media	5. TYPE OF REPORT & PERIOD COVERED Final <del>In-House</del> Oct 75 - Apr 76	6. PERFORMING ORG. REPORT NUMBER N/A
7. AUTHOR(s) Captain Guy E. Eller, USAF Captain Steven S. Russell, USAF	8. CONTRACT OR GRANT NUMBER(s) N/A	
9. PERFORMING ORGANIZATION NAME AND ADDRESS Rome Air Development Center (DCLF) Griffiss AFB, NY 13441	10. PROGRAM ELEMENT, PROJECT, TASK AREA & WORK UNIT NUMBERS R2110101	
11. CONTROLLING OFFICE NAME AND ADDRESS Same	12. REPORT DATE February 1977	13. NUMBER OF PAGES 113
14. MONITORING AGENCY NAME & ADDRESS (if different from Controlling Office) Same	15. SECURITY CLASS. (of this report) UNCLASSIFIED	15a. DECLASSIFICATION DOWNGRADING SCHEDULE N/A
16. DISTRIBUTION STATEMENT (of this Report) Distribution limited to U. S. Government Agencies only; Test and Evaluation; February 1977. Other requests for this document must be referred to RADC (DCLF), Griffiss AFB NY 13441.		
17. DISTRIBUTION STATEMENT (of the abstract entered in Block 20, if different from Report) Same		
18. SUPPLEMENTARY NOTES None		
19. KEY WORDS (Continue on reverse side if necessary and identify by block number) Bipolar, Conditioned Diphase, Digital Transmission, Crosstalk, Bit Error Rate, Impulse Noise, Intersymbol Interference, Breadboard Hardware, Performance Curves.		
20. ABSTRACT (Continue on reverse side if necessary and identify by block number) This report was prepared for the Defense Communications Agency to study the performance of two waveforms competing for implementation in the Defense Communications System. The waveforms, Bipolar Alternate Mark Inversion (BAMI) and Conditioned Diphase (CDP), were studied both from a theoretical standpoint and with experimental breadboard hardware designed and built in-house. Theoretical performance curves for both waveforms operating in wideband gaussian noise were developed and the hardware was tested against wideband gaussian noise. The results of testing the waveform over (cont'd)		

DD FORM 1473

EDITION OF 1 NOV 65 IS OBSOLETE

UNCLASSIFIED

SECURITY CLASSIFICATION OF THIS PAGE (When Data Entered)

UNCLASSIFIED

SECURITY CLASSIFICATION OF THIS PAGE(When Data Entered)

Griffiss AFB cable plant are presented along with computer-generated distributions of data bit errors encountered. The effects and problems involved in recovering timing information from the two waveforms are not covered in this report.

The results indicate that, with white gaussian noise as the only transmission impairment, the two waveforms perform nearly identically. Their performances are also close when operation is over cables with moderate amounts of intersymbol interference and attenuation. However, when intersymbol interference and attenuation are severe (long cables, high data rates, and poor-condition cables), BAMl has an advantage of approximately 30 percent, expressed in terms of maximum usable bit rate for a given length of cable. Another conclusion reached was that impulse noise is the limiting impairment of the Griffiss AFB cable plant.

## TABLE OF CONTENTS

	<u>Page No.</u>
1.0 Introduction	1
1.1 Scope of the Experiment	2
2.0 Characterization of the Waveforms	3
2.1 Bipolar Alternate Mark Inversion (BAMI)	3
2.2 Conditioned Diphas (CD $\phi$ )	3
3.0 Signal Processing	8
3.1 Processing of the BAMI Waveform	8
3.1.1 Theoretical Bit Error Rate for BAMI	8
3.2 Processing of the CD $\phi$ Waveform	16
3.2.1 Relationship Between CD $\phi$ Sample Errors and Bit Errors	17
3.2.2 Theoretical Bit Error Rate for CD $\phi$	18
3.3 Consideration of Sample Correlation	28
3.4 Spectrum Occupancy of CD $\phi$ and BAMI	30
4.0 Hardware to Test BAMI and CD $\phi$	36
4.1.1 DICEF Laboratory Cable Plant	36
4.1.1.1 Characterization of DICEF Cable	36
4.1.2 Griffiss AFB Cable Plant	42
4.1.2.1.1 Amplitude and Phase Characteristics	43
4.1.2.1.2 Impulse Noise and Wideband Noise	54
4.2 Performance of Experimental Hardware	58
4.2.1 Performance in White Gaussian Noise (WGN)	61
4.2.2 Performance on 5-Mile Base Loop	63
4.2.3 Error Occurrence Analysis	67
4.3 Summary of Hardware Performance	74
Appendix 1	81
Appendix 2	85
References	88

## LIST OF FIGURES

	<u>Page No.</u>
2.2-1 Examples of Waveforms for CD $\phi$ with Supervisory Signalling	6
3.1-1 Block Diagram for BAMI Receiver	9
3.1.1-1 BAMI Waveform with Intersymbol Interference	10
3.1.1-2 Probability Distribution of the BAMI Waveform with Additive Noise	13
3.1.1-3 Error Area Under Gaussian Distribution	15
3.2-1 Block Diagram for CD $\phi$ Receiver Decoder	18
3.2.1-1 CD $\phi$ Processing Delay = T	19
3.2.1-2 CD $\phi$ Processing Delay = T/2	22
3.2.2-1 CD $\phi$ Waveform with Gaussian Noise Distribution	24
3.2.2-2 Plot of Theoretical Error Rates for CD $\phi$ and BAMI	27
3.4-1 Power Spectral Density for BAMI	31
3.4-2 Power Spectral Density for Conditioned Diphas	33
3.4-3 Integration of Power Spectral Densities	34
3.4-4 Signal Attenuation vs Data Rate for BAMI and CD $\phi$	35
4.1.1.1-1 Attenuation vs Frequency for 19 GA Plastic Insulated Cable (.083 f/M.)	37
4.1.1.1-2 Test Setup for Crosstalk Measurement	38
4.1.1.1-3 Oscilloscope Photographs of Cable Crosstalk	39
4.1.2-1 Map of 5-Mile Loop	44
4.1.2.1.1-1 Test Setup for Transfer Measurement	45
4.1.2.1.1-2 Transfer Function for 5-Mile Loop	46
4.1.2.1.1-3 Transfer Function for 10-Mile Loop	47
4.1.2.1.1-4 Test Setup to Measure Frequency Response of 5-Mile Cable Loop	48
4.1.2.1.1-5 5-Mile Base Cable Attenuation vs Frequency	49
4.1.2.1.1-6 Conditioned Diphas Transmitted and Received Power Spectrum	50
4.1.2.1.1-7 BAMI Transmitted and Received Power Spectrum	51
4.1.2.1.1-8 Conditioned Diphas Transmitted and Received Power Spectrum	52
4.1.2.1.1-9 BAMI Transmitted and Received Power Spectrum	53
4.1.2.1.2-1 Test Configuration for Impulse Noise Measurement	55
4.1.2.1.2-2 Bit Error Rate Upper Bound in Impulse Noise	59
4.2-1 Test Setup for Testing Breadboard Hardware	60
4.2.1-1 Performance of CD $\phi$ and BAMI in WGN	62
4.2.2-1 Performance of CD $\phi$ and BAMI over 5-Mile Loop No Equalization	64



### LIST OF FIGURES

	<u>Page No.</u>
4.2.2-2 Performance of CD $\phi$ and BAMl Over 5-Mile Loop with Equalization	65
4.2.2-3 Performance of CD $\phi$ and BAMl on 10-Mile Base Loop	68
4.2.3-1 Test Configuration for Error Pattern Characterization	69
4.2.3-2 Error Distributions - CD $\phi$ 5-Mile Loop No Equalization	71
4.2.3-3 Error Distributions - CD $\phi$ 5-Mile Loop with Equalization	72
4.2.3-4 Error Distributions - BAMl 5-Mile Loop with Equalization	75
4.2.3-5 Error Distributions - CD $\phi$ 10-Mile Loop/No Equalization	76
4.2.3-6 Error Distributions - BAMl 10-Mile Loop/No Equalization	77
4.3-1 BAMl Maximum Distance vs Bit Rate for Error Rate of $10^{-8}$	79
A2-1 SD 360 Spectrum Analyzer Setup for Measurement of System Transfer Function	86

### LIST OF TABLES

	<u>Page No.</u>
3.1.1-1 Mathematical Notations Used in Derivations	12
4.1.2.1.2-1 Impulse Rates on Griffiss AFB Cable	57

## Digital Loop Signalling Techniques Test Program

### 1.0 Introduction

The motivation for this test program came from the DOD Interoperability Committee's Transmission Considerations Working Group. The objective was to determine a signalling scheme by which timing and data could be transmitted over subscriber loops to and from multiplex nodes of a digital communications system. Four wire operation was to be used to achieve maximum common mode noise rejection and facilitate full duplex operation. Thus over each line data and timing would have to be transmitted in some combined form so that at the receiving end the timing and data phasing could be established.

Two waveforms were identified by the working group as potential candidates. These were: Bipolar with Alternate Mark Inversion (BAMI) and Conditioned Diphas (CD $\phi$ ).

At the receiving end, both waveforms require equalization to compensate for the delay distortion incurred in the lines, amplification to recover the loss of signal strength, and timing recovery to regenerate the data and timing signals. These three basic processing needs can be met by many different methods, and are only limited by tradeoff between mission essential needs and economy of implementation and, since all three of the above processes interact with each other a wide range of transmitter/receiver implementations can be used to achieve the same ends. These implementations are limited only by the designer's ingenuity and his knowledge of the transmission medium.

Thus the purpose of this report will be to assemble pertinent knowledge of the cable medium, relate this knowledge to the BAMI and CD $\phi$  waveforms, and to determine the relative performance of these waveforms under a variety of

transmission conditions. These conditions will be simulated with existing cable at the RADC Digital Communications Experimental Facility (DICEF). The system will also be exposed to a sample of a real communications link by transmission over the Griffiss AFB cable plant.

### 1.1 Scope of the Experiment

The scope of this experiment will be defined in terms of the flexibility in implementing the waveform generators including their optimal filters, amplifiers, equalizers and timing recovery units. That is, any element of the transmission system which will eventually be a product of the creativity of the designer and his economic constraints will not be considered in the test. Therefore, we have simplified the waveform generator/receiver, now called a modem, design so that the receiver operates with no preprocessing equipment other than a low pass filter for most of the tests. This will allow very objective comparisons of performance to be made between the two waveforms used. Timing recovery will be ideal. For this test an external clock triggered by the transmit clock and properly delayed will be the source of timing used at the receiver. This will insure that the effects of the channel on the signal can be viewed independent of any other receiver function. Since the experiment will involve evaluation of a wide variety of data rates, 4.8 KBps to 76.8 KBps, timing recovery problems become negligible and a relative performance of every rate can be clearly established. Also, observing the performance and the waveforms against a stable reference will allow designers to determine what sort of distortion can be expected during transmission and thus the characteristics of the signals impinging on their timing recovery units.

There are a variety of impairments which can be found in transmission links which are characteristic of the cable medium. These are: signal strength loss, envelope delay, thermal noise and transient noise. Another impairment which would arise in a system of transmission lines is crosstalk arising from capacitive imbalance and mutual inductance between cables. The experiments performed will focus on these impairments.

## 2.0 Characterization of the Waveforms

The waveforms compared in this experiment are of two types: 1. bipolar with alternate mark inversion; 2. conditioned diphase. Their generation and recovery will be described below.

### 2.1 Bipolar Alternate Mark Inversion (BAMI)

This waveform is a three-level encoded signal used in the Bell T-carrier System over digital repeatered lines (Ref 3). The line signal is a 50% duty cycle pulse representing a "mark," with each alternate "mark" being inverted in polarity. The "spaces" are at ground potential.

One of the virtues of this form of data transmission is that overhead signalling information can be forced onto the data stream and extracted at the receiver without affecting the data. For example, since alternate data "marks" must be opposite in polarity, the rule can be broken to insert extra "marks" which serve signalling and supervision purposes. Disadvantages of this waveform are that when the data source is idling or has a long "space" output, no pulses are provided to the timing recovery network thus resulting in clock drift at the receiver. Thus for a given stability of local clock source a given number of "marks" must be inserted to suppress strings of successive "spaces." For example, the bipolar six zero suppression (B6ZS) code is used in the Data Service Unit (DSU) and Office Channel Unit (OCU) of the Bell Digital Data System (DDS), (Ref 4, 14).

### 2.2 Conditioned Diphase (CD $\phi$ )

This waveform is a two level waveform alternating above and below ground. The data incoming in NRZ form with timing is conditioned by a flip-flop so



that the "marks" appear as transitions. This signal is then used to modulate the phase of the transmit clock. Thus, a "mark" is a  $180^\circ$  phase shift of the clock. Here, as in BAMI, alternate "marks" are opposite in polarity. A representative waveform chart is given in Figure 3.2.1-1.

The advantage of the  $CD\phi$  signal in timing recovery is that there exists at least one transition in every bit transmitted, be it a "mark" or "space," allowing the timing circuitry to be simpler and the oscillator less stable and therefore cheaper.

$CD\phi$  offers the ability (as does BAMI) to transmit supervisory or overhead data in the form of mark polarity violations. However the method is more complicated than that used for BAMI (bipolar violations). Figure 2.2-1 depicts waveforms illustrating one method of implementing  $CD\phi$  supervisory signalling. The line labeled  $CD\phi$  gives the normal  $CD\phi$  waveform for the NRZ data on the top line. The line labeled "B bit" shows the  $CD\phi$  waveform with the B bit, a mark, also used as signalling bit. It has the wrong voltage polarity. This condition can be detected and used for signalling purposes in the same way as bipolar violations are used for signalling in BAMI. The other waveforms show other "marks" used as supervisory signalling bits. There are no ambiguous situations generated by this scheme but additional processing is required at both the transmitter and receiver. The additional circuitry to insert the supervisory information at the transmit end would not be much. However, at the receiver the extra circuitry would be more extensive. It would have to detect the additional waveform patterns allowed such as those in Figure 2.2-1 and, depending upon the implementation, it may have to restore the waveform to a standard  $CD\phi$  waveform before the information is decoded. This is because the  $CD\phi$  supervisory bits would decode as errors if the standard "delay and exclusive OR" decoding were performed.

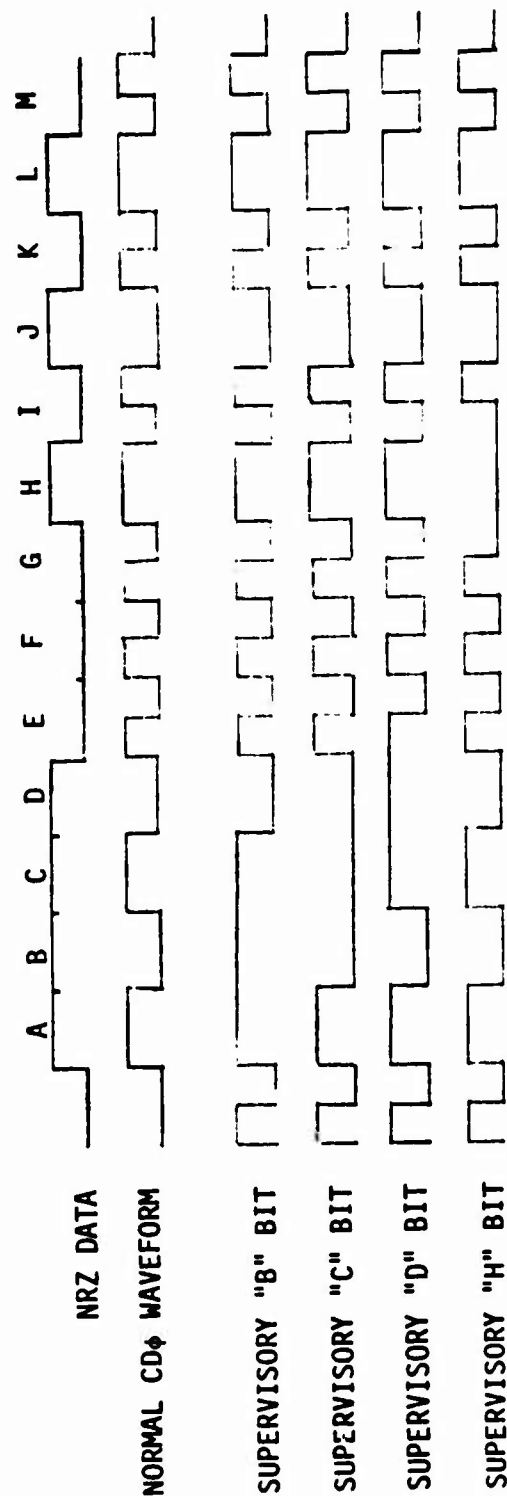


Figure 2.2-1  
 EXAMPLES OF WAVEFORMS  
 FOR CDφ WITH SUPERVISORY SIGNALLING

This scheme would cause an increase in the error rate in situations where ISI is severe. This is because the  $CD\phi$  waveform can be in the same state for as long as three symbol intervals instead of the one symbol interval maximum experienced for  $CD\phi$  without a supervisory channel. A sample error in the receiver would cause an ambiguity which would tend to cause the receiver to decode the resulting waveform as containing a supervisory bit. BAMI has this problem but it is not as severe in BAMI because a sample error in BAMI would more likely cause the BAMI receiver to decode the sample errors as a "space" than to decode it as a bipolar violation.

### 3.0 Signal Processing

The generation of these waveforms at the transmitter is straightforward and only the processing at the receiver will be examined. The virtues of balanced operation are discussed in Ref 5, Sec 3.5.4.3.1 and 3.5.4.3.2.

#### 3.1 Processing of the BAMI Waveform

After passing through the differential amplifier to reduce common mode noise, the signal is fed to two differential comparators to separate positive from negative "marks." The negative side of the differential comparators is set to the threshold voltage which is the "Mark-space" decision level. The same threshold can be set on both differential receivers.

The input signal level and the threshold will set the allowable noise margin. A block diagram for a BAMI receiver without equalization is shown in Figure 3.1-1.

##### 3.1.1 Theoretical Bit Error Rate for BAMI

The eye pattern for the BAMI signal is shown in Figure 3.1.1-1. To detect the BAMI signal only one sample needs to be taken per data bit and it is compared to the two thresholds. In the ideal case (no distortion, no noise) the threshold can be set on any value within its range limits and the sampling signal can occur any time within  $(0, T/2)$ . On the other hand for a distorted signal the threshold must be set according to expected Intersymbol Interference (ISI) and noise, and at the point in time where the signal reaches the maximum value. Hence there is very little choice in setting the sampling signal phase; it would have to occur just before  $T/2$ . The threshold due to intersymbol interference is best determined from the worst case condition, i.e., all "marks" followed by a "space" in the data stream. If the rise time of the

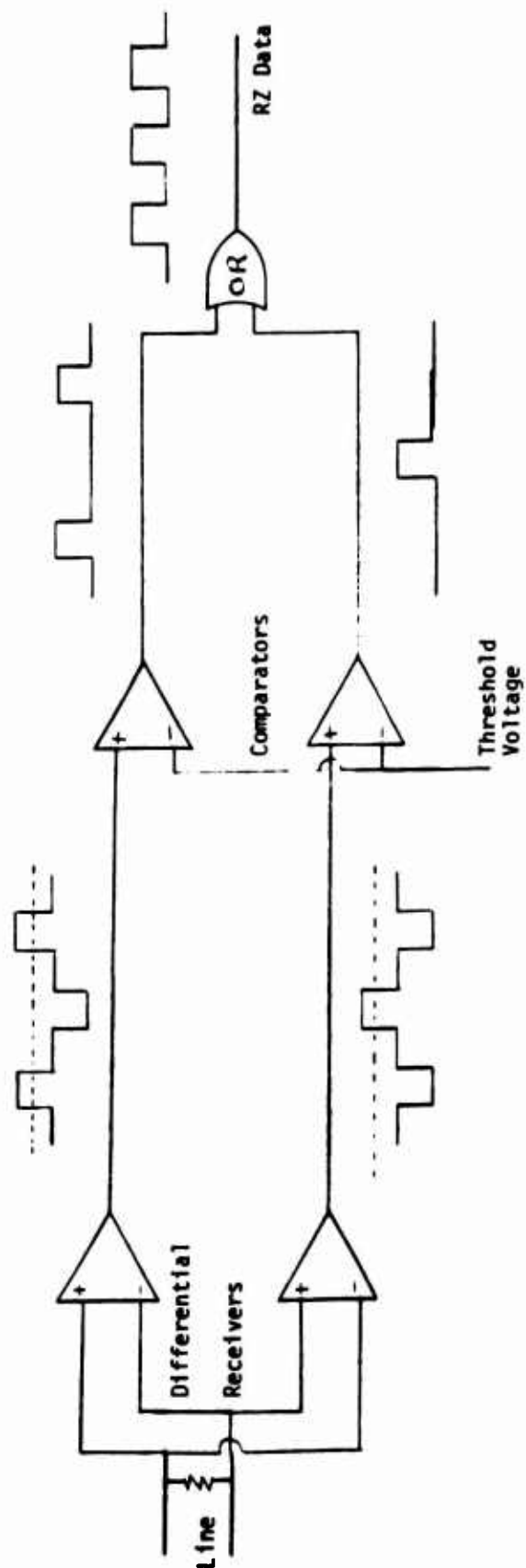


Figure 3.1-1  
BLOCK DIAGRAM FOR BAM RECEIVER



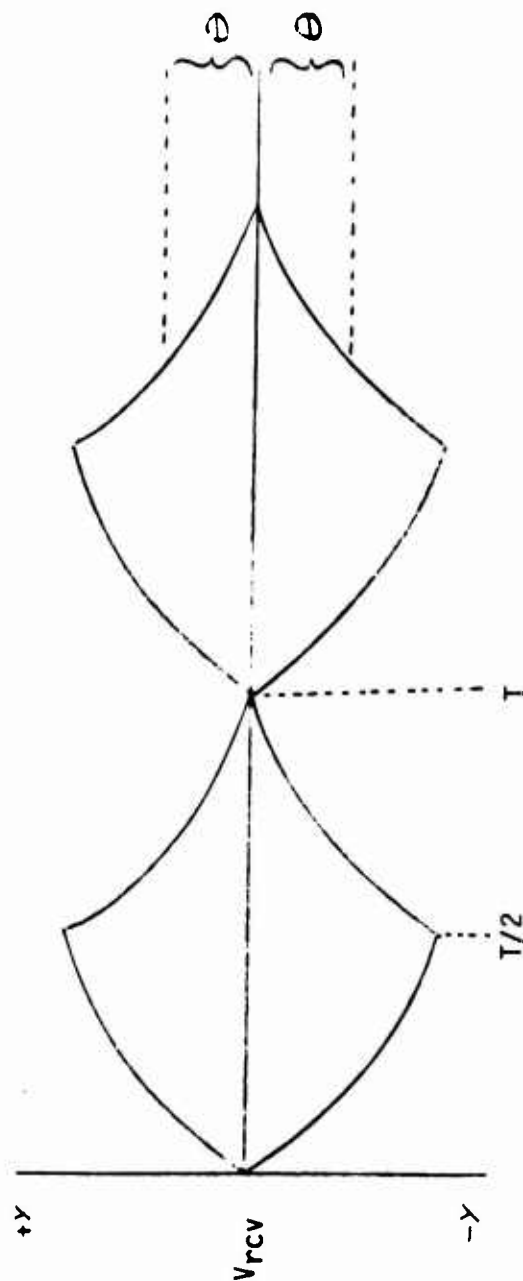


Figure 3.1.1-1  
BAMI WAVEFORM WITH  
INTERSYMBOL INTERFERENCE

signal is equal to the fall time then the ISI would be zero; however, if the fall time is longer then the combined ISI can be calculated from Ref 5, pp 60.

In the presence of ISI the threshold,  $\theta$ , should be set at a voltage one half of the receiver input signal for both positive and negative portions of the waveform (see Figure 3.1.1-1). The noise margin at the receiver is the voltage from the received signal to the threshold, and the probability of a sample error is the probability that the noise voltage exceeds the noise margin at the sampling instant. Then at the sampling instant (see notations, Table 3.1.1-1), circled numbers represent areas from the figure,

$$P_{be} = P_{se} = P(|y| > \theta) \text{ for space detection}$$

and

$$P_{se} = P(|y| < \theta) \text{ for mark detection}$$

using conditional probabilities

$$P_{se} = P(rcv1|xmit0) + P(rcv0|xmit1)$$

converting from conditional to total probabilities (see Figure 3.1.1-2)

$$\begin{aligned} P_{se} &= P(|y| > \theta) P(xmit0) + P(y < \theta) P(+1) + P(y > -\theta) P(-1) \\ &= [1 + 2] P(0) + [4] P(1) + [3] P(-1) \end{aligned}$$

Given the symmetry of the waveform, i.e.,  $|y_1| = |y_2|$ , equal threshold levels,  $\theta = \frac{1}{2}|y_1| = \frac{1}{2}|y_2|$ , and the even noise pdf.

$$\textcircled{1} = \textcircled{2} = \textcircled{3} = \textcircled{4}$$

Thus

$$P(y < \theta) = P(y > -\theta)$$

Since

$$\begin{aligned} P(y < \theta) + P(y > -\theta) &= P(|y| < \theta) \\ \textcircled{3} + \textcircled{4} &= P(|y| < \theta) \end{aligned}$$

$P_{be}$  - Probability of Bit Error  
 $P_{bc}$  - Probability of Bit Correct  
 $P_{se}$  - Probability of Sample Error  
 $P_{sc}$  - Probability of Sample Correct  
 $\theta$  - Threshold Voltage  
 $Y$  - Received Signal plus noise  
 $X_{mit1}$  - A "one" was Transmitted  
 $X_{mit0}$  - A "zero" was Transmitted  
 $rcv1$  - A "one" was Received  
 $rcv0$  - A "zero" was Received  
 $P(+1)$  - Probability that Mark has "plus" Polarity  
 $P(-1)$  - Probability that Mark has "minus" Polarity

Table 3.1.1-1  
 Mathematical Notations Used in Derivations

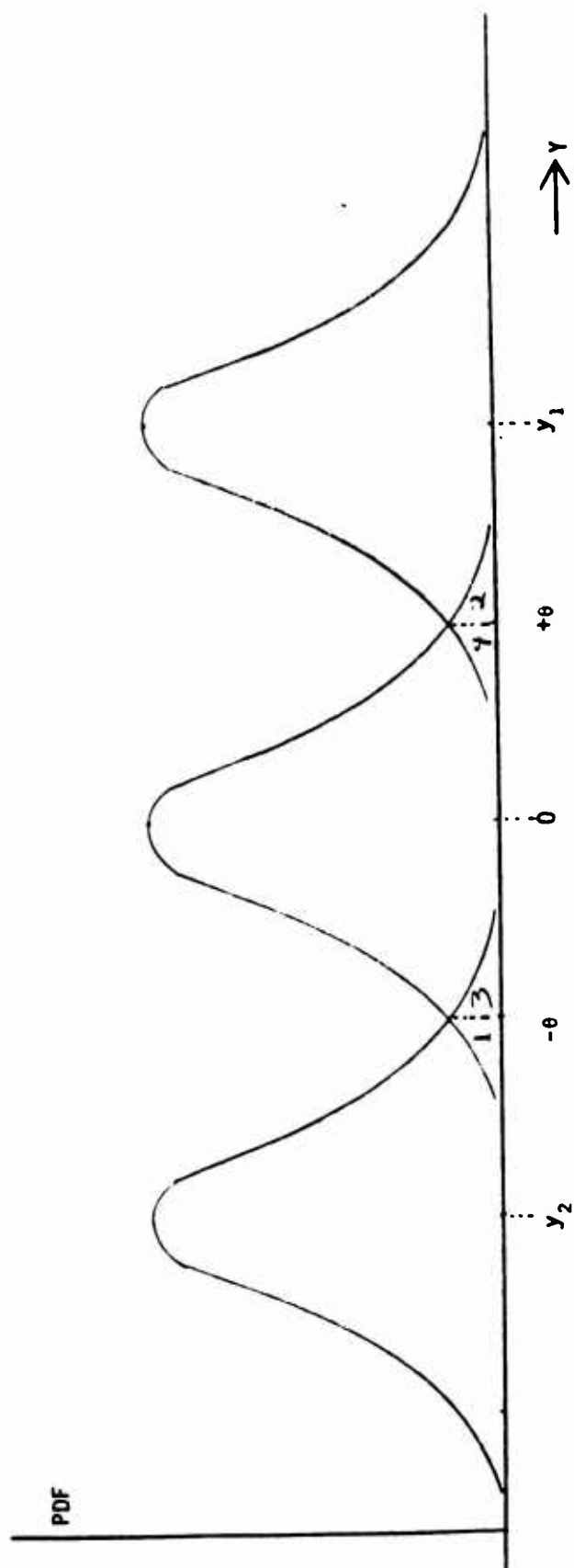


Figure 3.1.1-2  
PROBABILITY DISTRIBUTION OF THE  
BAMI WAVEFORM WITH ADDITIVE NOISE

But from Eq 3

$$3 + 4 = 1 + 2$$

Now we have

$$P(|y| < -\theta) = P(|y| > \theta)$$

For random data

$$P(x_{mit}0) = \frac{1}{2}, P(+1) = P(-1) = \frac{1}{4}$$

From Eq 2 and 4

$$P_{se} = P(|y| > \theta) \frac{1}{2} + P(y < \theta) \frac{1}{4} + P(y > -\theta) \frac{1}{4}$$

$$P_{se} = P(|y| > \theta) \frac{1}{2} + P(|y| > \theta) \frac{1}{4}$$

$$P_{se} = 3/4 P(|y| > \theta)$$

Thus the probability of a sample error is equal to 3/4 the probability that the signal plus noise ( $y$ ) deviate from normal by more than the threshold voltage  $\theta$ . This can be seen by noting that when a zero is being sampled, a deviation by more than  $\theta$  always causes an error but when a +1 or -1 is being sampled a deviation by more than  $\theta$  sometimes helps and sometimes hurts.

This probability can be evaluated assuming Gaussian noise by use of the error function as follows: (See Figure 3.1.1-3)

First, a change to normalized variables is required to be able to evaluate the error function.  $\mu$  is the noise mean and  $\sigma$  is its standard deviation.

$y$  becomes  $z$  and  $\theta$  becomes  $\frac{\theta - \mu}{\sigma}$ . The  $P_{se}$  is the shaded area where  $z > \frac{\theta - \mu}{\sigma}$ . In terms of the error function this is

$$P_{se} = \frac{3}{4} p(|z| > \frac{\theta - \mu}{\sigma}) = \frac{3}{4} (1 - \text{ERF}(\frac{\theta - \mu}{\sigma}))$$

Where

$$\text{ERF}(X) = \frac{1}{\sqrt{2\pi}} \int_{-X}^X e^{-y^2/2} dy$$



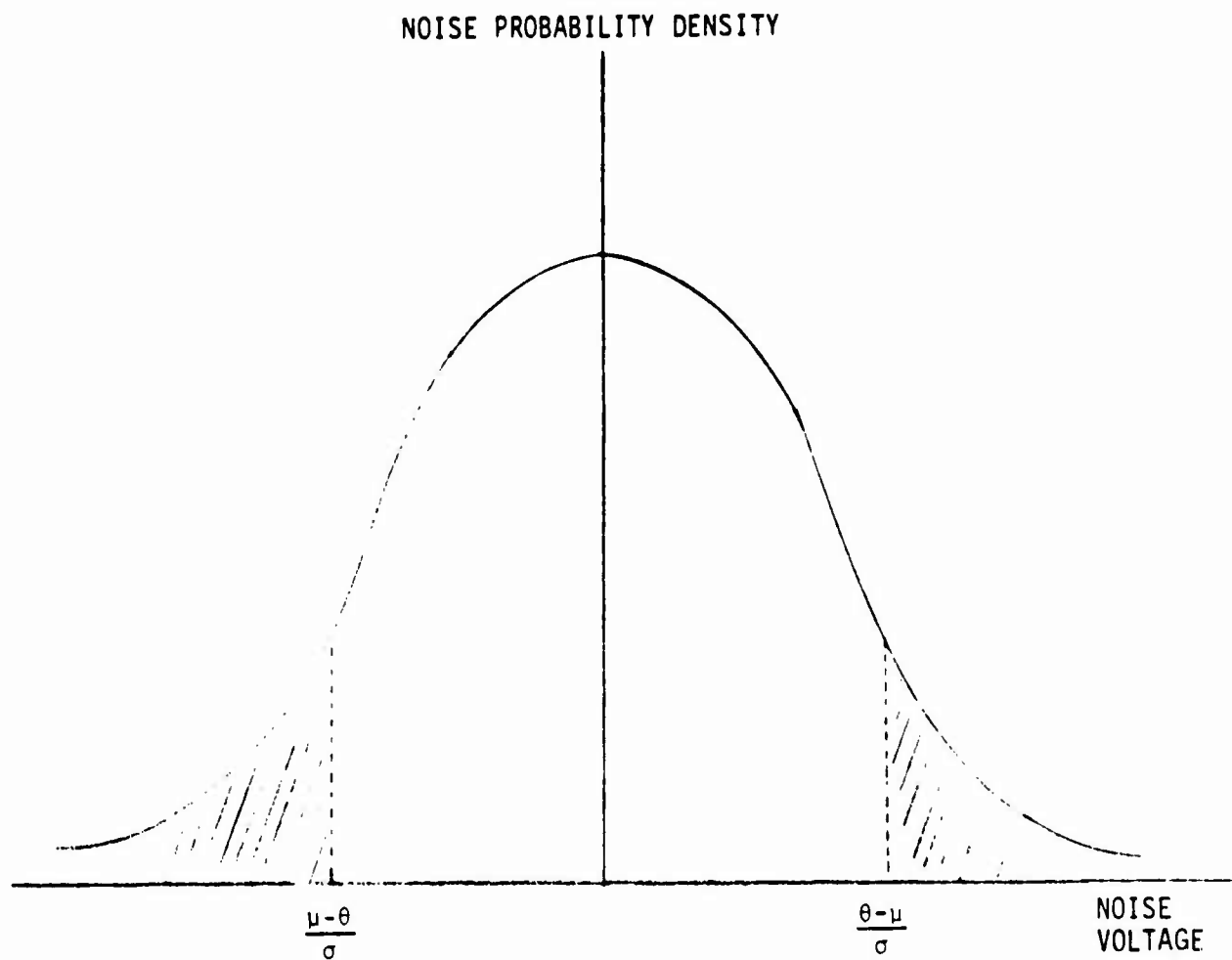


Figure 3.1.1-3  
ERROR AREA UNDER GAUSSIAN DISTRIBUTION

To generate a performance curve of BER vs S/N ratio it is required to vary  $\sigma$  for each point. The abscissa (SNR in db) is calculated:

$$\text{SNRdb} = 20 \log \left( \frac{\theta - u}{\sigma} \right)$$

In the no ISI case:

$$\theta = \frac{1}{2} V_{rcv}$$

and if the cable is modelled as a low pass RC filter:

$$V_{rcv} = V_{xmt} (1 - \exp(-\frac{2.2t}{t_r}))$$

where  $V_{xmt}$  is the transmitted pulse voltage and  $t_r$  (ref 20, pg 44) is the rise time of the signal having passed through the cable and  $t$  is the sampling instant:  $t = 0$  or  $T/2$ , and generally will be equal to  $T/2$ .

The value of  $\sigma$  for the noise is its true rms power. The bandwidth of the noise is determined from the input filters to the receiver. These front end filters should be wide enough to allow 90% of the signal power to pass. As such for the BAMI signal, this bandwidth would be 1.2 times the data rate (Figure 3.4-3).

### 3.2 Processing of the CD $\phi$ Waveform

This waveform is also received in the differential mode but one threshold suffices for the decision at sampling time. But unlike the BAMI signals, two samples are required to determine the sense of the bit sent.

Since in the conditioned diphase signal the "mark" is transmitted as a phase change, two samples of the received signal's amplitude must be made to determine if a phase change occurred. This polarity sensing is performed when the output of the differential receiver is delayed to be used as one of the inputs to the mod two addition to recover the NRZ data signal.

In Figure 3.2-1 the  $CD\phi$  signal is clocked into the delay flip flops one half bit at a time. This is performed by clocking the flip flops at a rate twice that of the data. The resultant delay is one data clock period as required. Timing diagrams showing the decoding process are given in Figures 3.2.1-1 and 3.2.1-2.

### 3.2.1 Relationship Between $CD\phi$ Sample Errors and Bit Errors.

As already noted two samples are needed to determine the sense of a received  $CD\phi$  data bit. If the two samples are on opposite sides of the threshold the data bit is a space and if the two samples are on the same side of the threshold the data bit is decoded as a mark. This section discusses what happens when one of the two samples is in error. Two methods of  $CD\phi$  decoding are discussed: first, where the received waveform is delayed a whole symbol interval ( $T$ ) before decoding, and second where the delay is half a symbol interval.

Figure 3.2.1-1 shows the pertinent waveforms for a data pattern and the effects of sample errors. In this discussion a distinction is made between "data bits" and "bits." A "bit" is one of the two  $CD\phi$  samples that make up an NRZ "data bit." Data bits A, D, F, G, J, M, and N have sample errors introduced. The sample errors introduced in data bits A and D do not cause bit errors. The reason is that the second sample of the two-sample pair for these data bits is the erroneous one and when the delay is equal to  $T$  no error can occur. This can be seen by noting that since the transmitted NRZ data is first reduced to RZ data, the data bit information is carried only in the first half of  $T$ . The second half of  $T$  ends up carrying timing information due to the exclusive OR of the RZ waveform and the clock. Thus if a  $CD\phi$  sample error occurs in the "timing" portion of the  $CD\phi$  waveform the information is

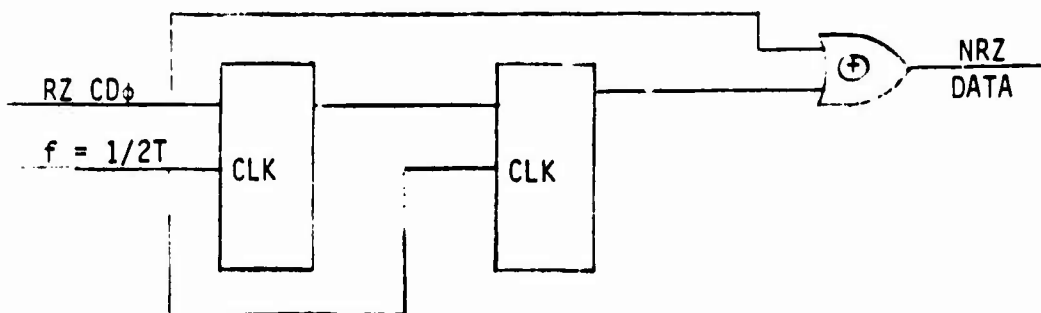
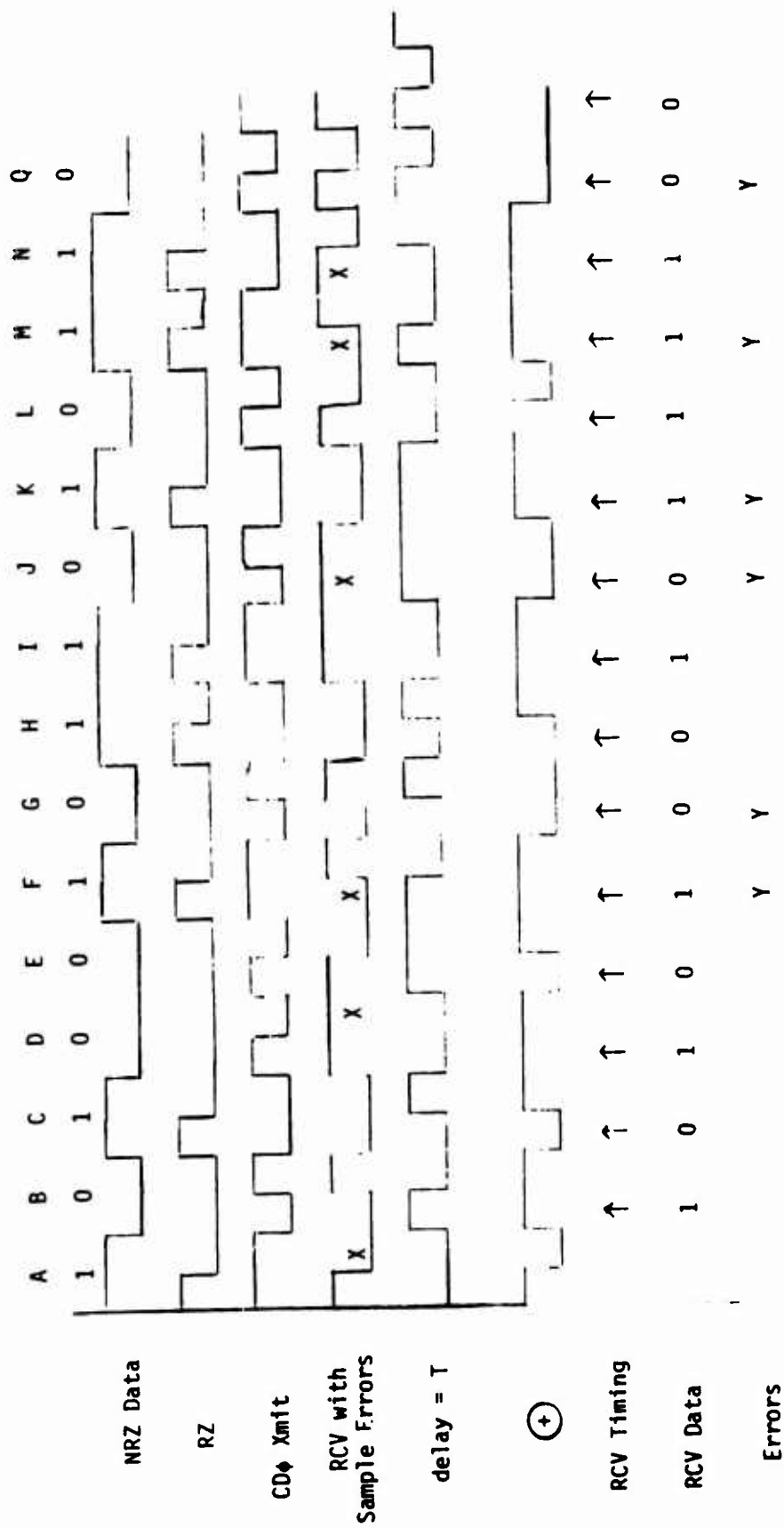


Figure 3.2-1  
BLOCK DIAGRAM FOR CDφ RECEIVER DECODER



T = NRZ bit time

X = sample errors

Y = bit errors

Figure 3.2.1-1

CDφ Processing Delay = T



not affected if the waveform is delayed by  $T$ . Where delay =  $T$  the "erroneous timing" sample is exclusive ORed with another "timing" bit and not an information carrying bit. If random data and independent occurrence of sample errors are assumed, it is concluded that half the sample errors cannot cause a data bit error.

These "timing" sample errors have an insignificant effect on the recovery of timing at the receiver since their only purpose is to insure that a sufficient number of transitions occur in the  $CD\phi$  waveform for the receiver phase locked loop to track.

When the sample error occurs in the information portion of the  $CD\phi$  waveform, such as at data bits F, G, J, M, and N, either one or two errors are produced. In the case where there are not two information sample errors in succession (bits F and J) two data bit errors will be produced: one at the instant the sample error occurs and one when the sample error is delayed and exclusive ORed with the incoming  $CD\phi$  waveform.

For the case where two or more information sample errors in a row occur (bits M and N) only the first and last sample errors will cause bit errors. The bits in between the end sample errors will be decoded properly because both of their sample bits have been detected on the wrong side of the sampling threshold and the decoding process only cares about whether samples are on the same side or opposite sides of the threshold, and not what the sides are. This property is inherent in the exclusive OR portion of the decoding process.

The probability that more than one information bit sample in succession is erroneous is assumed to be low since these digital systems will typically operate in environments where bit error rates are  $10^{-5}$  errors/bit or lower. This implies a high SNR which means most sample errors will be spaced far

apart. If the receiver incorporates a low pass front end filter, the assumption that sample errors will seldom occur in succession holds true for impulse noise as well. In fact, reference 14, page 942, shows that the expected number of errors per impulse is only  $3/16$ . Also the data presented in Section 4.2.3 indicates that only 5% of the data bit errors are adjacent.

To summarize, half the sample errors will not cause a bit error and the large majority of the other sample errors will cause two bit errors yielding close to one-to-one correspondence between sample error rate and data bit error rate.

The  $CD\phi$  decoding process where the delay is  $T/2$  instead of  $T$  is depicted in Figure 3.2.1-2. Sample errors are introduced in the same positions as the case for delay =  $T$  and the resulting bit errors are shown. Six sample errors generate six bit errors. Following logic as before it can be seen that this one-for-one correspondence will always be the case because with the delay equal to  $T/2$  a sample error in the "timing" bit will be delayed to line up with an information bit for the exclusive OR process and vice versa. Thus it is concluded that both methods of decoding  $CD\phi$  are essentially the same in performance, i.e., the bit error rate and the sample error rate are very close to the same.

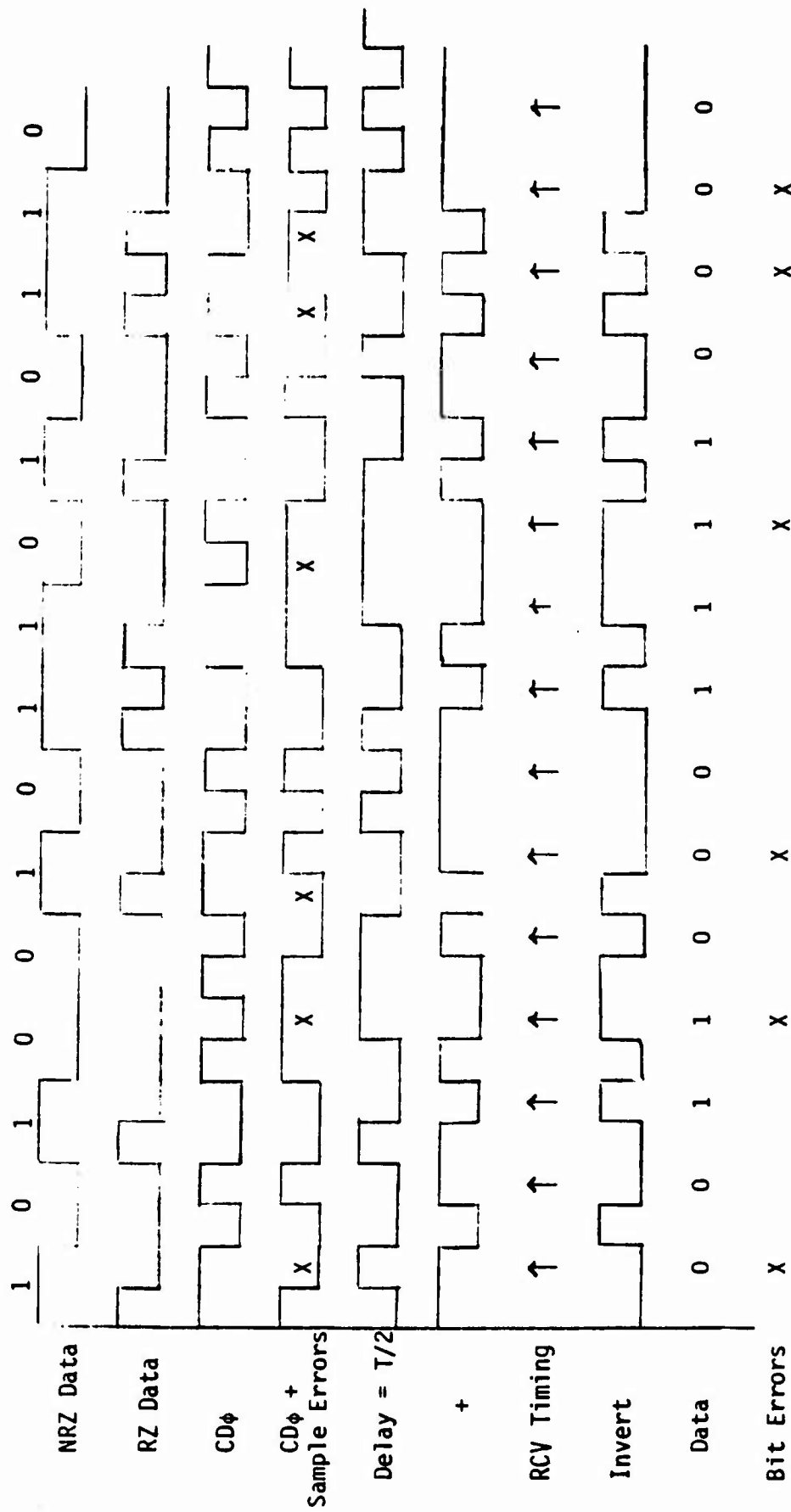


Figure 3.2.1-2  
CDφ Processing Delay = T/2

### 3.2.2 Theoretical Bit Error Rate for CD $\phi$

This derivation is based on the following assumptions:

- a. The only transmission impairment is Wideband Gaussian noise with mean  $\mu = 0$  and variance  $\sigma^2$ .
- b. The probability of occurrence of a mark equals the probability of occurrence of a space.
- c. There is no intersymbol interference (ISI).

A CD $\phi$  waveform with superimposed gaussian distributed noise is shown in Figure 3.2.2-1. This waveform has amplitude levels of  $\pm y$  and no ISI. The waveform is sampled at times A, B, C, and D. The noise margin (sample threshold) is  $\theta$ . The sample that occurs at time A will be described in detail.

The voltage at time A will be  $\pm y \pm N$  where  $N$  is the value of the additive gaussian noise. If  $N$  is positive at time A the sample will be correct because the amplitude of the waveform at time A will be  $Y + N$  which actually enhances the distance from the sample level to the threshold level. However, when the noise  $N$  at time A is negative, one of two conditions can occur. If  $|N| < \theta$  ( $\theta$  = threshold margin) the sample will still be correct because the noise was not of sufficient magnitude to cause the value  $y - N$  to be on the other side of the sampling threshold. The other case where  $|N| > \theta$  and  $N$  is negative at time A will be an error condition because the sum of  $y - N$  will be on the wrong side of the sampling threshold. To summarize the conditions at time A, if  $N$  is positive no error will occur, but if  $|N| > \theta$  and  $N$  is negative a sample error will occur.

Due to the symmetry of the Gaussian probability density function we can write

$$P(+N) = P(-N) = \frac{1}{2}$$

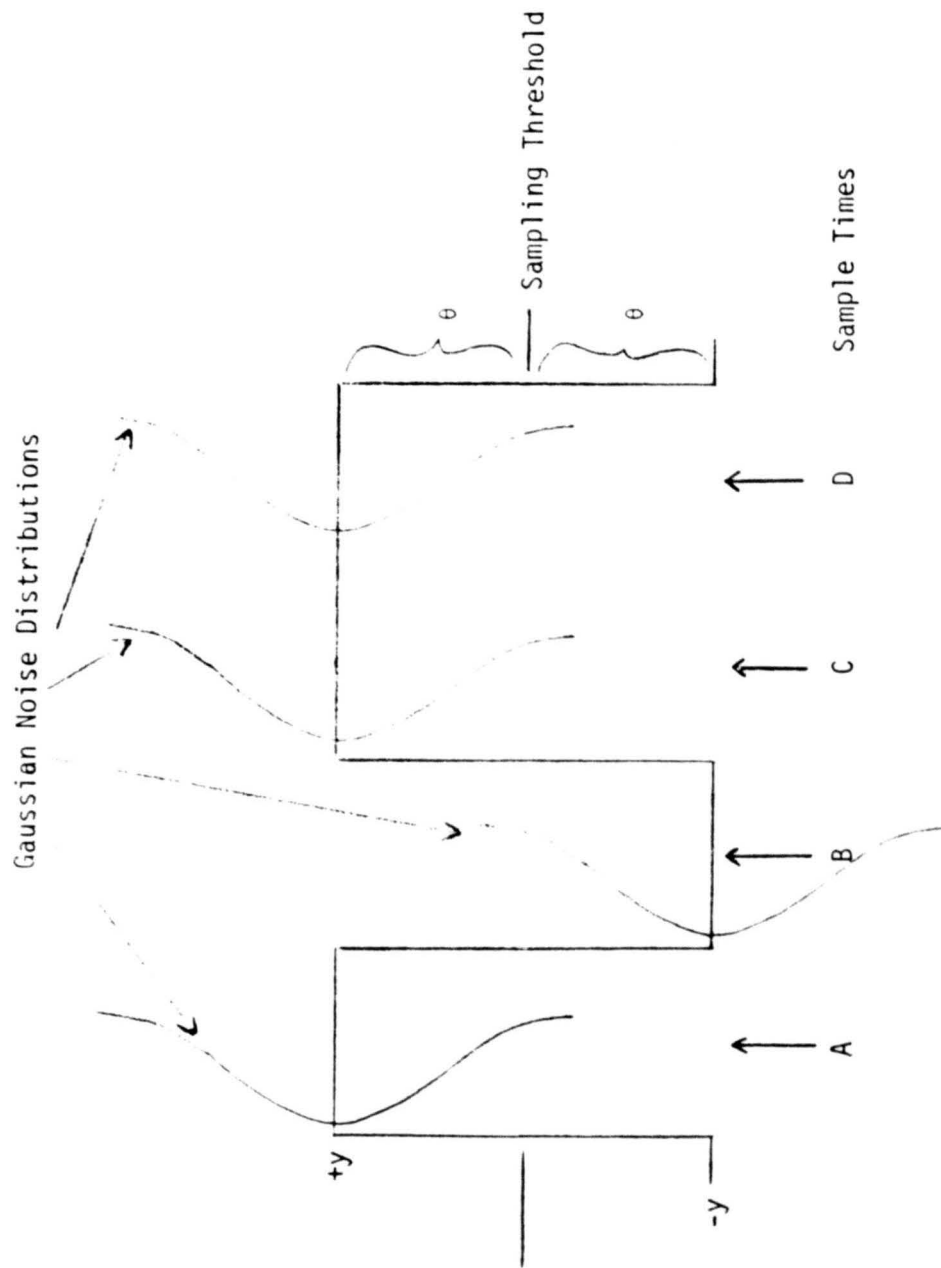


Figure 3.2.2-1  
 $CD\phi$  Waveform with Gaussian Noise Distributions

The only condition where a sample error occurs is when we have  $-N$  and specifically when we have the case where  $|N| > \theta$ . Now we can determine the probability of a sample error ( $P_{se}$ ). If we assume that the polarity of the noise and its amplitude are independent events we can write:

$$\begin{aligned} P_{se} &= P(-N) P(|N| > \theta) \\ &= \frac{1}{2} P(|N| > \theta) \end{aligned}$$

Next we want to relate the  $P_{se}$  to the Bit Error Rate (BER). First note (Section 3.2.1) that

$$P_{se} \approx P_{be}$$

where  $P_{be}$  is the probability of a bit error. A conversion is needed to get the BER from the  $P_{be}$  since  $P_{be}$  is a dimensionless quantity while BER has units ERRORS/BIT. Since there are two samples per bit in  $CD\phi$ , each with an associated  $P_{se}$  we can write

$$\begin{aligned} BER &= (SR)(P_{se}) \\ &= (SR)(P_{be}) \end{aligned}$$

where  $SR$  is the sample rate which is two per bit. Combining we get

$$\begin{aligned} BER &= (SR)(P_{be}) = 2(\frac{1}{2}P(|N| > \theta)) \\ &= P(|N| > \theta) \text{ per bit} \end{aligned}$$

To plot this function for the general case we can normalize the function as we did for BAMI (Section 3.1.1) to get

$$BER = P(|N| > \frac{\theta - \mu}{\sigma}) = 1 - \text{ERF}(\frac{\theta - \mu}{\sigma})$$

where

$$\text{ERF}(N) = \frac{1}{\sqrt{2\pi}} \int_{-N}^N e^{-y^2/2} dy$$

Plots of the BER for both CD $\phi$  and BAMI are given in Figure 3.2.2-2. The abscissa is defined as

$$\text{SNRdb} = 20 \log \left( \frac{\theta - \mu}{\sigma} \right)$$

In Figure 3.2.2-2 the curves show the calculated results for CD $\phi$  and BAMI having equal threshold margins  $\theta$ . This occurs when the BAMI waveform has twice the peak-to-peak amplitude level compared to CD $\phi$ . In this case the BAMI error rate is 75% of the CD $\phi$  error rate. Allowing the BAMI peak-to-peak amplitude to be twice that of CD $\phi$  should cause no problem in an implemented system for the following reason. The amplitude (voltage swing) of a given signal is limited to keep crosstalk at a tolerable level. The major contributor to crosstalk is caused by the capacitive coupling between the wires. The magnitude of the crosstalk due to capacitive coupling in a given set of wires is determined by the magnitude of the voltage transition. For the situation where the BAMI signal has a peak-to-peak amplitude twice that of CD $\phi$ , the magnitude of all voltage transitions is equal since BAMI is a 3-level signal and CD $\phi$  is a 2-level signal. The BAMI signal always stops at 0 volts before proceeding to one of its amplitude extremes while CD $\phi$  always goes from one amplitude extreme to the other.

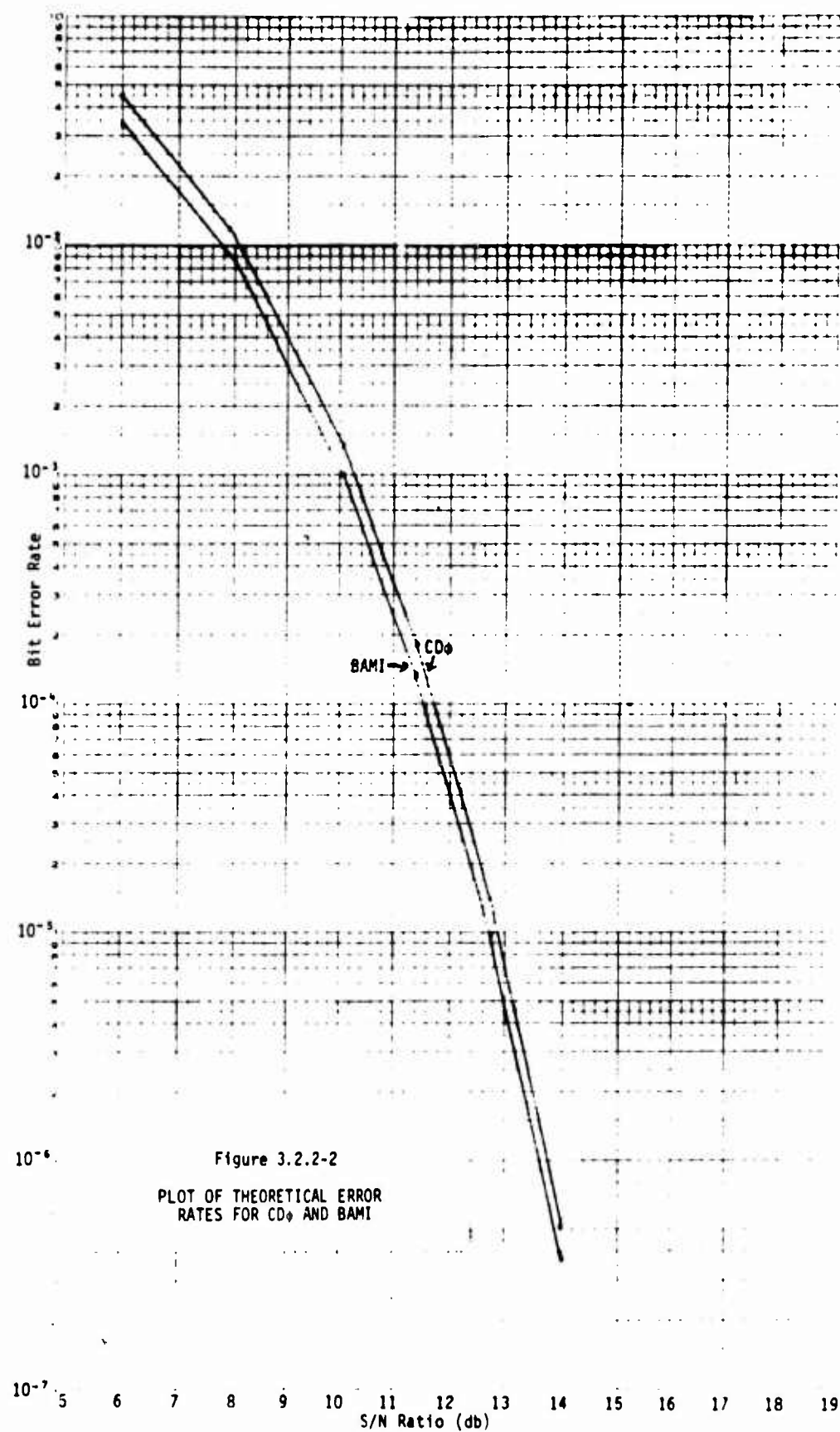


Figure 3.2.2-2  
PLOT OF THEORETICAL ERROR  
RATES FOR CD AND BAMI



### 3.3 Consideration of Sample Correlation

An additional consideration in the  $P_{be}$  calculation is the degree of correlation between samples. The data is assumed independent. Therefore, for BAMI, in the absence of noise, the magnitudes of successive samples are uncorrelated. For  $CD\phi$  the same condition holds because of the randomness of the phase modulation by the random data.

On the other hand, if noise is present a degree of correlation may exist and this degree of correlation is a function of the bandwidth of the noise. Again, assuming gaussian noise, the bandwidth of the receiver front end filters will depend on the timing recovery mechanism but the wider the bandwidth of the filters, the more likely the probability of error due to noise because of the increased noise power. Because of side lobe characteristics of their spectral power distributions the two types of waveforms will admit more or less noise with an increase of filter BW.

Figure 3.4-3 can be used to determine the filter bandwidth necessary to admit a given amount of signal power for each waveform and how much the filter bandwidths would have to be increased to admit a given increase in signal power.

This filtering effect will give rise to a correlation in the noise samples. This correlation can be found from:

$$\rho_n(\tau) = \frac{\psi_n(\tau)}{\sigma^2}$$

(from Ref 9, pp A-42). The parameters are the correlation function of the noise,  $\psi_n(\tau)$ , and the noise power,  $\sigma^2$ . This correlation coefficient will yield the correlation between two samples spaced  $\tau$  seconds apart. From Reference 9:

$$\psi(\tau) = \int_0^\beta N_0 \cos 2\pi f \tau df$$

$$\begin{aligned} &= \frac{N_0}{2\pi\tau} \sin 2\pi\beta\tau \\ &= N_0\beta \frac{\sin \pi 2\tau\beta}{2\pi\beta\tau} \end{aligned}$$

where an ideal filter is assumed and  $N_0$  is noise power spectral density then

$$\rho_n(\tau) = \frac{\sin 2\pi\beta\tau}{2\pi\beta\tau}$$

Letting  $\beta$  take on the value  $1.2f_d$  for BAMI and  $1.7f_d$  for CD $\phi$ , where  $f_d$  is the data rate, then for BAMI successive samples,  $T$  sec apart ( $T = \frac{1}{f_d}$ )

$$\rho_{BAMI}(T) = \frac{\sin 2\pi 1.2f_d/f_d}{2\pi 1.7f_d/f_d} = 0.126$$

and CD $\phi$  at successive samples are correlated by a factor of

$$\rho_{CD\phi}(\frac{T}{2}) = \frac{\sin 2\pi 1.7f_d/2f_d}{2\pi 1.7f_d/2f_d} = -0.15$$

These correlations are small and not expected to influence the  $P_{be}$  to any significant degree. The signs of the correlation coefficients indicate the trends toward which the errors will gravitate. That is, the positive correlation will effect "spaces" to be read as "marks" in the BAMI case, while the negative correlation will effect "marks" to be read as "spaces."

### 3.4 Spectral Occupancy of CDφ and BAMl

To determine the spectral distribution of the signal power in the BAMl and CDφ waveforms references 9, 18, and 13 were used. The purpose for determining the signal power spectrum was to be able to identify the power content and its location in frequency. Primarily the strength of the signal components which would yield the timing would have to be found. Then receiver filters would have to be implemented to maximize the signal to noise ratio at the decision time.

The BAMl with equally likely "marks" and "spaces" has the following power spectral density:

$$PDS = \frac{1}{2T} |G(f)|^2 (1 - \cos 2\pi fT)$$

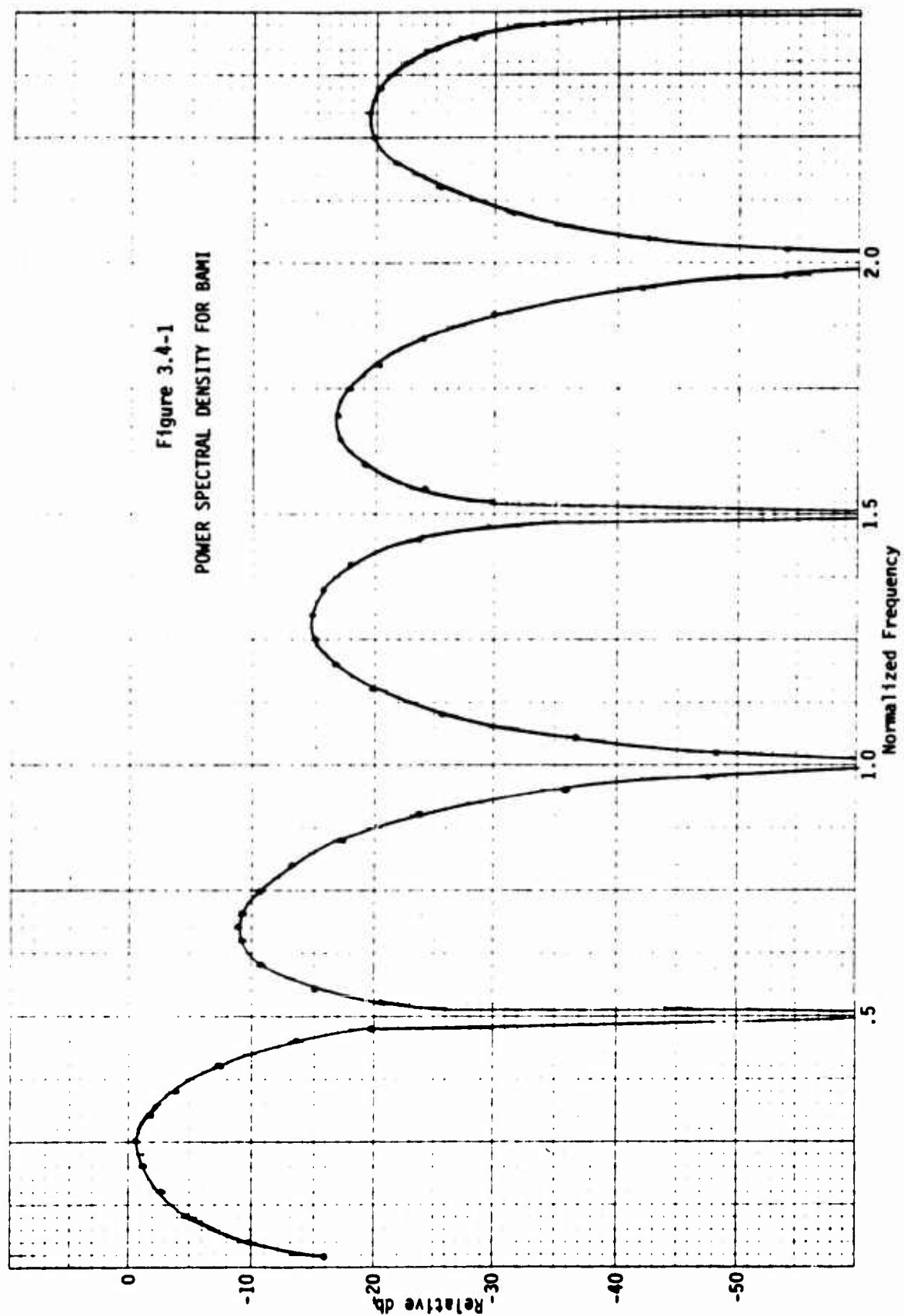
where

$$G(f) = \frac{\sin \frac{\pi fT}{2}}{\frac{\pi fT}{2}}$$

This distribution does not have discrete spectral components [Figure 3.4-1] since the BAMl transmission system uses balanced positive and negative pulses, i.e., pulses of equal duty cycle and magnitude. The signal power around  $\frac{1}{2T}$  is the source of the timing signal, and the discrete components at the timing frequency,  $\frac{1}{T}$ , can be derived by rectification of the incoming data pulses.

The CDφ power spectrum is given by:

$$PSD = 2T \left[ \left( \frac{\sin \frac{\pi fT}{2}}{\frac{\pi fT}{2}} \right)^2 - \left( \frac{\sin \pi fT}{\pi fT} \right)^2 \right]$$

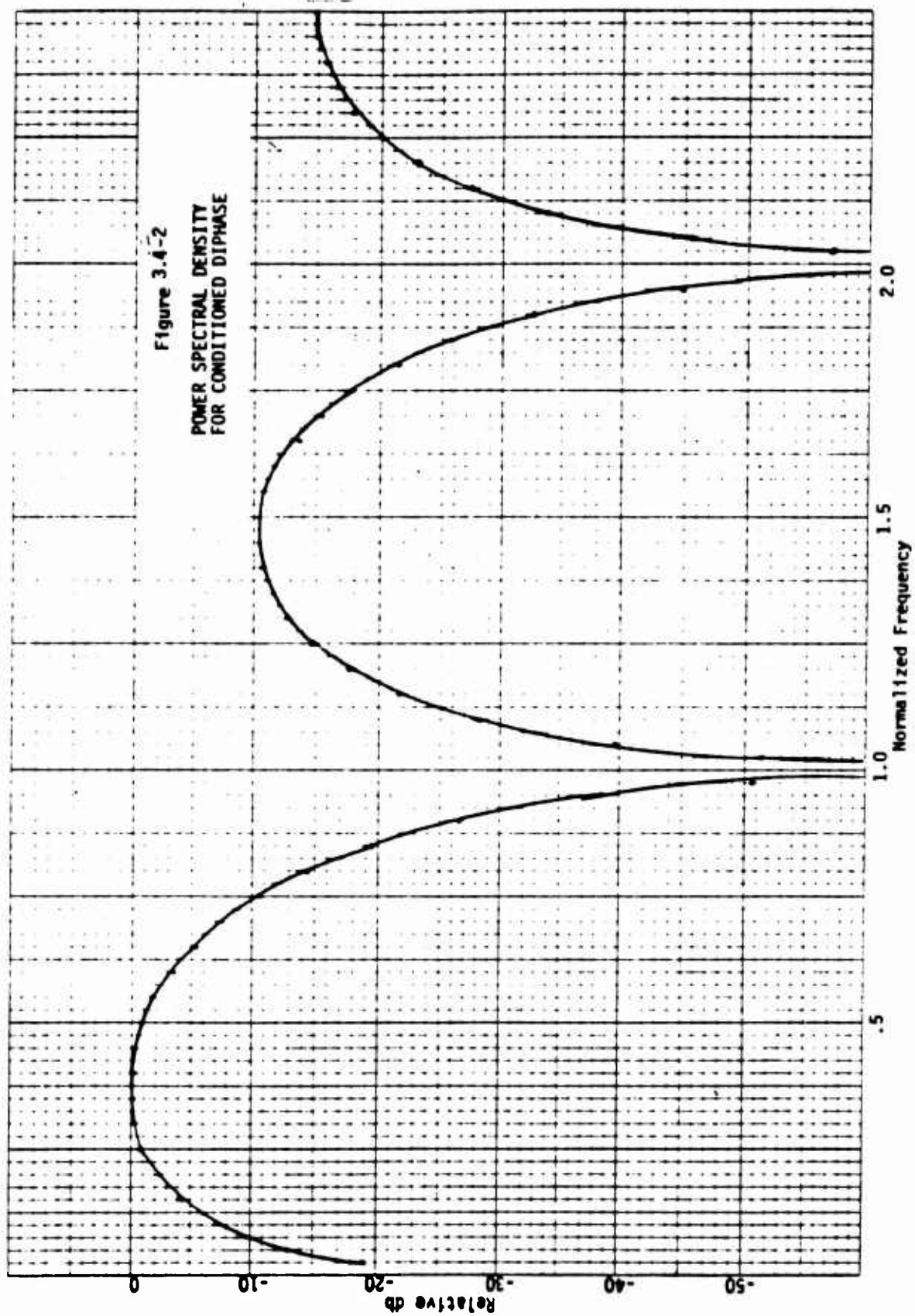


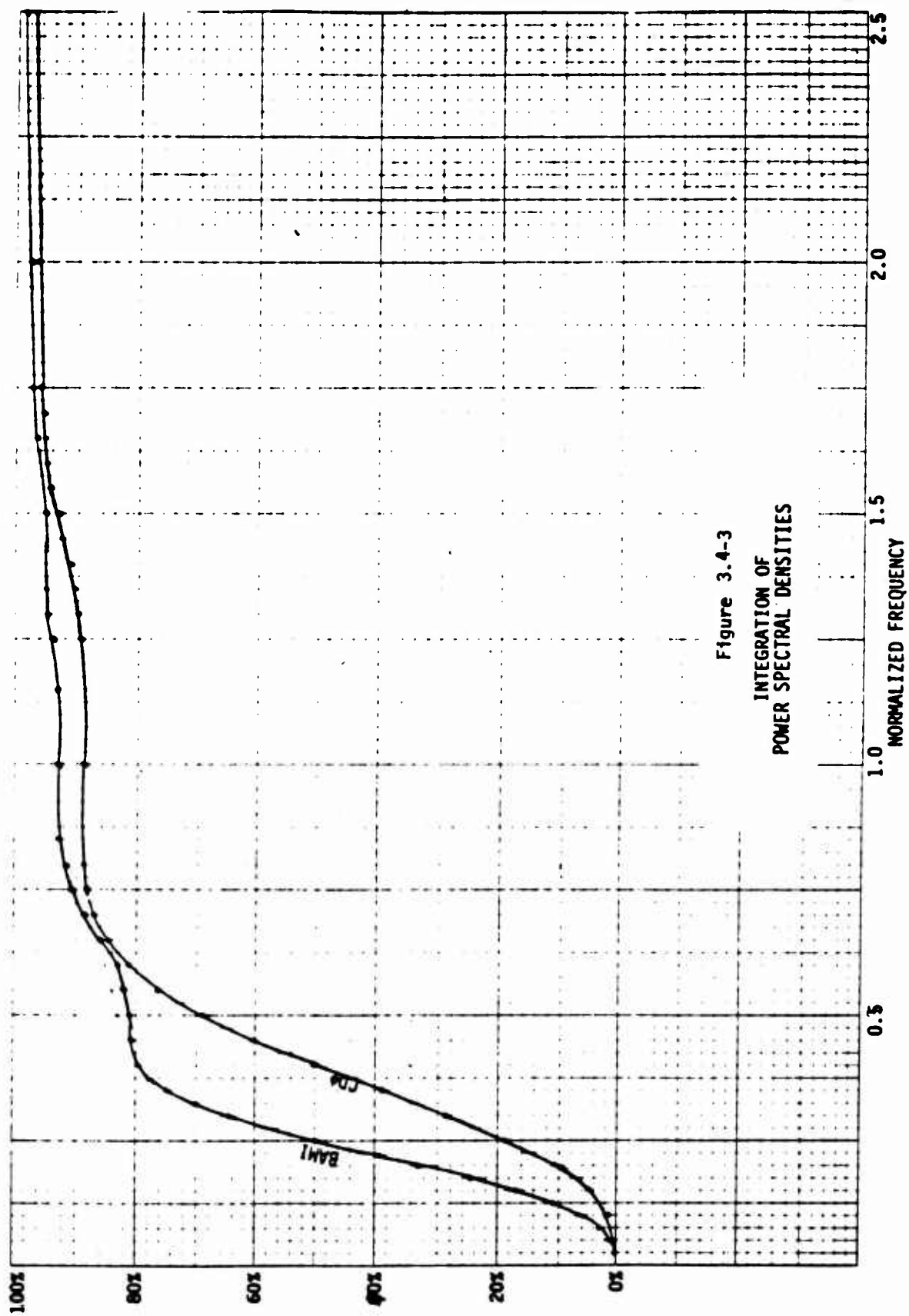
The spectrum is shown in Figure 3.4-2. Here also, the lack of discrete spectrum components is evident. The timing will be recovered from components about the data frequency,  $\frac{1}{T}$ .

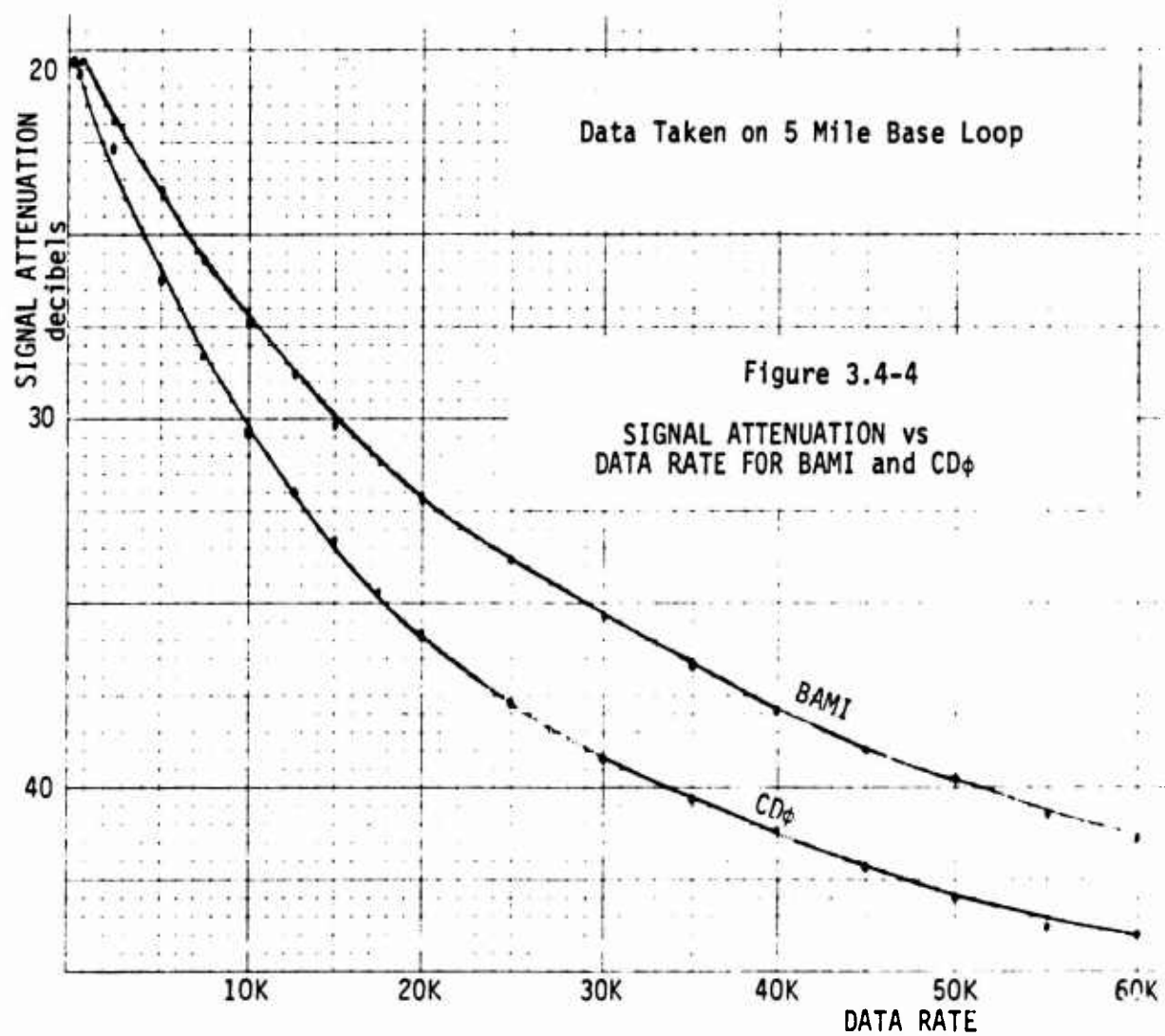
As for BAMI the  $CD\phi$  timing recovery process is nonlinear requiring slicing, differentiating and rectification.

BAMI enjoys an advantage over  $CD\phi$  in terms of spectrum occupancy. Comparison of Figures 3.4-1 and 3.4-2 shows that at a normalized frequency of 1.0 (data rate) BAMI is at its second null where  $CD\phi$  is at its first. This means that there is relatively less low frequency energy in the  $CD\phi$  waveform. This is emphasized by Figure 3.4-3 which is an integration of the magnitude of the two spectra. At normalized frequency of 1.0, BAMI is up to 92.5% of its total energy and  $CD\phi$  is at 88.9%. This in itself is not significant. What is significant is that the BAMI curve begins to peak much lower in frequency than  $CD\phi$ . Since the telephone cable is essentially a low pass filter the BAMI waveform is therefore transmitted in the region of lower attenuation of the telephone cable. This gives BAMI an inherent advantage over  $CD\phi$  in terms of its ability to resist attenuation by the telephone cable.

Figure 3.4-4 gives the results of an experiment to determine quantitatively the extent of advantage. For rates below 4K bits/sec the received power differs by less than 3 db and above 13K bits/sec the difference remains about 7 db. Looking at this another way BAMI can typically have a 50% higher data rate than  $CD\phi$  before it suffers the same power loss. This difference compares favorably with the results of section 4.3 where comparative tests were run over the 5 and 10 mile loops. If the data rates at which the error rates show a sharp increase are compared, BAMI out-performed  $CD\phi$  by approximately 30% for both the 5 and 10 mile loops.









#### 4.0 Hardware to Test BAMl and CD $\phi$

The hardware can be broken into two categories; first, the real and simulated media and second, the BAMl and CD $\phi$  waveform generator. The first part of Section 4 describes the media and the second part describes the performance of the waveform generator on the various media. The waveform generator was designed and built in-house. The schematics for it are given in the appendices.

##### 4.1.1 DICEF Laboratory Cable Plant

This cable consists of 6000 ft reels of AWG 19 plastic insulated copper wires. The ends of the cables are brought into three terminal boxes where equipment can be patched onto them, or the 6000 ft lengths can be connected in tandem to a maximum length of 150 miles. These cable plants are idealized in the sense that they are not strung next to other signal or power cables and therefore are not subject to external perturbations that are found in typical subscriber loops.

##### 4.1.1.1 Characterization of DICEF Cable

The nominal characteristics of 19-gauge cable are well known (refs 2, 10, 16). However, testing methods, cable test equipment, terminating impedance all vary so a short characterization of the DICEF cable was done. As stated above there is no impulse noise because the cables are physically isolated and their steel jacketing shields them from most RFI. A sample attenuation curve from reference 2 is given in Figure 4.1.1.1-1 for a cable of this type.

The wideband noise was measured at 2mv rms with a true rms voltmeter.

Crosstalk measurements were also made on the DICEF cables. The test setup is shown in Figure 4.1.1.1-2.

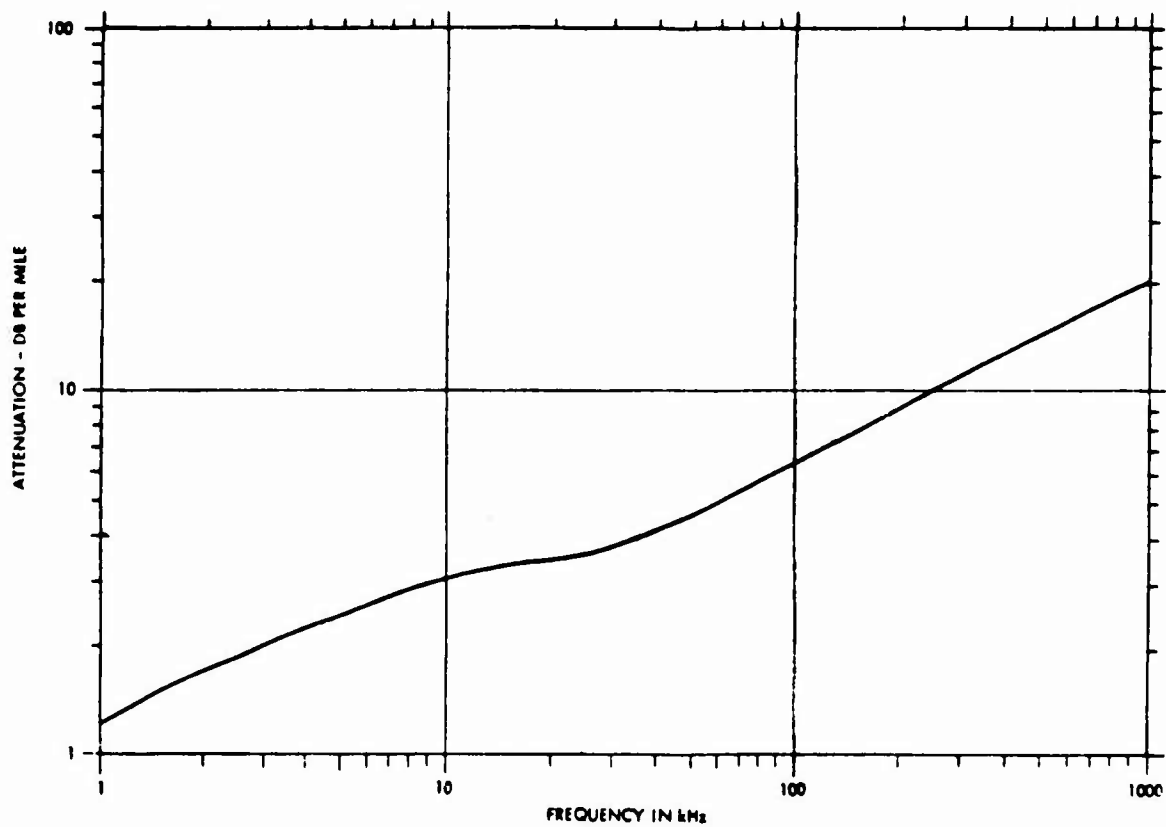


Figure 4.1.1.1-1  
Attenuation Versus Frequency for 19 GA  
Plastic Insulated Cable (.083  $\mu\text{f}/\text{Mi}$ )

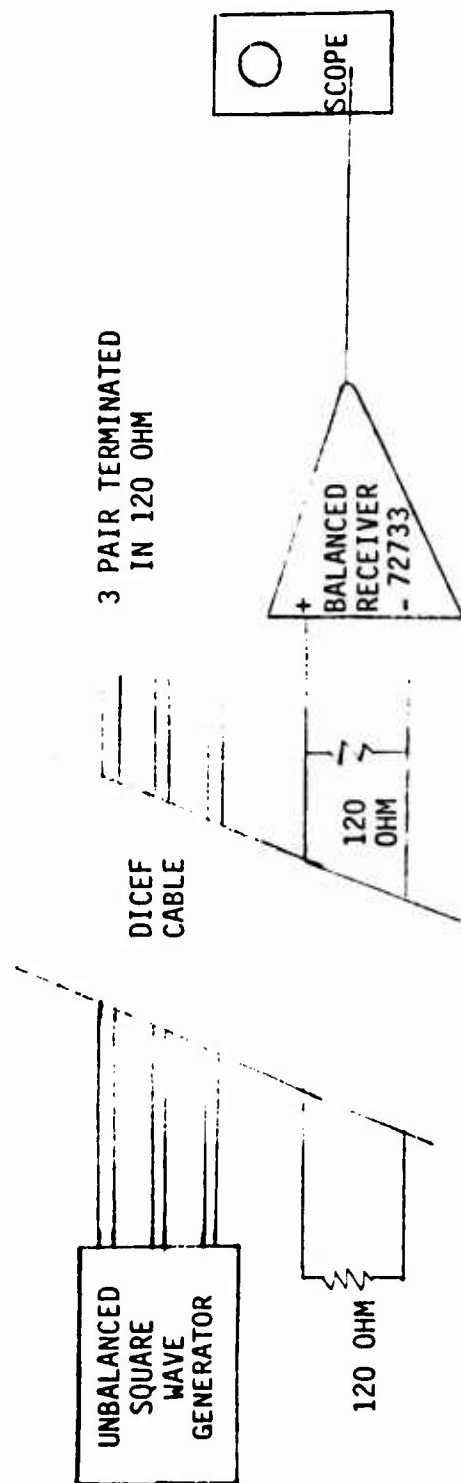
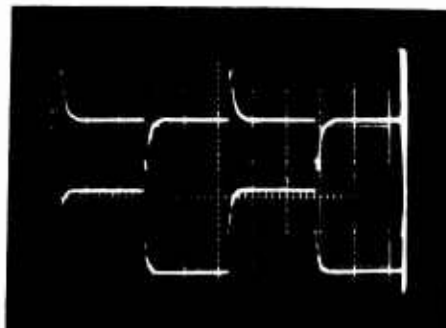


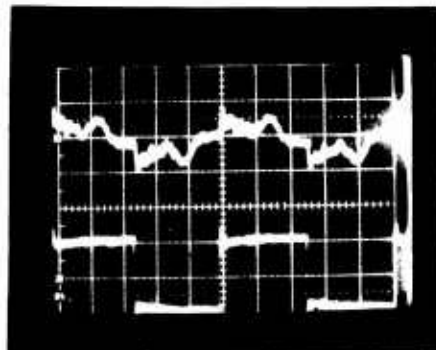
Figure 4.1.1.1-2  
TEST SETUP FOR CROSSTALK MEASUREMENT

A



Top Trace 2.5 mv/div (Crosstalk)  
"1 KHZ Rate"  
Bottom Trace 2.0 v/div (Disturbing Signal)

B



Top Trace 5 mv/div (Crosstalk)  
"100 KHZ Rate"  
Bottom Trace 1 v/div (Disturbing Signal)

Figure 4.1.1.1-3  
OSCILLOSCOPE PHOTOGRAPHS OF CABLE CROSSTALK

When the tests were planned both near-end (NEXT) and far-end (FEXT) crosstalk tests were to be conducted. However it was not possible to do far-end crosstalk tests because of the physical layout of the DICEF cable. Both ends of the cable are brought into the same connection box (which is sealed) in the laboratory. This caused the "far-end" crosstalk to be masked by crosstalk at the near end, thus no valid far-end crosstalk measurements could be taken. Fortunately, it is the near-end crosstalk which is the worst offender because the interfering signals at the near-end are larger in amplitude and contain higher frequency components than at the far end. As the interfering signal passes through the cable it is attenuated in amplitude, and the low pass characteristics of the cable reduce the higher frequency components. Another reason why near-end crosstalk is greater than far-end is that the currents induced in the disturbed pair by capacitive coupling flow in opposite directions to those induced by inductive coupling at the far end but flow in the same direction at the near end (Ref 3, page 287).

Figure 4.1.1.1-3 shows photographs of crosstalk induced by a square wave. The unbalanced square wave was applied in phase to three pairs in a cable bundle and the differential near end crosstalk was observed in a fourth pair. In these photographs the upper trace is the crosstalk and the lower trace is the disturbing signal. Part A is a 1 KHz square wave and the crosstalk appears as a voltage spike at each square wave transition which decays exponentially back to 0 volts before another transition occurs. Part B is the case when the square wave frequency has been increased to 100 KHz. The period of the disturbing signal is short enough that the spikes do not have a chance to decay to zero before another one of the opposite polarity occurs. The cumulative effect is the noisy signal on the upper trace of Part B. If we define

the crosstalk loss as the ratio of peak-to-peak disturbing signal to peak-to-peak crosstalk we get for Part A:

$$\text{Crosstalk loss db} = 20 \log \frac{4800\text{mv}}{7\text{mv}} = 56.7 \text{ db}$$

For Part B:

$$\text{Crosstalk loss db} = 20 \log \frac{2000\text{mv}}{8\text{mv}} = 47.9 \text{ db}$$

These numbers are representative only since they vary depending upon how close the pairs are in the cable and individual cable differences. This example is typical for the pairs tested.

Reference 3 performed a comprehensive study (Chapter 27) on NEXT and FEXT. The results there for 1000 ft of 50 pair, AWG 22 cable with 49 disturbing pairs show that the average NEXT loss at 3 MHz is 44db. This result is not directly comparable to the one performed in this test since the reference 3 results were for non-synchronized disturbing signals and other parameters are different. However, a general idea of the magnitude of crosstalk to be expected can be obtained from the above. Also these results are worst case examples since more than one disturbing pair was involved; and, for the tests at DICEF, the signal generator was unbalanced because a balanced square wave generator was not available. An unbalanced disturbing signal creates more crosstalk than a balanced one. Reference 9 on page 130 gives results for coupling of sine wave signals averaged over many pairs in the same cable layer and from layer to layer over the frequency range of 320 Hz to 3 KHz. Their results show approximately 100 db of NEXT crosstalk loss at 3 KHz. This is quite a bit more than the other figures mentioned above but this is to be expected since Reference 9 tests were for a single disturbing pair with a sine wave at low frequency.

The conclusion is NEXT crosstalk loss can be expected to be 50 db or more, except in worst case conditions where many signals are driven synchronously into one cable bundle. Bell laboratories (Ref 14) in a study on local cable distribution systems concluded that at 56 KHz there is only a 1% chance of NEXT between cable pairs being less than 72 db (non-synchronous disturbers). They also considered the case of synchronous disturbing lines and concluded that with a decision level-to-crosstalk ratio of 18 db, even 50 disturbing pairs did not degrade the performance appreciably. The overall conclusion on crosstalk is that it will not be a major problem in baseband digital transmission on telephone cables up to the limits discussed in Section 4.3.

#### 4.1.2 Griffiss AFB Cable Plant

The Griffiss AFB cable system is AWG 19, AWG 22, and AWG 24 cable in 1200, 600, 200, 51, and 26 pair lead-jacketed cables. The insulation is either paper or plastic with AWG 22 paper insulation being the most common. The 5-mile and 10-mile loops used in this test are a conglomeration of all these types, since the loops were patched together with available empty lines. In addition to the mixture of cable types, another factor caused degraded performance by the cables. The factor is that parallel taps have been made off of the cables during their lifetime to allow routing of telephone connections between points on base where there are no direct cable runs. A cable may have as many as eight branches tapped off of it and there are no restrictions against branches off of branches. An attempt was made to get a complete map of our 5-mile and 10-mile cables but too much manpower would have been involved to compile and cross reference the various charts. It was decided to characterize the base cables by other means, such as measuring wideband noise, impulse noise, and the transfer function. One conclusion is that any

cables one might be allotted at Griffiss AFB will probably be a mixture of cable types along with a quantity of parallel branches. This means that the performance of any modem over the lines cannot be accurately predicted but must be measured. A general map of the 5-mile loop is shown in Figure 4.1.2-1.

#### 4.1.2.1.1 Amplitude and Phase Characteristics

Several tests were performed on the Griffiss cable plant to determine its loss and delay characteristics. Several of these were done using a Digital Signal Processor (Appendix 2) using the test setup of Figure 4.1.2.1.1-1.

Figures 4.1.2.1.1-2 and 4.1.2.1.1-3 are the measured functions for the 5-mile and 10-mile base loops taken with the Digital Signal Processor. The absolute attenuation at 1 KHz was measured at 22 db for the 5-mile loop and 37 db for the 10-mile loop. The graph becomes distorted at frequencies higher than 75 KHz because that is the cut-in frequency for the aliasing filters in the Digital Signal Processor.

The magnitude response of the 5-mile base cable shown in Figure 4.1.2.1.1-2 compares very favorably with the loss measured with a different technique. The test setup for the alternate technique is shown in Figure 4.1.2.1.1-4.

The attenuation in decibels is shown in Figure 4.1.2.1.1-5 and was calculated using:

$$\text{db of attenuation} = 20 \log_{10} \frac{V_{\text{out}}}{V_{\text{in}}}$$

The curve stops at 25 KHz because of the limited sensitivity of the rms voltmeter.

Figures 4.1.2.1.1-6 through 4.1.2.1.1-9 show plots of the transmitted power spectrum and the received power spectrum for Conditioned Diphas and BAM1. The increasing attenuation with frequency can clearly be seen. In this



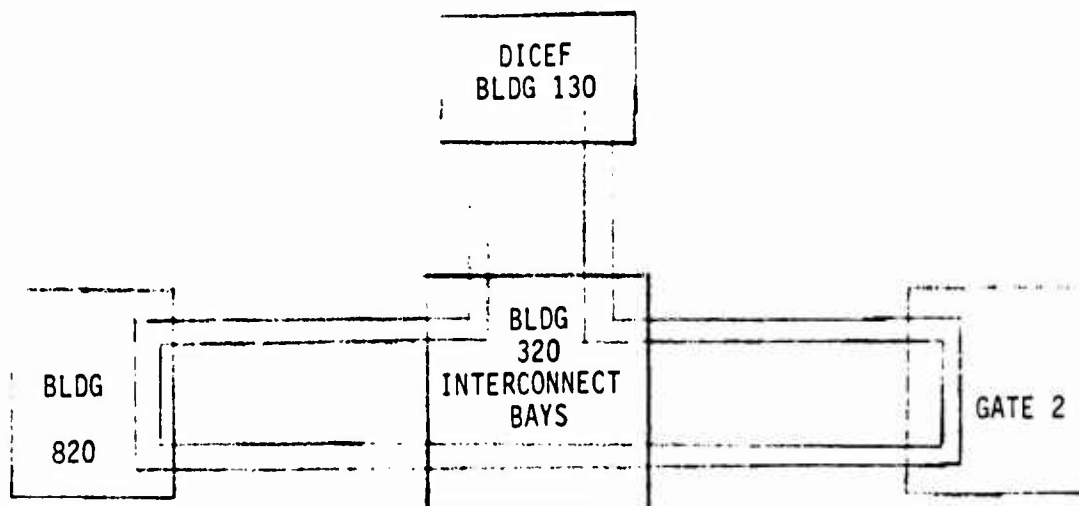


Figure 4.1.2-1  
MAP OF 5-MILE LOOP

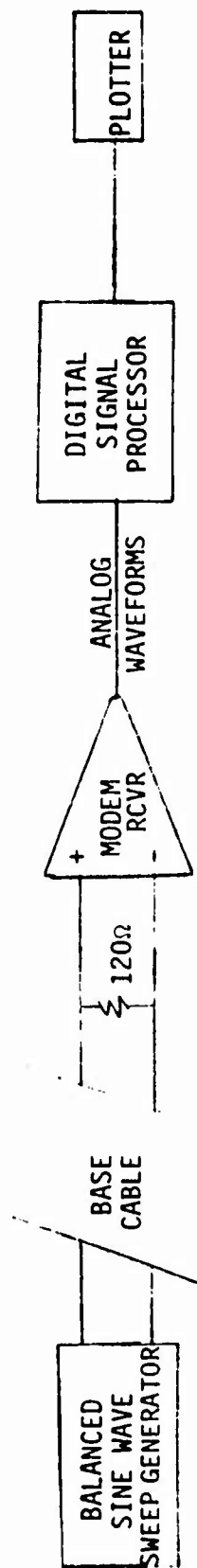


Figure 4.1.2.1.1-1  
TEST SETUP FOR TRANSFER FUNCTION MEASUREMENT

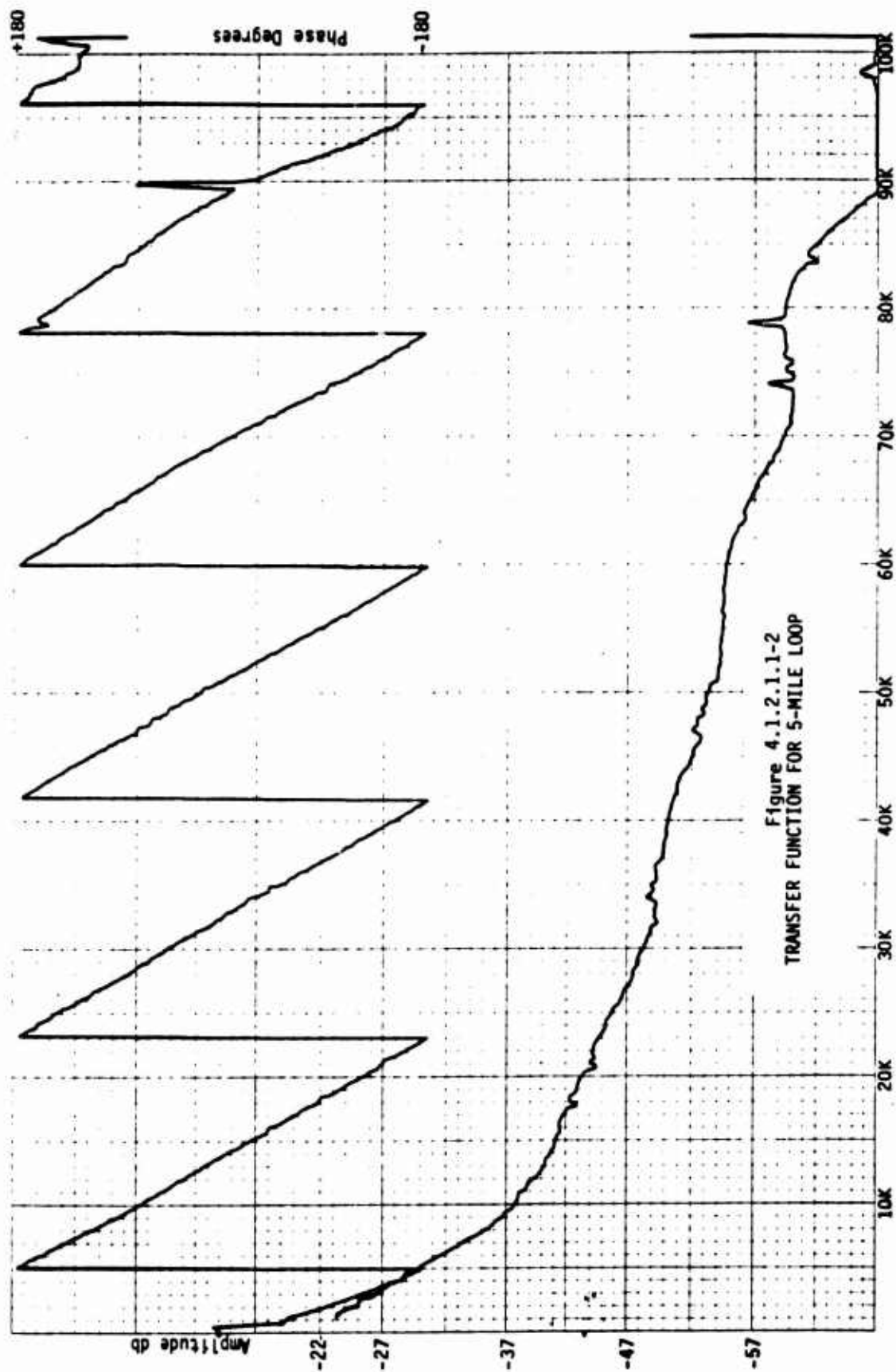
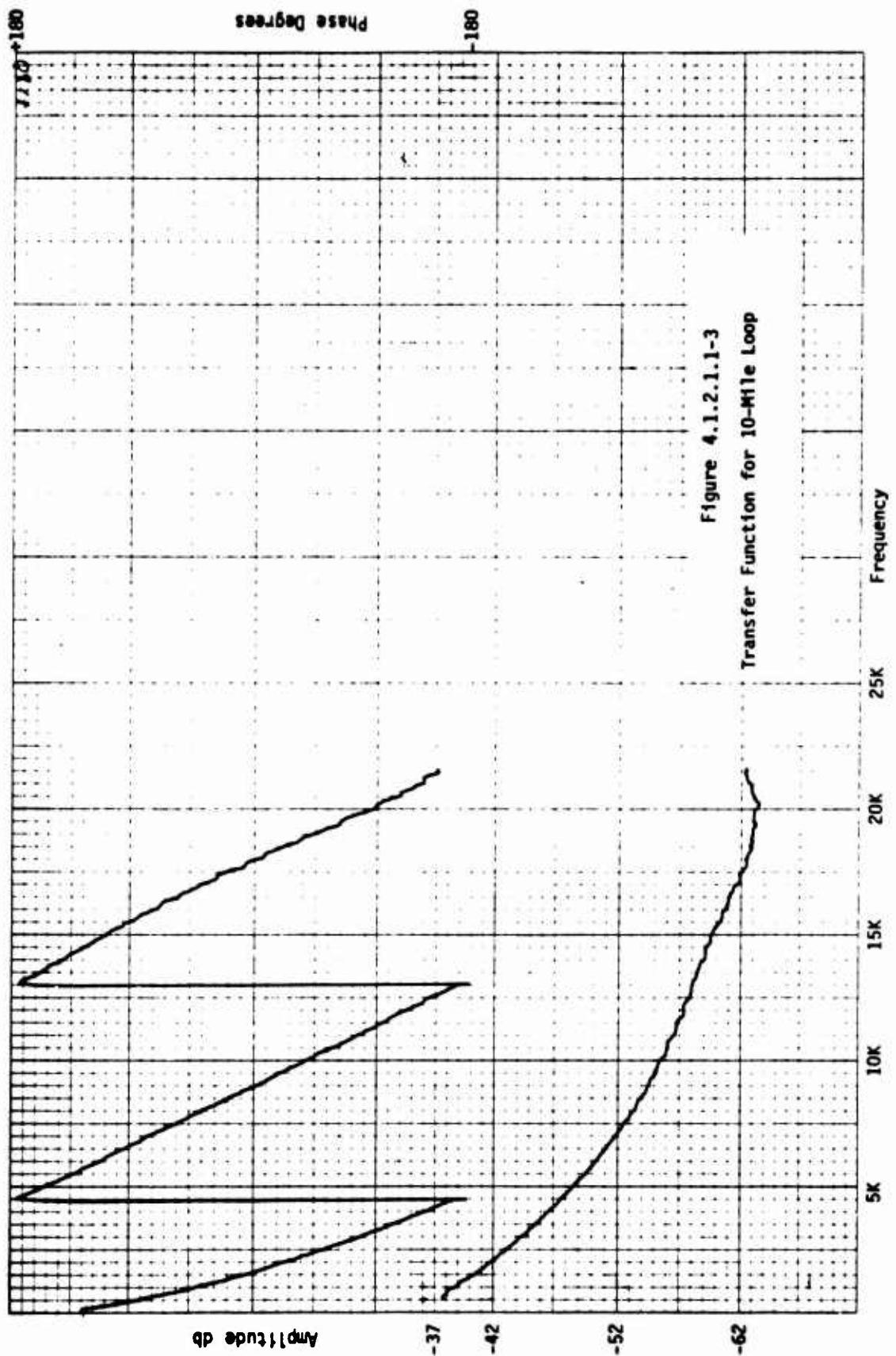


Figure 4.1.2.1.1-2  
TRANSFER FUNCTION FOR 5-MILE LOOP



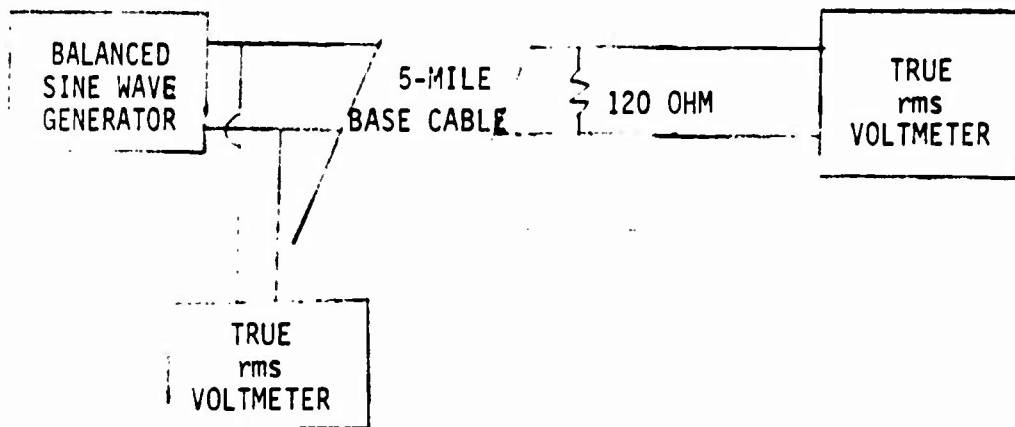
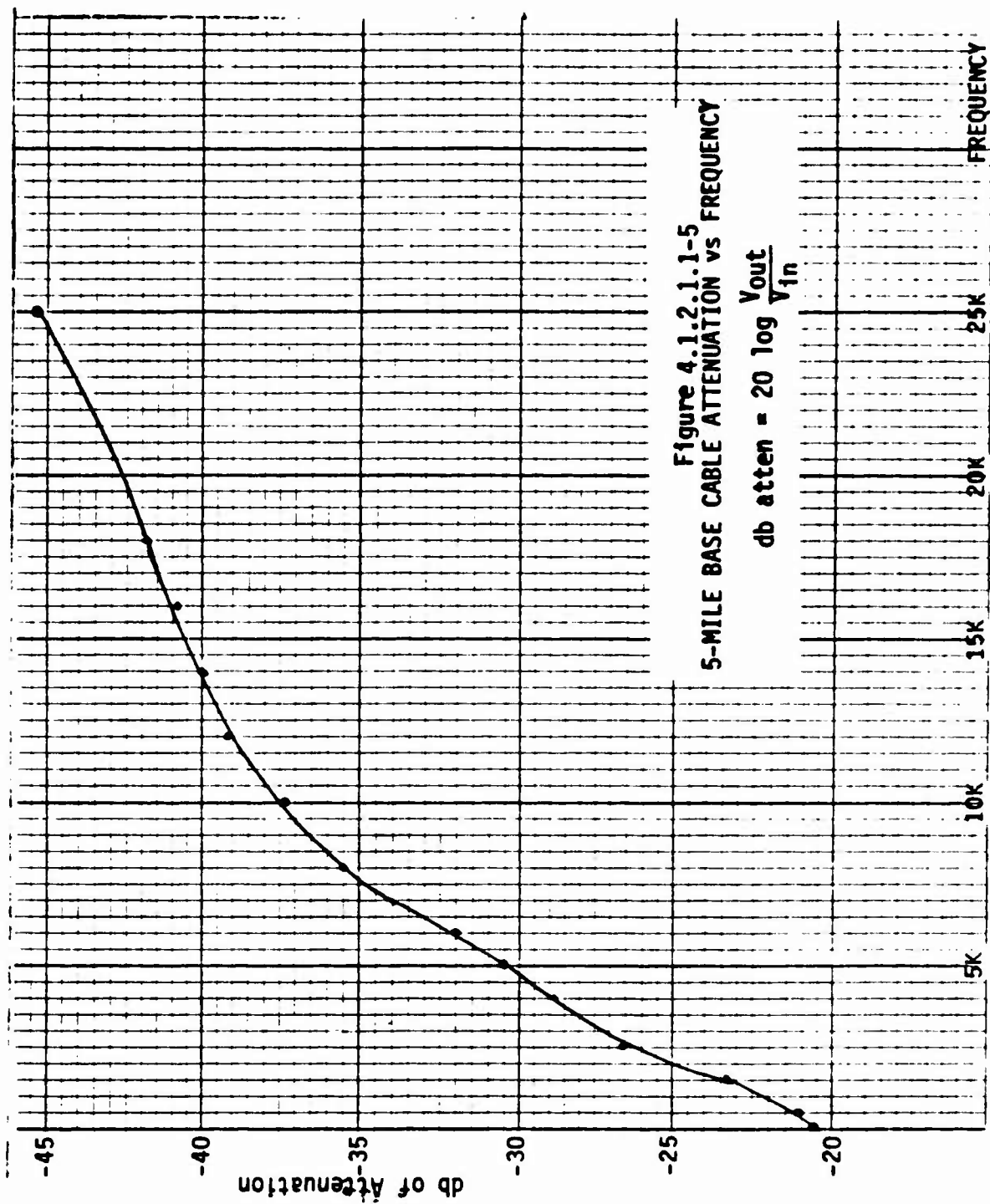
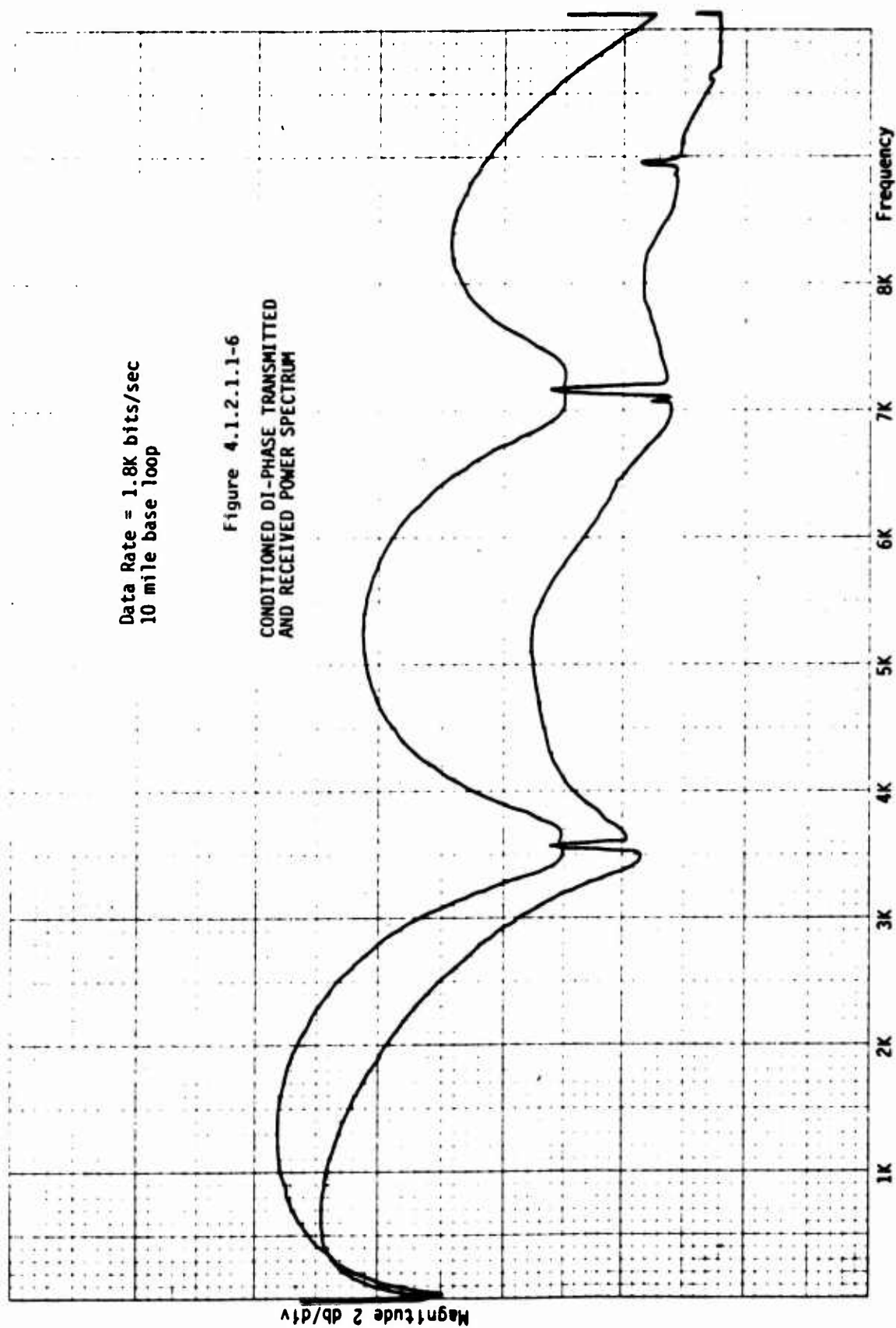
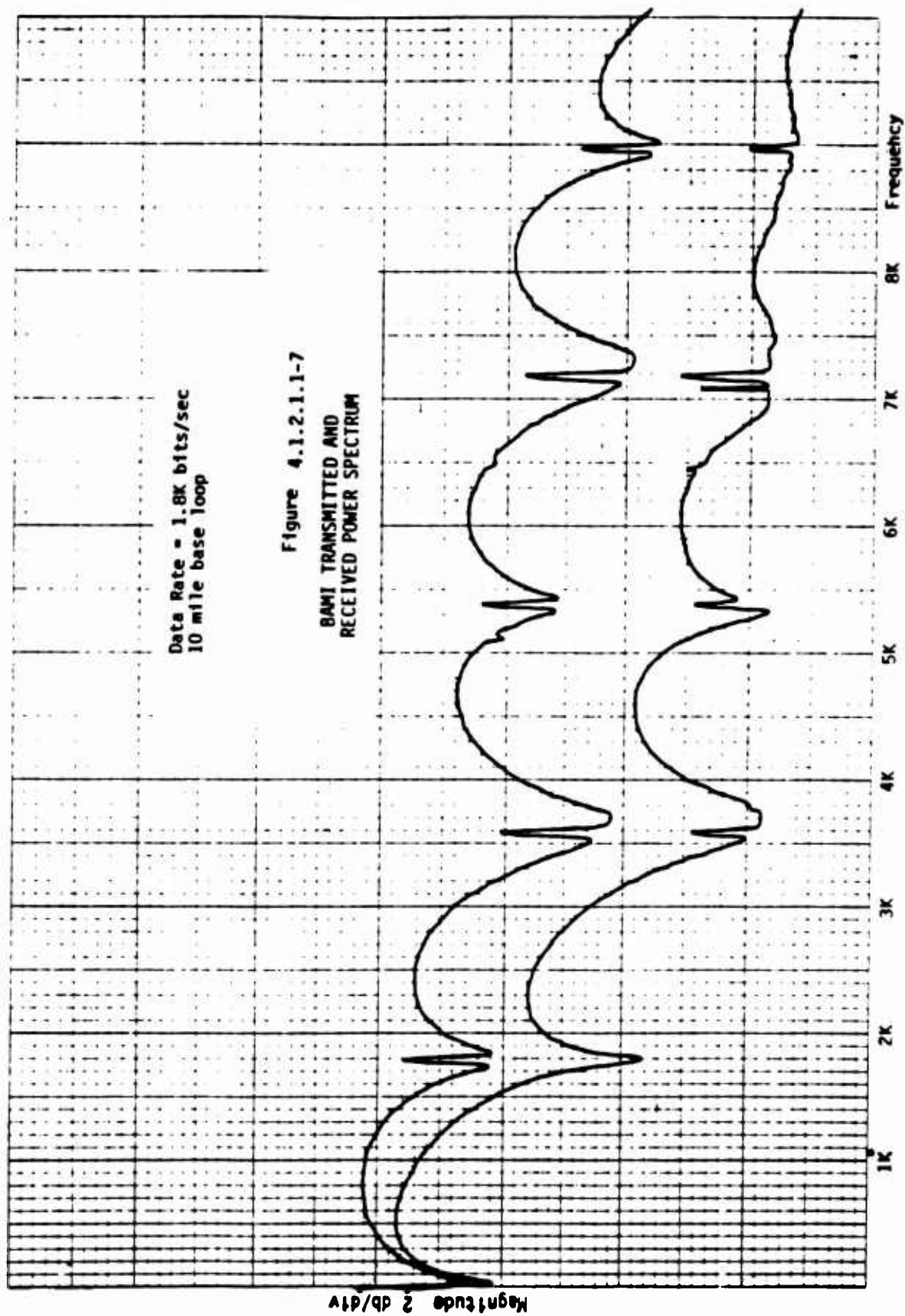


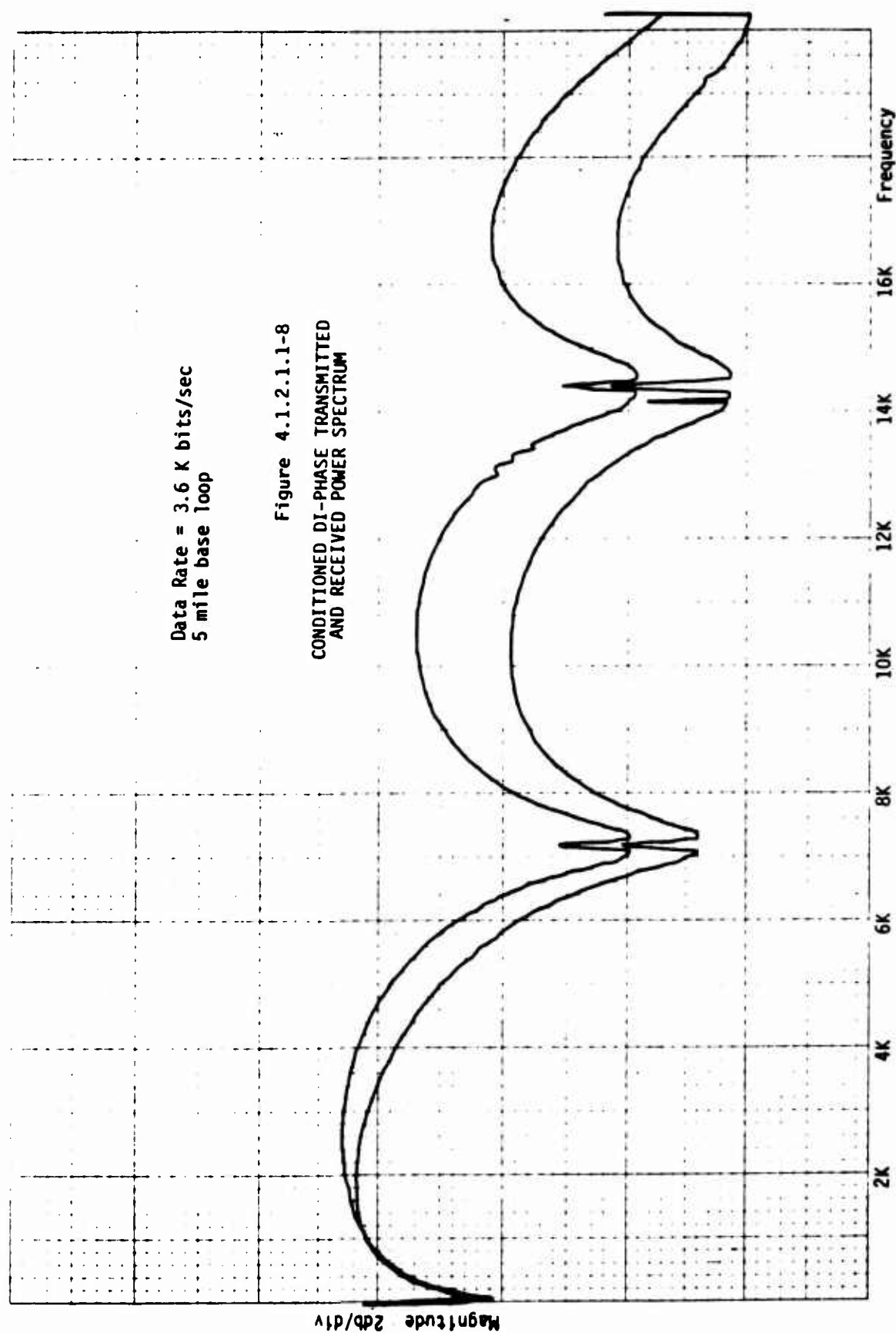
Figure 4.1.2.1.1-4  
TEST SETUP TO MEASURE FREQUENCY RESPONSE  
OF 5-MILE CABLE LOOP

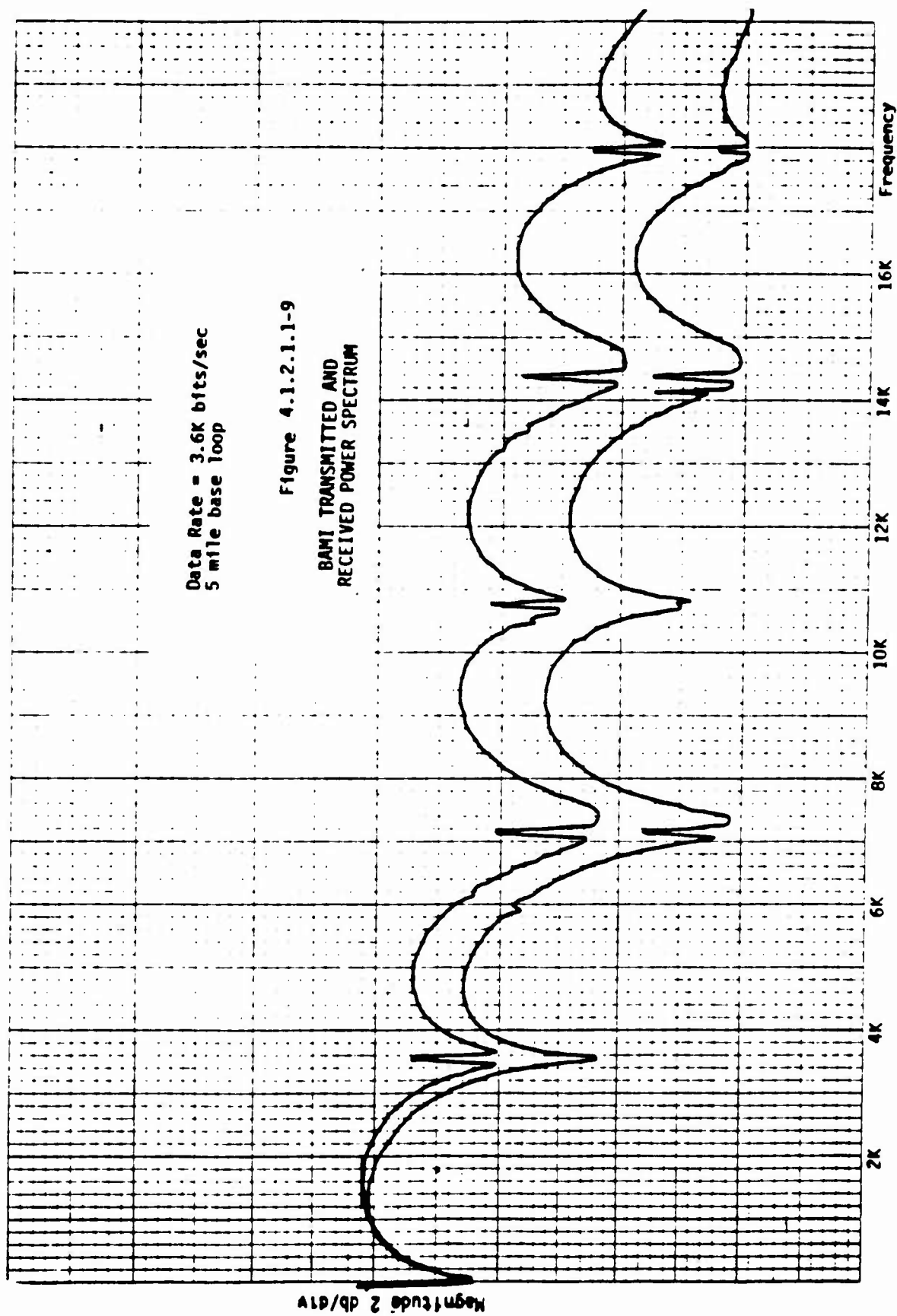












series of figures the spectra for received signals were taken with no equalizer and at the output of the balanced receiver in the modem receiver. The spikes in the nulls that appear to be discrete frequency components are in reality clock noise induced onto the signals by capacitive coupling and power bus feed-through in the breadboard hardware.

#### 4.1.2.1.2 Impulse Noise and Wideband Noise

The impulse noise was measured using the test setup shown in Figure 4.1.2.1.2-1. The impulse measuring set used was a Northeast Electronics Corporation Model TTS-58A. The set measures impulses in mutually exclusive ranges set by dials on the instrument. The impulses are measured in terms of dbrn where 0 dbrn is -90 dbm (1 pico watt). However, we are interested in measuring the impulses in terms of peak values and not power since the CD $\phi$  and BAM I devices sample at a given time instant and not after a signal integration period as used in some signalling techniques. The Model TTS-58A defines 90 dbrn as .775 volts peak into 600 ohms. It treats peak values as rms values and with the appropriate scale conversions can be calibrated to measure peak values of impulses. The base lines were terminated in 135 ohms instead of 600 ohms since the impedance of the cables is closer to 135 ohms than 600 ohms for pulse transmission. The final conversion factor from dbrn as defined on the TTS-58A to peak impulse volts is:

$$\begin{aligned} \text{Peak impulse volts} &= \sqrt{\frac{(.775)^2}{600\Omega} \cdot 135\Omega} \cdot 10\left(-\frac{90}{20}\right) \cdot 10\left(\frac{K\text{dbrn}}{20}\right) \\ &= 1.1625 \times 10^{-5} \cdot 10\left(\frac{K\text{dbrn}}{20}\right) \end{aligned}$$

where Kdbrn is the dbrn setting on the TTS-58A, the square root factor is for the impedance difference, and the  $10\left(-\frac{90}{20}\right)$  factor changes the reference level to -90 decibels.

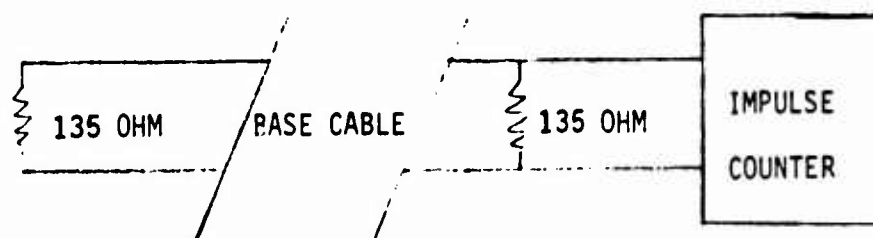


Figure 4.1.2.1.2-1  
TEST CONFIGURATION FOR  
IMPULSE NOISE MEASUREMENT

The data shown in Table 4.1.2.1.2-1 were taken with the three ranges on the TTS-58A set as shown below along with the equivalent peak impulse volts calculated with the foregoing formula.

A range = 20 dbrn to 30 dbrn (116.25  $\mu$ v to 367.61  $\mu$ v)

B range = 30 dbrn to 40 dbrn (367.61  $\mu$ v to 1.16 mv)

C range = above 40 dbrn (above 1.16 mv)

The runs listed in Table 4.1.2.1.2-1 each covered a 60 minute period. The rates shown in the table are not completely accurate since the TTS-58A has a bandpass filter characteristic on the input. The bandpass is from 3 KHz to 12 KHz. From observation of impulses on the oscilloscope and analysis with the Digital Signal Processor it is estimated that approximately 50% of the energy in an impulse is detected by the TTS-58A. Thus the impulse level for a given rate in Table 4.1.2.1.2-1 is really higher than the calculated value for the A, B, and C ranges. An experiment to determine the error introduced indicated that for impulses of 50  $\mu$ s duration the voltages were off by about a factor of 2 from the calculated ones.

If it is assumed that impulses are the predominant cause of errors, these impulse rates can be used to estimate an upper bound for the error rates as follows: practical implementations of CD $\phi$  and BAMI modems use eye openings on the order of tens of millivolts, therefore, only impulses with amplitudes in that range can cause errors. This corresponds to C range in Table 4.1.2.1.2-1, impulses greater than 1.16 mv. If we assume that each impulse causes an error we can establish a relation between bit rate and bit error rate given an impulse rate as follows:

$$\text{Bit Error Rate} = \frac{\text{Impulse Rate}}{\text{Bit Rate}}$$

Run #	A RANGE	B RANGE	C RANGE
1	9005	4290	442
2	7404	3059	224
3	8366	4363	236
4	9698	4589	298
5	7494	3895	201
6	8647	4240	246
7	9175	4103	247
8	8520	3824	220
9	9740	4977	257
10	7094	2170	177
11	10256	4744	356
Average Impulses Per Second	2.4	1.1	.073

Table 4.1.2.1.2-1  
IMPULSE RATES ON GRIFFISS AFB CABLE

A plot of this using an impulse rate of  $7.3 \times 10^{-2}$  impulses/sec (the C range average) is shown in Figure 4.1.2.1.2-2. Since not all impulses will cause an error (they are not of sufficient magnitude or do not occur at the sampling instant) this curve represents an upper bound neglecting other effects.

Other effects not considered in this upper bound are errors caused by timing jitter on the sampling signal and the width of the impulse. If the impulse spans more than one bit interval it may cause more than one error. These effects would have progressively more severe degradation on the signal as the data frequency is increased.

During the tests on the breadboard modems the bit error rates generally conformed to the bound shown in Figure 4.1.2.1.2-2 with the majority of the exceptions occurring at the higher frequencies.

Wideband noise was measured at typically 0.8 mv rms.

#### 4.2 Performance of Experimental Hardware

Breadboard models were built for the BAMI and CD $\phi$  modems and tested over the DICEF laboratory cable and the 5-mile and 10-mile base loops. The tests performed for this report were designed to study the effects of ISI, attenuation, and noise on BAMI and CD $\phi$ . Considerations of timing extraction from the waveforms are not covered here. The receiver timing was synchronized directly to the transmitter timing with an appropriate delay.

The general test setup is shown in Figure 4.2-1. The wideband noise generator was not used when data was being taken over the cables. Its function in that case was in adjusting the threshold detectors and clock delay to optimum values before data taking commenced. The other function for the

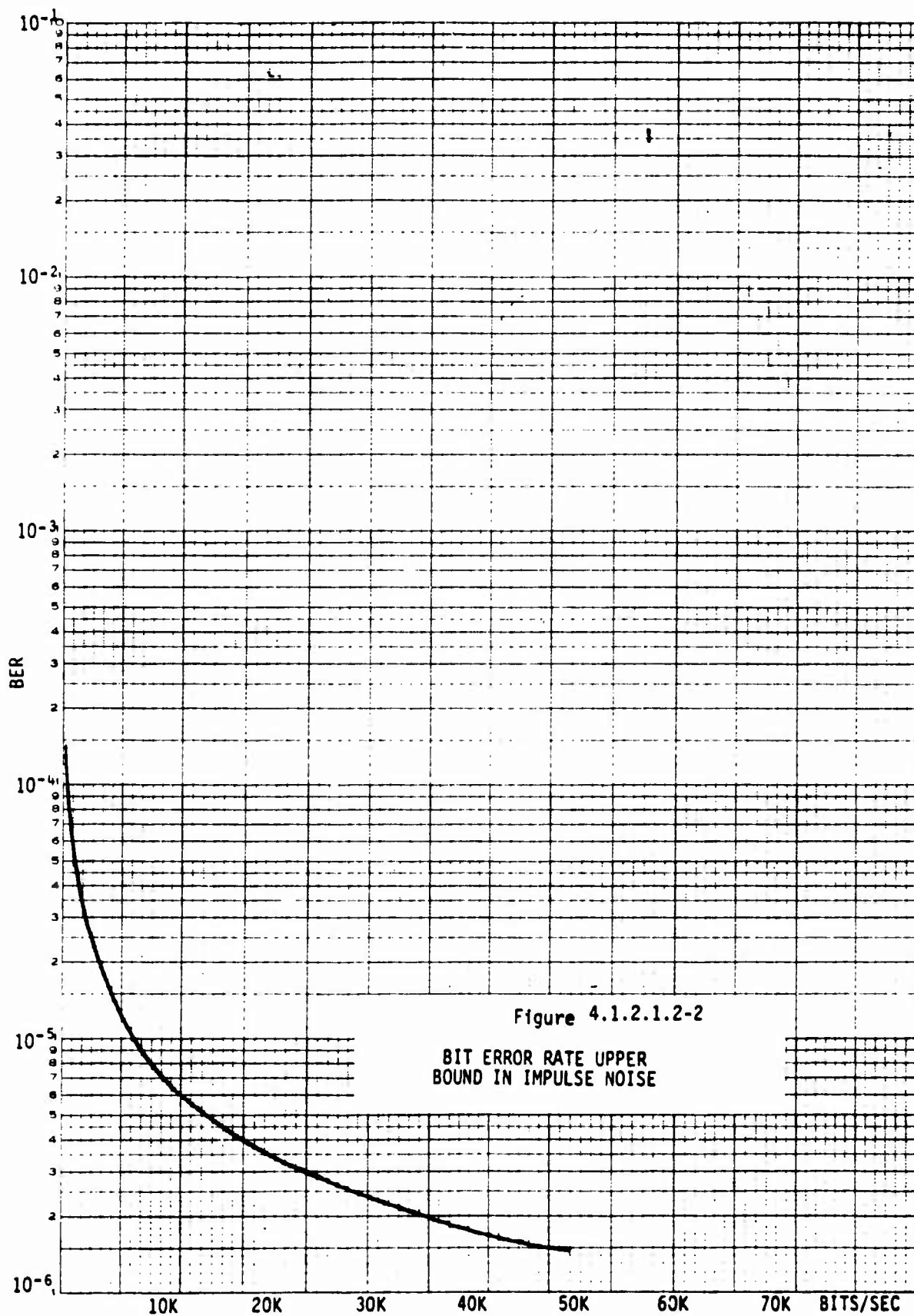


Figure 4.1.2.1.2-2

BIT ERROR RATE UPPER  
BOUND IN IMPULSE NOISE



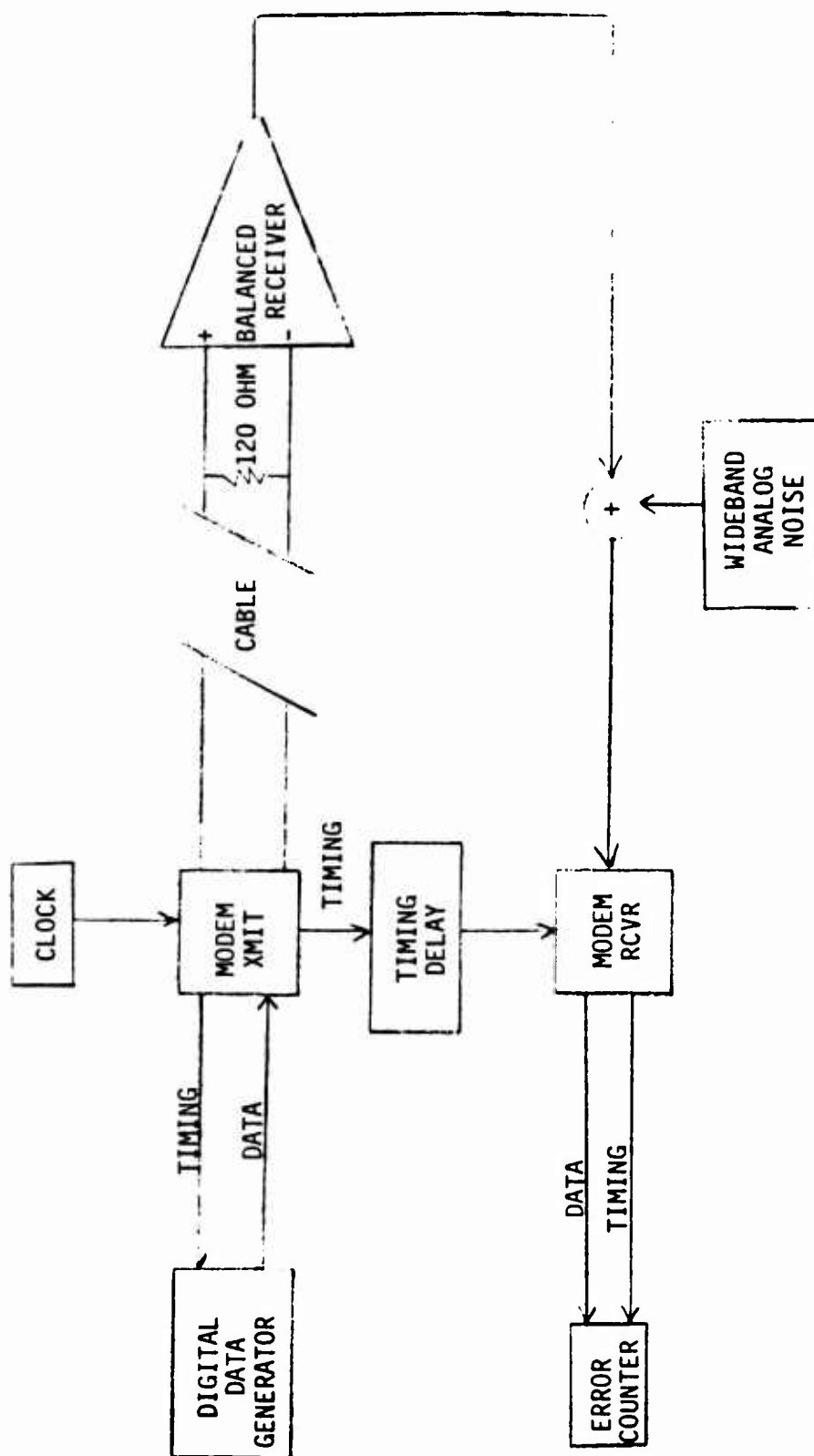


Figure 4.2-1  
TEST SETUP FOR TESTING BREADBOARD HARDWARE

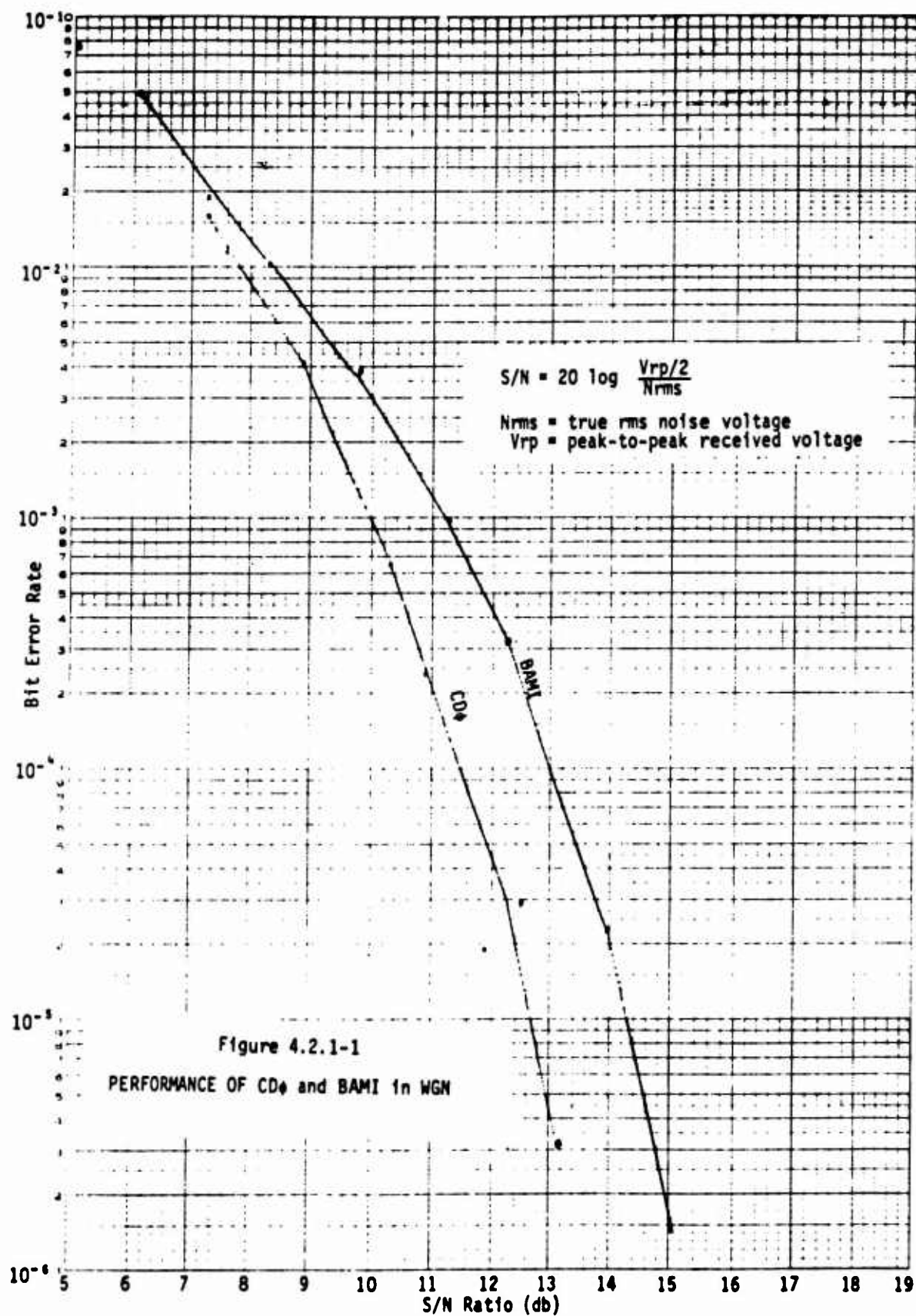
wideband noise generator was to get performance of the hardware as a function of signal-to-noise ratio without intersymbol interference. For those tests the wideband noise generator amplitude was varied to change the S/N ratio effectively at the receiver input, and an attenuator substituted for the cables. It should be noted that with this setup the wideband noise was added as differential noise and not common mode noise. This is desirable since with current technology balanced receivers have a common mode rejection ratio of 60 db or more. It is the differential noise due to cable unbalance that units in the field will have to contend with; therefore the breadboard was subjected to differential noise and not common mode noise.

The line drivers for CD $\phi$  and BAMI were built to generate the same peak-to-peak voltages which were 4 Vpp. This value was picked because it was large enough to give reasonable signal levels at the receive end of the base loops and small enough that other users of the base cables were not unduly affected by crosstalk noise. Since the peak-to-peak voltage values were the same, the power transmitted in the BAMI waveform was 6 db less than the CD $\phi$  waveform: 3 db because BAMI is return-to-zero (RZ) and, assuming random data, another 3 db since no energy is transmitted for space data bits.

#### 4.2.1 Performance in White Gaussian Noise (WGN).

For these tests the cable was replaced with an attenuator, and the WGN generator (500 KHz bandwidth) output was varied to change the S/N ratio. A true rms voltmeter was used to measure the rms value of the noise and an oscilloscope was used to measure the amplitude of the signal without noise

This setup, with the cable replaced by an attenuator, eliminates intersymbol interference (ISI). The voltage between the received signal without noise and the sampling threshold will be the same for all samples of a given



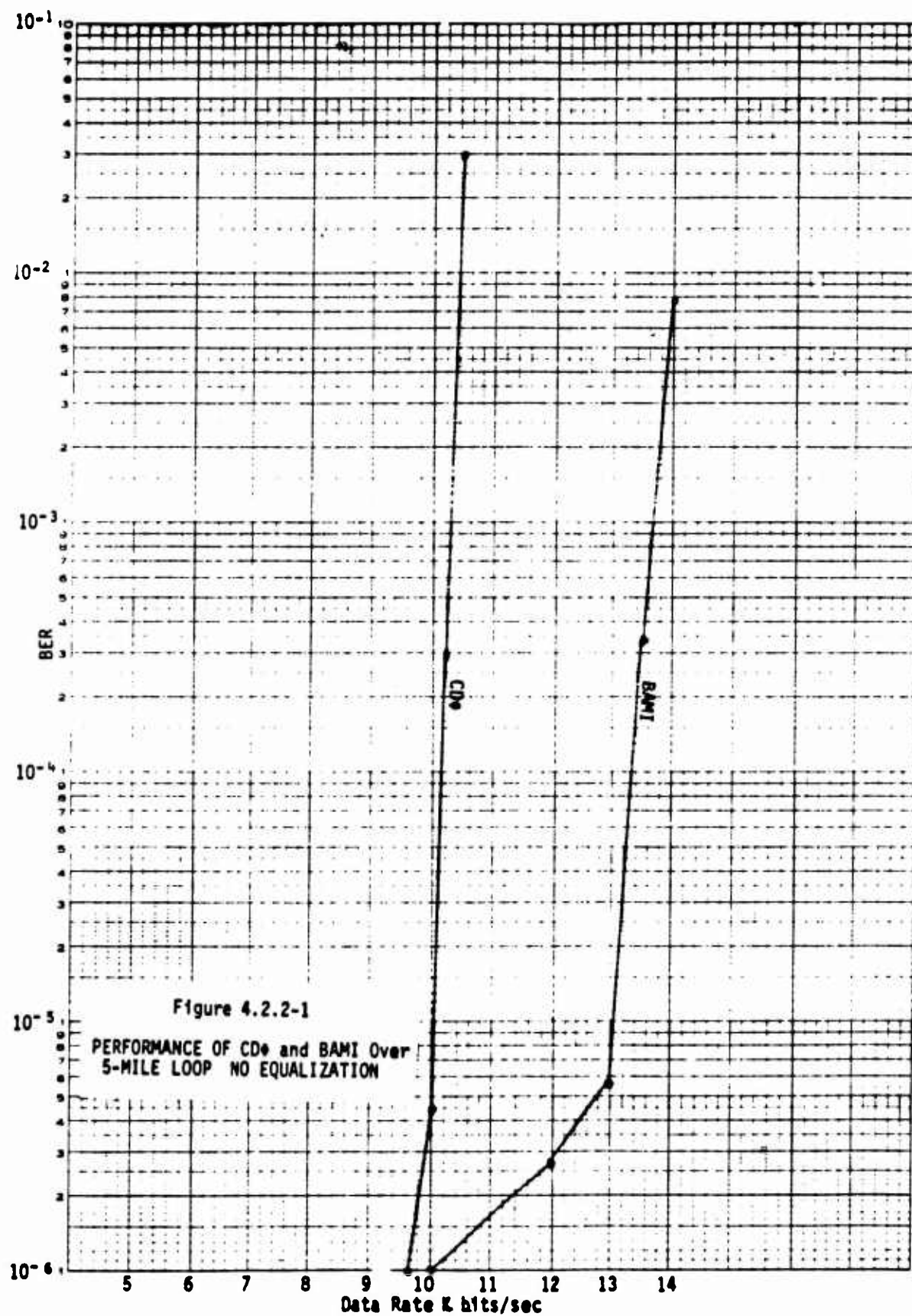
waveform. However BAMI is a three level waveform while  $CD\phi$  is only a two level waveform, therefore, the voltage between the received signal and the sampling threshold will be twice as large for  $CD\phi$  as for BAMI if the peak voltages for both waveforms are the same. See Section 3.1.1 and 3.2.2 for a derivation of the calculated curves for  $CD\phi$  and BAMI.

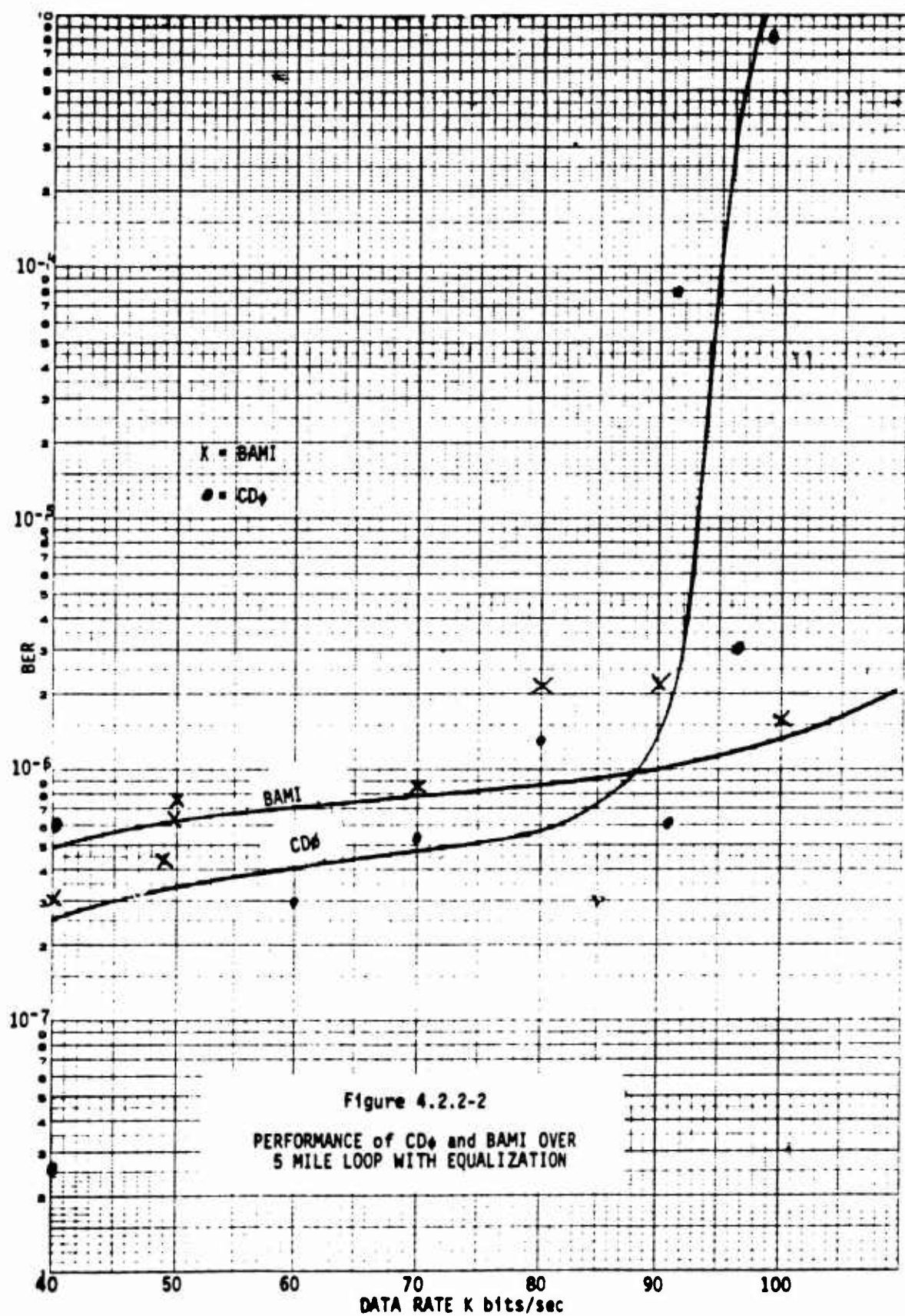
The experimental results are shown in Figure 4.2.1-1.  $CD\phi$  outperformed BAMI by about 2 db in the lower BER region. These curves represent the case where the BAMI amplitude is twice that for  $CD\phi$ .

#### 4.2.2 Performance on 5-Mile Base Loop.

Both waveforms were tested on the 5-mile loop at various data rates. They were tested with and without equalization. Figure 4.2.2-1 gives the results for no equalization. Both waveforms exhibited a very sharp increase in error rate as their eye patterns began to close.  $CD\phi$  broke down around 10 K Bits/Sec and BAMI around 13 K Bits/Sec. This can be related to the discussion in Section 3.4 concerning the relative attenuation vs data rate for  $CD\phi$  and BAMI. Figure 3.4-2 indicates 30 db of attenuation at 10 K Bits/Sec data rate for  $CD\phi$  while BAMI does not suffer this much attenuation until 15 K Bits/Sec. Overall signal attenuation is not the only factor to be considered in comparing  $CD\phi$  and BAMI performance because their threshold margins are different with  $CD\phi$  having a larger threshold margin. The result is that BAMI does not break down when it reaches the same attenuation as  $CD\phi$  but before that point, 13 K Bits/Sec in this case.

The waveforms were tested over the 5-mile loop with equalization and the results shown in Figure 4.2.2-2. The equalizers used were very simple and







better ones could be manufactured using careful design which would yield better performance than that showed in Figure 4.2.2-2. The equalization tests were performed for two reasons; first, to get an idea of how much improvement could be expected, and second to check the difference in performance between CD $\phi$  and BAMI with some of the ISI removed. As noted previously CD $\phi$  has higher frequency energy than BAMI, therefore ISI will degrade CD $\phi$  more. Equalization to remove some of the ISI should help CD $\phi$  more than BAMI and tend to bring their performance closer together.

Figure 4.2.2-2 shows that the error rates tended to be fairly similar between CD $\phi$  and BAMI and degraded more slowly than they did without equalization. The difference in performance seldom differed by more than a factor of two. The data points for a given waveform exhibited a relatively large variation because with the low error rates long runs were required to generate the data points, typically 200 megabits, and the base phone lines do not exhibit much stationarity. That is, occasionally they will have a large number of strong impulses and at other times they will be relatively quiet. This sort of activity tends to spread the error rates so a smooth curve cannot be drawn. It was not practical to have runs long enough to insure a good number of noisy and quiet periods for each data point since each run would have to be hours long. A good example of this spread in data points is the two points at 96 K Bits/Sec for CD $\phi$  in Figure 4.2.2-2. The low error rate point was taken on a Sunday afternoon when activity on the base phone system was low. The high-BER point was done on a normal workday. The difference will not be as great as this in general because the CD $\phi$  signal was nearing its upper limit (eye almost closed) at 96 K Bits/Sec. The CD $\phi$  eye closed at about 100 KHz for this test. The BAMI eye pattern was mostly closed at about

150 K Bits/Sec. CD $\phi$  has a slightly better performance than BAMI until its eye pattern closes but BAMI continued to operate after CD $\phi$  did not.

An important point to be made here is that the BER performance is less affected less by the choice of waveform than by activity on the telephone network. An example is the two data points at 40 K Bits/Sec for CD $\phi$  in Figure 4.2.2-2. The  $2.6 \times 10^{-8}$  point was taken on a Sunday and the  $6.0 \times 10^{-6}$  point on a Monday. This order of magnitude difference is much more than the difference between the two waveforms given equal operating environments.

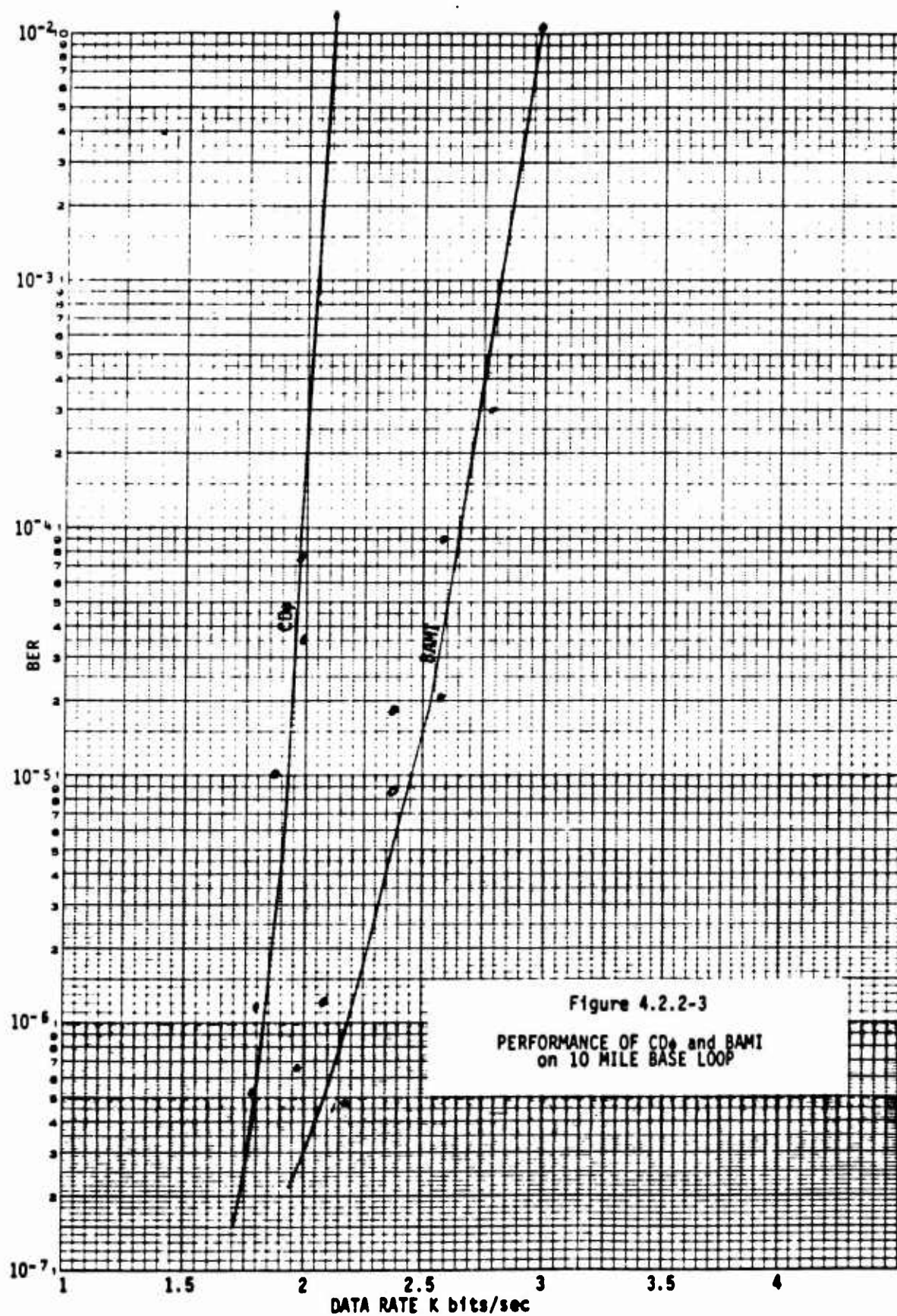
The waveforms were tested without equalization on the 10-mile base loop. The results are displayed in Figure 4.2.2-3. The threshold nature of CD $\phi$  and BAMI transmission is very evident here. Both schemes had a very low error rate at around 1.5 K Bits/Sec and a very high rate around 3 K Bits/Sec. BAMI again outperformed CD $\phi$ . At the lower data rates in this test the performances tend to be closer together. This is because there is less ISI as the data rate is decreased and CD $\phi$  is more vulnerable to ISI distortion than BAMI.

#### 4.2.3 Error Occurrence Analysis

The DICEF laboratory has the capability to completely characterize the occurrences of errors in a digital data stream. It is done using the test configuration shown in Figure 4.2.3-1.

The ADX 9303 computer is the data source and data sink. It generates a pseudorandom binary data stream, sends it to the modem and channel combination, receives the data, determines which bits are in error, and logs the error position data on an output magnetic tape. This tape is then processed on RADC's Honeywell 6180 computer to produce the graphs shown in this section.





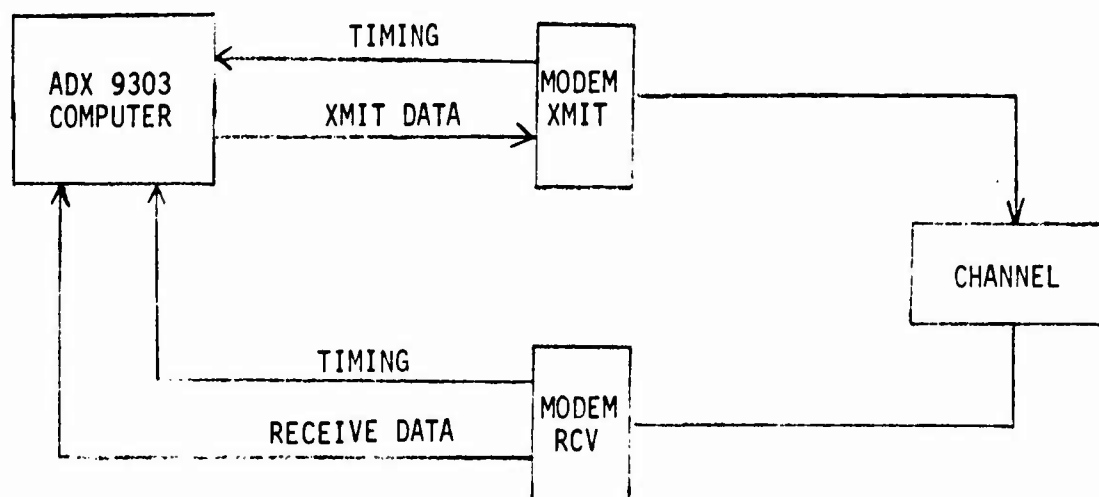


Figure 4.2.3-1  
TEST CONFIGURATION FOR  
ERROR PATTERN CHARACTERIZATION

The graphs give more information than a simple Bit Error Rate (BER) calculation. From the graphs one can determine such things as throughput vs block length, whether errors tend to occur in bursts or singly, how long bursts are, the probability of having a given number of good bits before an error occurs, etc. These tests were performed over the 5 and 10 mile base loops, with and without equalization.

Figure 4.2.3-2 is the probability distribution and density for CD $\phi$  operating over the 5-mile loop at 8.5 K Bits/Sec with no equalization. From the cumulative part of the graph (the plot of "C's") it can be seen that 50% of the time more than 25 K bits separated the occurrence of errors and 14% of the time errors occurred in succession (error free interval = 0.0). Another way of looking at this is that if you have an error there is a 14% chance it will be a multiple bit error. From the cumulative plot we can see that the probability there will be less than 4 good bits after the occurrence of an error until another error occurs is 23%. At an error free interval (EFI) of 1000 the probability of having less than 1000 good bits between errors is only up to 33%, or saying it another way the probability of having more than 1000 good bits in succession is 67%.

From the probability density portion of the graph it can clearly be seen that when an error occurs it generally falls into two categories. Either it is relatively close to another error (less than 5 bits away) or relatively far from an error (10 K bits or more), with half of the EFI being 25 K bits or more in length.

This graph can be used to justify the assumption that the main error causing mechanism is impulse noise. An impulse will cause either one error or multiple errors. Wideband noise on the other hand is not confined in short

TEST DURATION (min):

DATA RATE: 8.5

CONDITIONS: 8.5K DATA

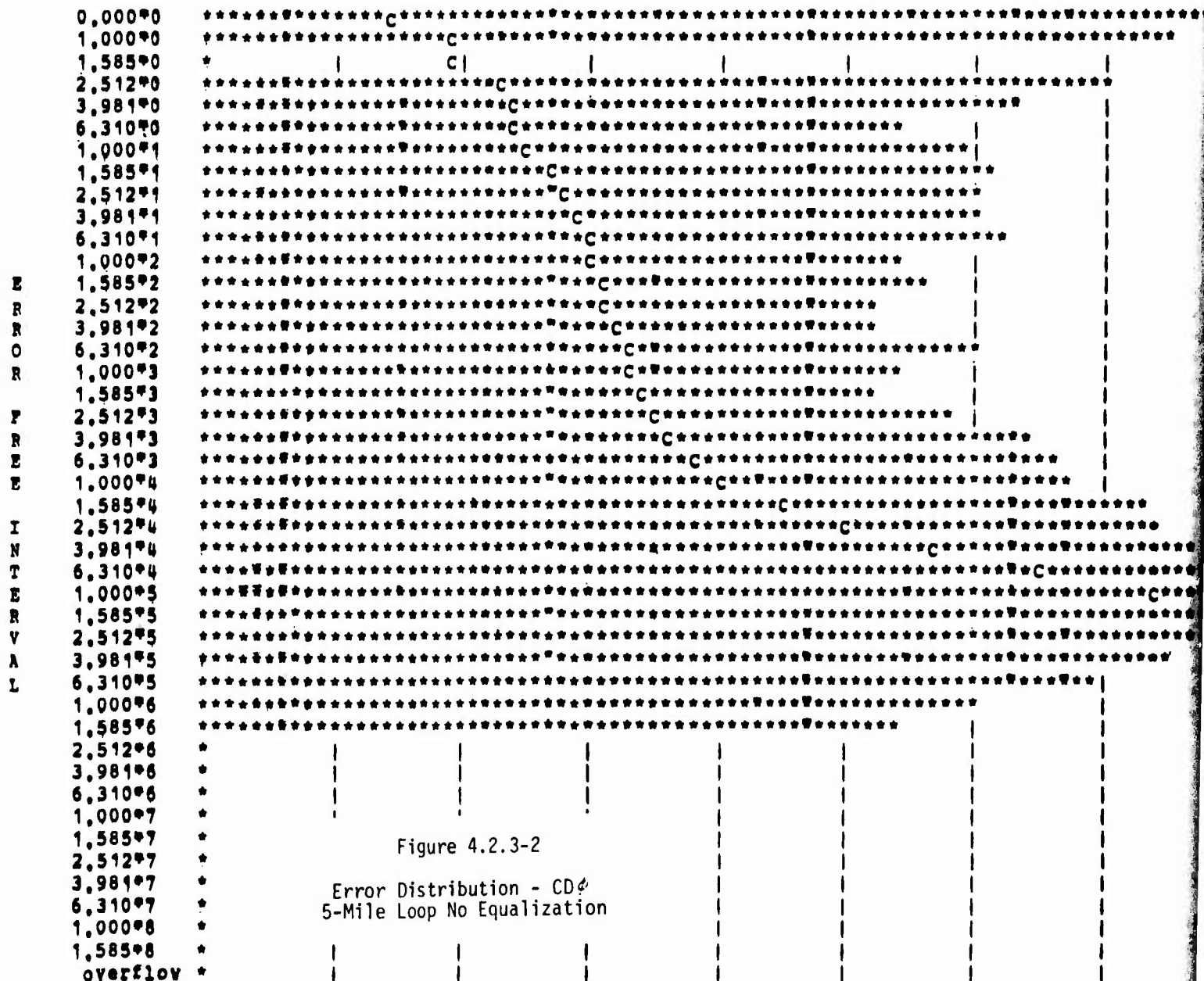
$$\text{Mean} = 1.086 \pm 05$$

Std Dev=1.987+05

```

,          bit_error_rate= 9.19321576e-006 number_of_bits_transmitted= 8.39749680e+007;

```



* coordinate	1,00-05	3,16-05	1,00-04	3,16-04	1,00-03	3,16-03	1,00-02	3,16-02
C coordinate	0%	10%	20%	30%	40%	50%	60%	70%

OP' RATOR: ELLER  
TEST ITEM:  
CONDITIONS: 8.5K DATA

TEST NUMBER: 001 AFSC RADC DICEF  
CHANNEL: 5 MILE BASE LINE  
LINE#: 140

```

plot of ERROR FREE INTERVAL          Mean=1.086+05  Var=3.949+10  Sample Size= 773
plot of ERROR FREE INTERVAL          Std Dev=1.987+05  SD/mean=1.829+0
9321576e-006 number_of_bits_transmitted= 8.39749680e+007;

```

[illegible]

Figure 4.2.3-2

**Distribution - CD<sup>4</sup>  
Pop No Equalization**

1,00-04	3,16-04	1,00-03	3,16-03	1,00-02	3,16-02	1,00-01	3,16-01	1,00+00
20%	30%	40%	50%	60%	70%	80%	90%	100%

71

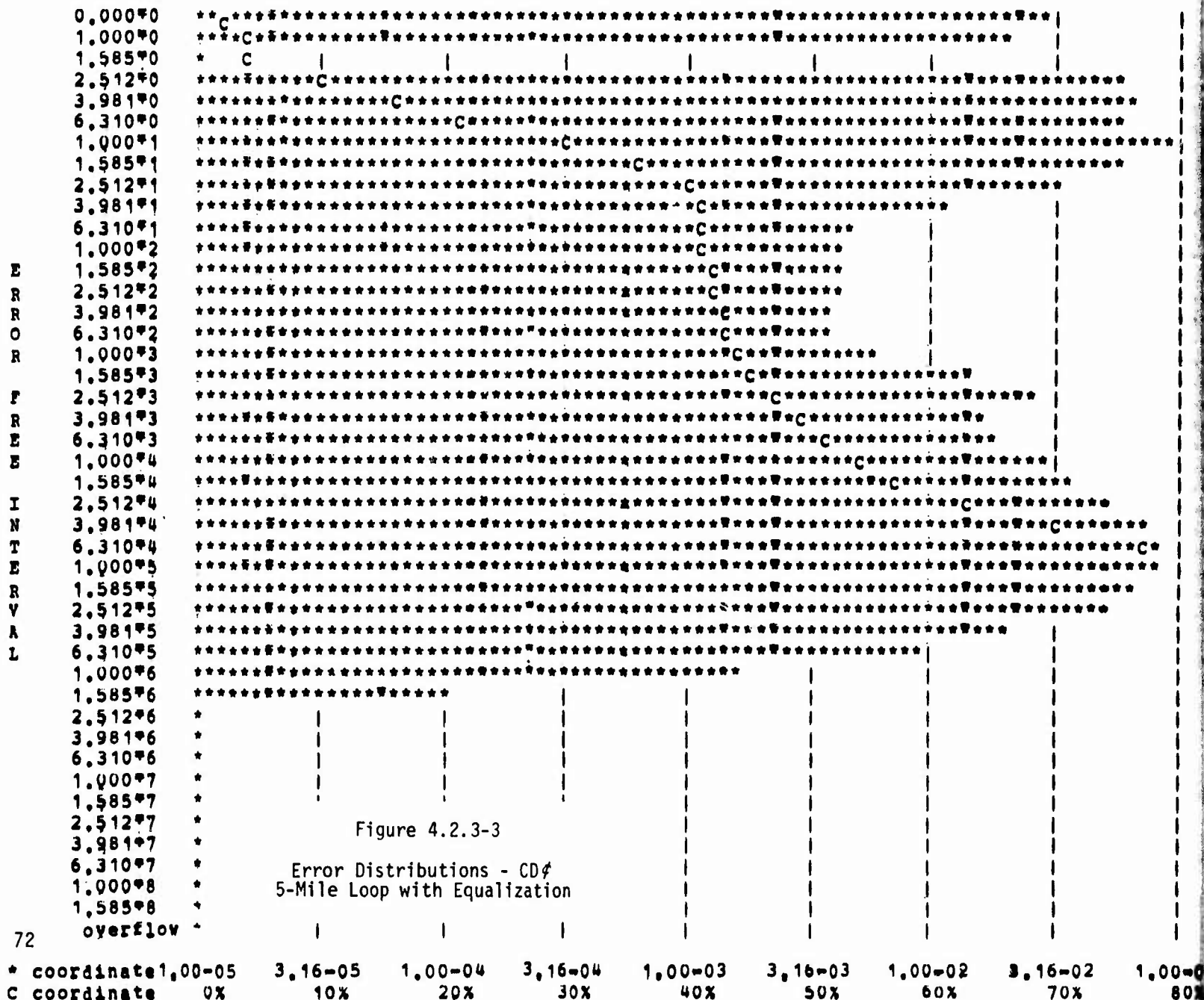
2

PROJECT; DCA LOOP TEST  
DATE; 3 MARCH 1976 HOUR: 1430  
ROUTE;

OPERATOR: ELLER  
TEST ITEM:  
CONDITIONS: 60.0K DATA

TEST DURATION (min):  
DATA RATE: 60.0

```
* represents a log probability plot of ERROR FREE INTERVAL      Mean=5.532+04   Var=
C represents a linear cumulative plot of ERROR FREE INTERVAL    Std Dev=1.050+05
.      bit_error_rate= 1.80730769e-005 number_of_bits_transmitted= 5.65703336e+00;
```



TEST NUMBER: 002 AFSC RADC DICEP

CHANNEL: 5 MILE BASE LINE C 19

LINE#: 140

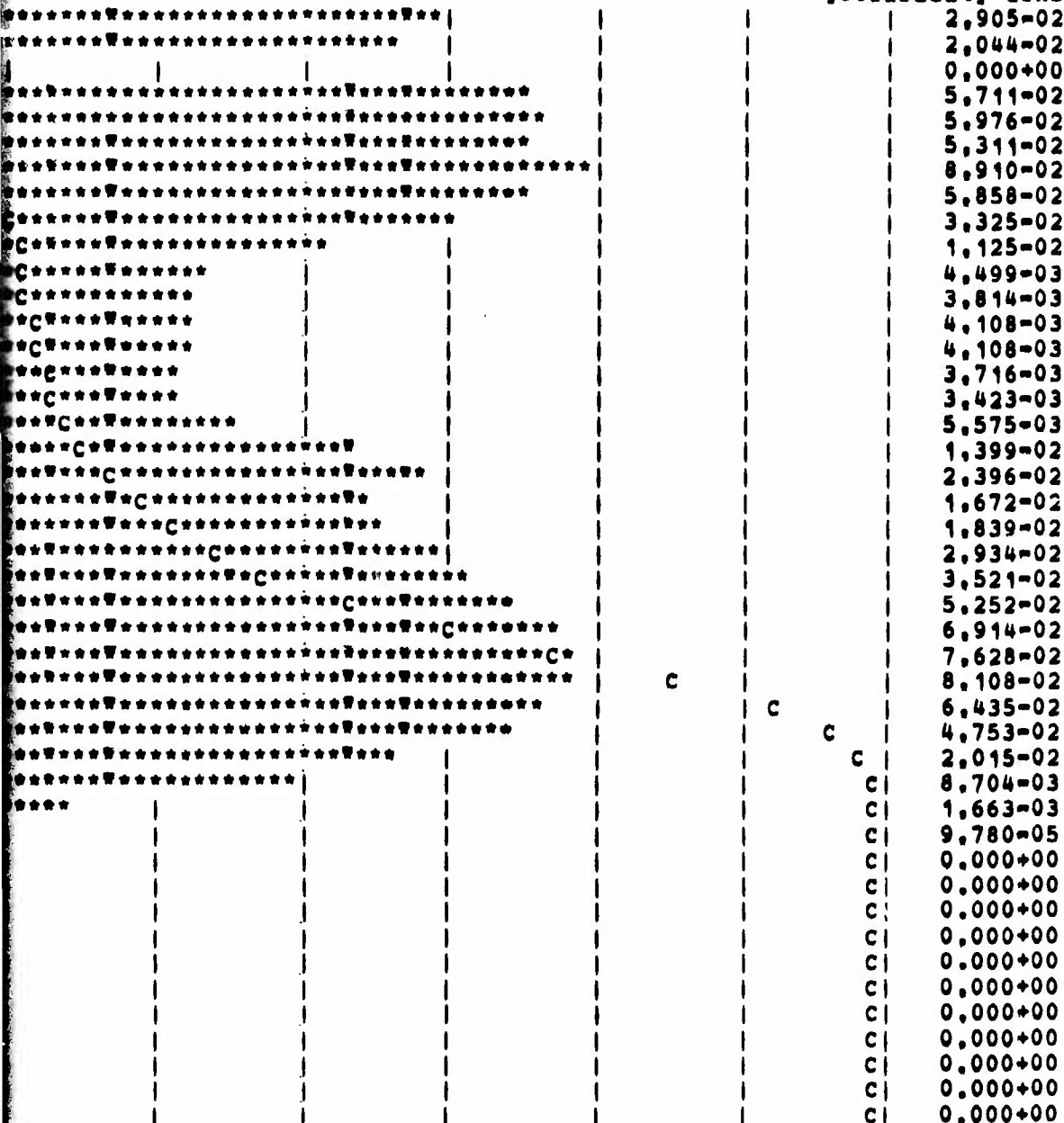
## DATA

```

VAL          Mean=5,532+04  Var=1,102+10  Sample size= 10225
ERRVAL       Std Dev=1,050+05  SD/mean=1,898+0
bits_transmitted= 5,65703336e+00H;

```

probability density



03	3,16-03	1,00-02	3,16-02	1,00-01	3,16-01	1,00+00
0%	50%	60%	70%	80%	90%	100%



time intervals as is impulse noise and it affects each and every bit's probability of being in error by the same amount. This would cause the EFI to trend towards one peak with a wide base, not two as shown in Figure 4.2.3-2. Impulse noise causes multiple errors which cause the large value at EFI less than four. The other large value occurs at EFI around 100 K bits. A connection between the latter peak and impulse noise can be established as follows: From Table 4.1.2.1.2-1 we note that the average rate of occurrence of impulse large enough to cause errors is .073 impulses/sec. This is one impulse every 13.7 seconds on the average. At a data rate of 8.5 KHz (rate used in Figure 4.2.3-2) 116.5 K bits are transmitted on the average, between impulses. This point is very near the center of the peak in the graph, thus it is concluded that this peak and the average impulse rate are closely related.

The EFI for CD $\phi$  operating over the 5-mile loop at 60 K Bits/Sec with equalization is shown in Figure 4.2.3-3. Again there are two predominant peaks. The one at the lower end of the EFI scale has been shifted right about 40 bits. This is due to the data rate being higher (a factor of 7). At a higher data rate a disturbance that spanned 5 bits at 8.5 K Bits/Sec would span  $7 \times 5 = 35$  bits at the higher rate, thus broadening the peak at the lower EFI's.

The peak around EFI = 100 K bits has not changed position or shape by much from the case where the data rate was 8.5 K Bits/Sec. This seemingly strange result is due to the extra attenuation the 60 K Bits/Sec signal suffers over the 8.5 K Bits/Sec. From Figure 4.1.2.1.1-2 we get a 20 db difference in attenuation. This is enough to get more than one range of impulses from Table 4.1.2.1.2-1. The eye opening at 8.5 K Bits/Sec without equalization was 50 mv so with 20 db of attenuation the opening at 60 K Bits/



Sec is on the order of 500  $\mu$ v which corresponds to the B range in the table. Assuming the B and C ranges are causing the errors at 60 K Bits/Sec, the most likely EFI calculated as above is 51.2 K Bits which is fairly near the center of the peak.

BAMI was run over the 5-mile loop at 60 K Bits/Sec with equalization and distribution of error free interval is given in Figure 4.2.3-4. The general shape of the distribution closely resembles the corresponding curve for CD $\phi$  except for the magnitude of the peaks. For BAMI the distribution shows fewer errors spaced close together and more of the errors spaced far apart. However, this is most likely caused by the difference in error rates. The CD $\phi$  BER was 5.4 times the BAMI BER in these tests. A high BER may indicate a very noisy channel which could easily cause the probability of a short EFI to increase.

Either the 5-mile loop was extra noisy the day these tests were run or both modems were misadjusted because the error rates for both BAMI and CD $\phi$  were higher than normal. Comparison with Figure 4.2.2-2 shows that BAMI BER for Figure 4.2.3-4 is half an order of magnitude higher than expected and for CD $\phi$  the difference is almost 1.5 orders of magnitude. Other examples are given in Figures 4.2.3-5 and 4.2.3-6.

#### 4.3 Summary of Hardware Performance

The CD $\phi$  modem outperformed BAMI by about 5 db in the S/N ratio when the amplitude of BAMI is limited (see Section 4.2.1). Under these conditions CD $\phi$  has a factor of two advantage in threshold margin since it is a two level signal and BAMI is a three level signal.

However, any real wireline channel will have ISI and when ISI becomes severe (combinations of long cables and/or high data rates) BAMI does better than CD $\phi$  in the sense that BAMI continues to operate after CD $\phi$  has a high

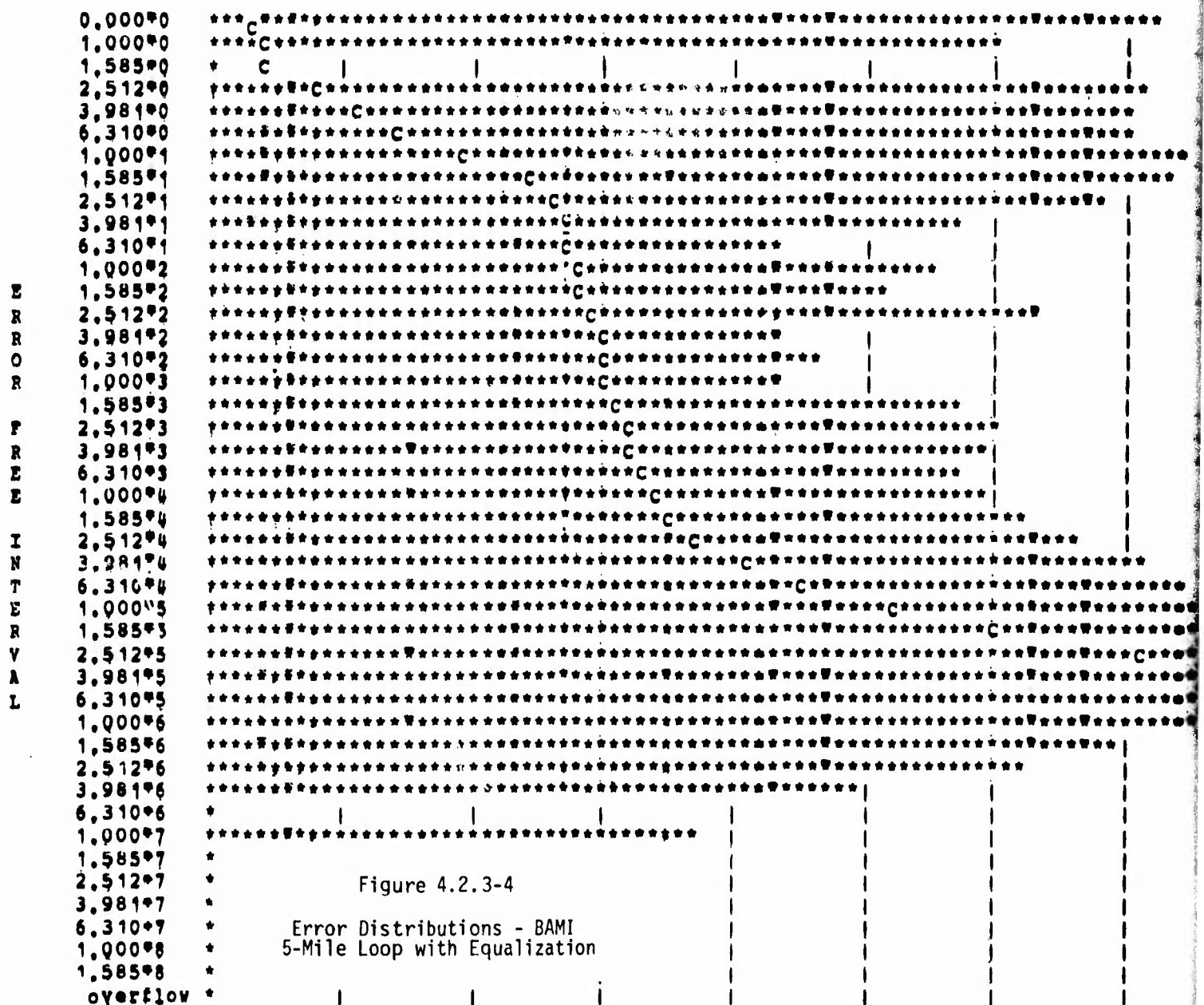
ERROR FREE INTERVAL

PROJECT: DCA LOOP TEST  
DATE: 4 MARCH 1976 HOUR: 0900  
ROUTE:

OPERATOR: ELLER  
TEST ITEM:  
CONDITIONS: 60.0K DATA

TEST DURATION (min):  
DATA RATE: 60.0

\* represents a log probability plot of ERROR FREE INTERVAL  
C represents A linear cumulative plot of ERROR FREE INTERVAL  
bit\_error\_rate= 3.36074157e-006 number\_of\_bits\_transmitted= 4,24013560e+008



\* coordinate 1.00-05 3.16-05 1.00-04 3.16-04 1.00-03 3.16-03 1.00-02 3.16-02  
C coordinate 0% 10% 20% 30% 40% 50% 60% 70%

<<<<<<<<<<<<<<< ERROR FREE INTERVAL >>>>>>>>>>>>>>>>

OPERATOR: ELLER  
TEST ITEM:  
CONDITIONS: 60.0K DATA

TEST DURATION (min):  
DATA RATE: 60.0

TEST NUMBER: 002 AFSC RADC DICEY  
CHANNEL: 5 MILE BASE LINE BAM.  
LINE#: 140

```

plot of ERROR FREE INTERVAL          Mean=2,973+05  Var=2,785+11  Sample Size= 1426
plot of ERROR FREE INTERVAL          Std Dev=5,277+05  SD/mean=1,775+0
0074157e-006 number_of_bits_transmitted= 4,24013560e+008;

```

[illegible]

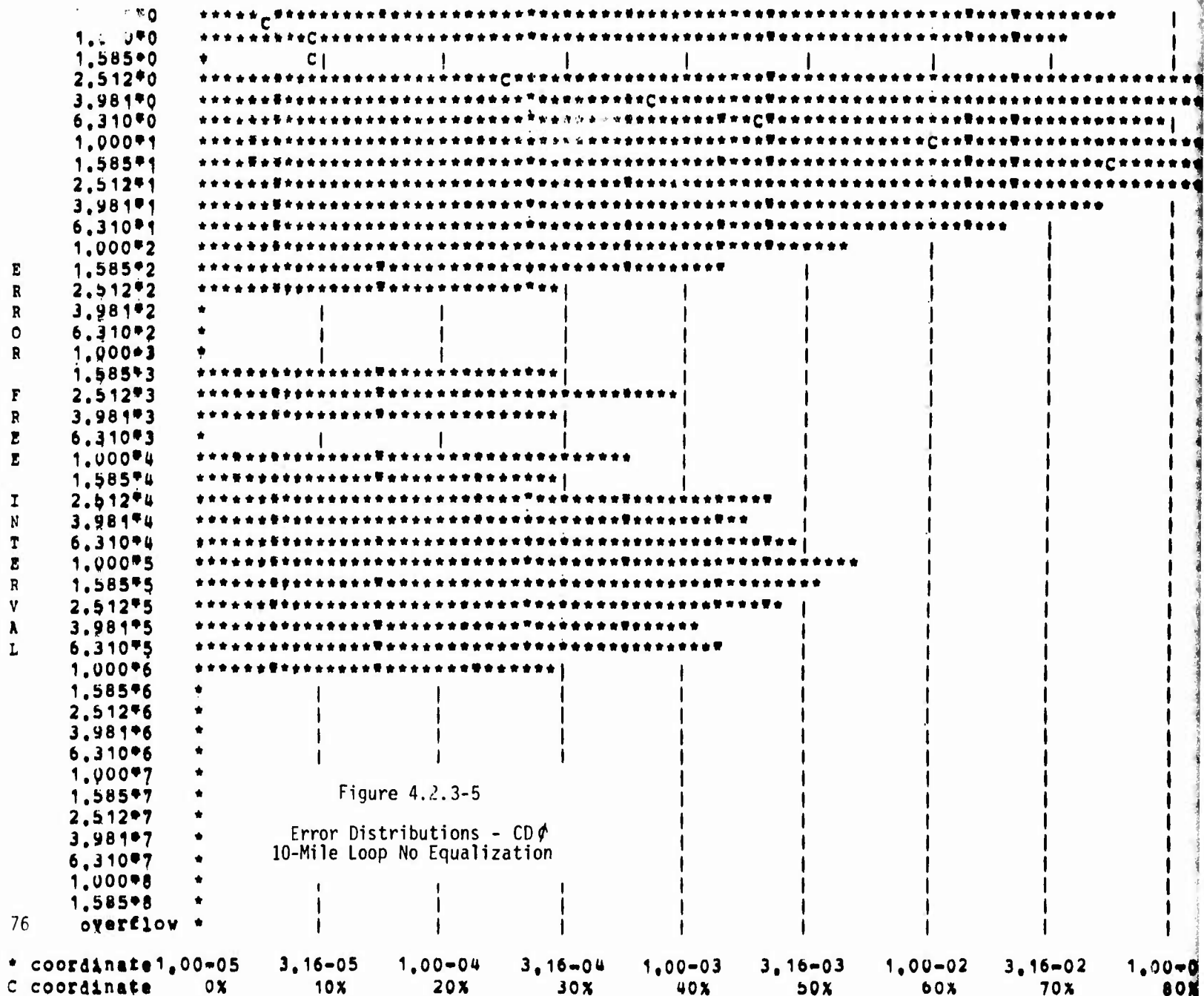
0,00-04	3,16-04	1,00-03	3,16-03	1,00-02	3,16-02	1,00-01	3,16-01	1,00+00
20%	30%	40%	50%	60%	70%	80%	90%	100%

PROJECT; DCA LOOP TEST  
DATE; 8 MARCH 1976 HOUR: 1300  
ROUTE; 1.6K DATA

OPERATOR: ELLER  
TEST ITEM:  
CONDITIONS:

TEST DURATION (min):  
DATA RATE: 60.0

```
* represents a log probability plot of ERROR FREE INTERVAL      Mean=3.677+03  Var=1
C represents A linear cumulative plot of ERROR FREE INTERVAL    Std Dev=3.732+04  S
.      Bit_error_rate= 2.71817560e-004 number_of_bits_transmitted= 1.28468520e+007;
```



TEST DURATION (min):  
DATA RATE: 60.0

```

L          Mean=3.677+03  Var=1.393+09  Sample Size=    3493
VAL          Std Dev=3.732+04  SD/mean=1.015+1
ts_transmitted= 1.28468520e+007;

```

[illegible]

03	3,16-03	1,00-02	3,16-02	1,00-01	3,16-01	1,00+00
%	50%	60%	70%	80%	90%	100%

* coordinate	1,00-05	3,16-05	1,00-04	3,16-04	1,00-03	3,16-03	1,00-02	3,16-02	1,00-01
C coordinate	0%	10%	20%	30%	40%	50%	60%	70%	80%

**<<<<<<<<<<<<<<<< ERROR FREE INTERVAL >>>>>>>>>>>>>>>>**

OPERATOR: ELLER  
TEST ITEM:  
CONDITIONS:

TEST DURATION (min):  
DATA RATE: 2.85

TEST NUMBER: 005 AFSC RADCD DICEF  
CHANNEL: 10 MILE BASE LINE BA  
LINE#:1140

```

plot of ERROR FREE INTERVAL          Mean=6.608+04  Var=5.041+09  Sample Size= 450
plot of ERROR FREE INTERVAL          Std Dev=7.100+04  SD/mean=1.074+0
992867e-005 number_of_bits_transmitted= 2.97365040e+007;

```

probability density

[illegible]

**Figure 4.2.3-6**

Contributions - BAMI  
Op No Equalization

1,00-04	3,16-04	1,00-03	3,16-03	1,00-02	3,16-02	1,00-01	3,16-01	1,00+00
20%	30%	40%	50%	60%	70%	80%	90%	100%

enough BER to become unusable (Section 4.2.2). Until this point is reached their performance in terms of BER is pretty much the same. BAMl does better than CD $\phi$  in severe ISI because it occupies a lower frequency band than does CD $\phi$  (Section 3.4). In these experiments BAMl would support a 30% to 50% higher data rate than CD $\phi$  for a given set of cable conditions. Reference 2, page 4-35, uses the general guide that BAMl can support twice the data rate of CD $\phi$ .

The maximum distance of data transmission attainable vs data rate for a given level of performance is an important parameter. Figure 4.3-1 shows curves for BAMl given a BER of  $10^{-8}$  (Ref 2, pg 928). This report did not cover this topic directly but the few data points generated agree with Figure 4.3-1.

The complexity of the hardware necessary for the BAMl and CD $\phi$  is about the same for CD $\phi$  and BAMl transmitters. For the receivers BAMl is more complex because of the necessity for two thresholds. Also for CD $\phi$  the threshold can be set once and work for all received signal levels whereas for BAMl the thresholds must be adjusted if the signal being sampled changes in amplitude. This would require a better AGC circuit for BAMl than is required for CD $\phi$ . However the difference in hardware complexity is judged small given the current state of integrated circuit technology.

There has been a question raised concerning the problem of a digital data source transmitting into a cable bundle at the same time it is receiving another digital data signal from the same cable bundle. The question is whether or not the transmitted signal will induce enough crosstalk into the received signal to make it unusable. The results of the tests performed at



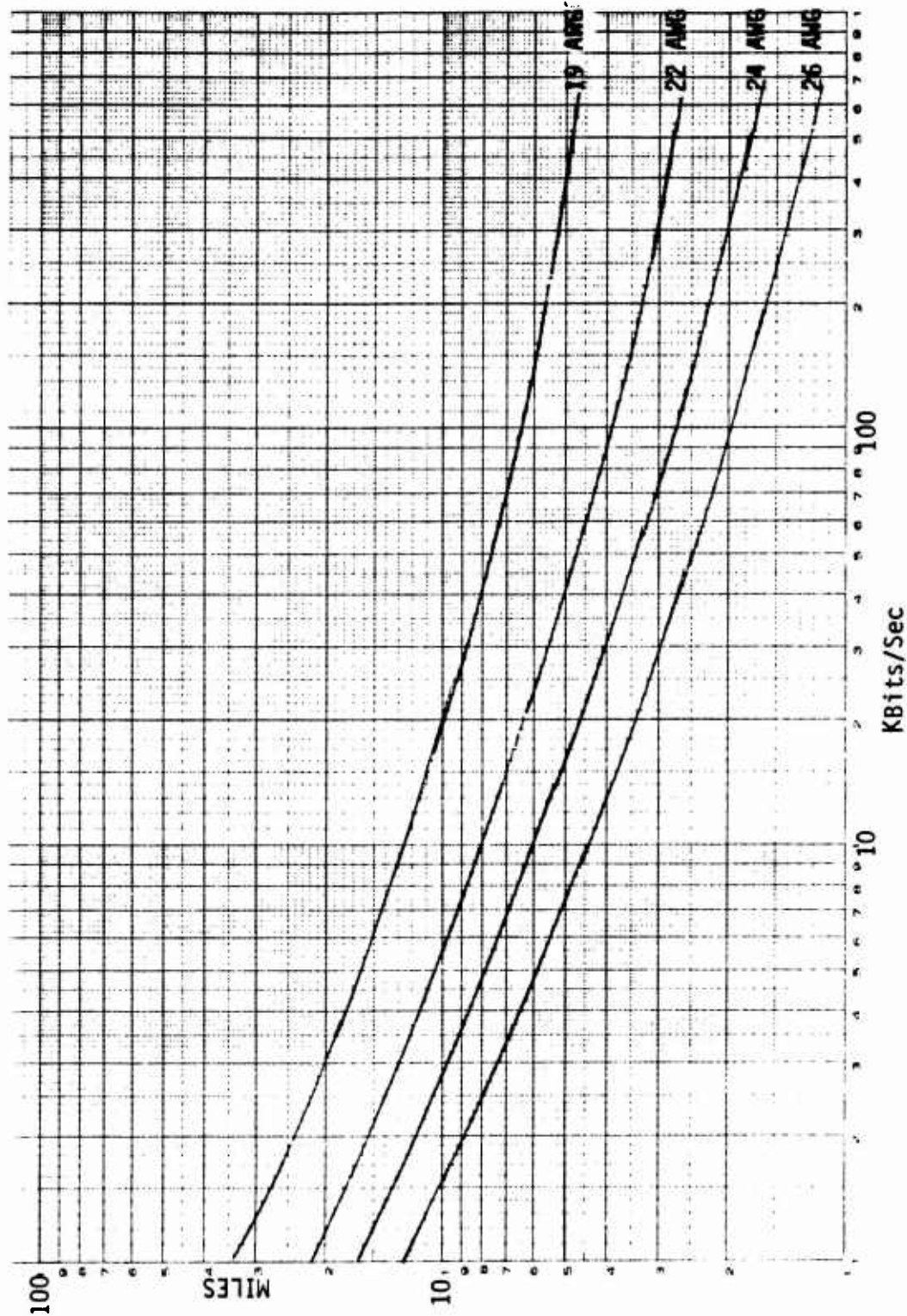


Figure 4.3-1

BAMI MAXIMUM DISTANCE VS BIT RATE  
for ERROR RATE OF  $10^{-8}$

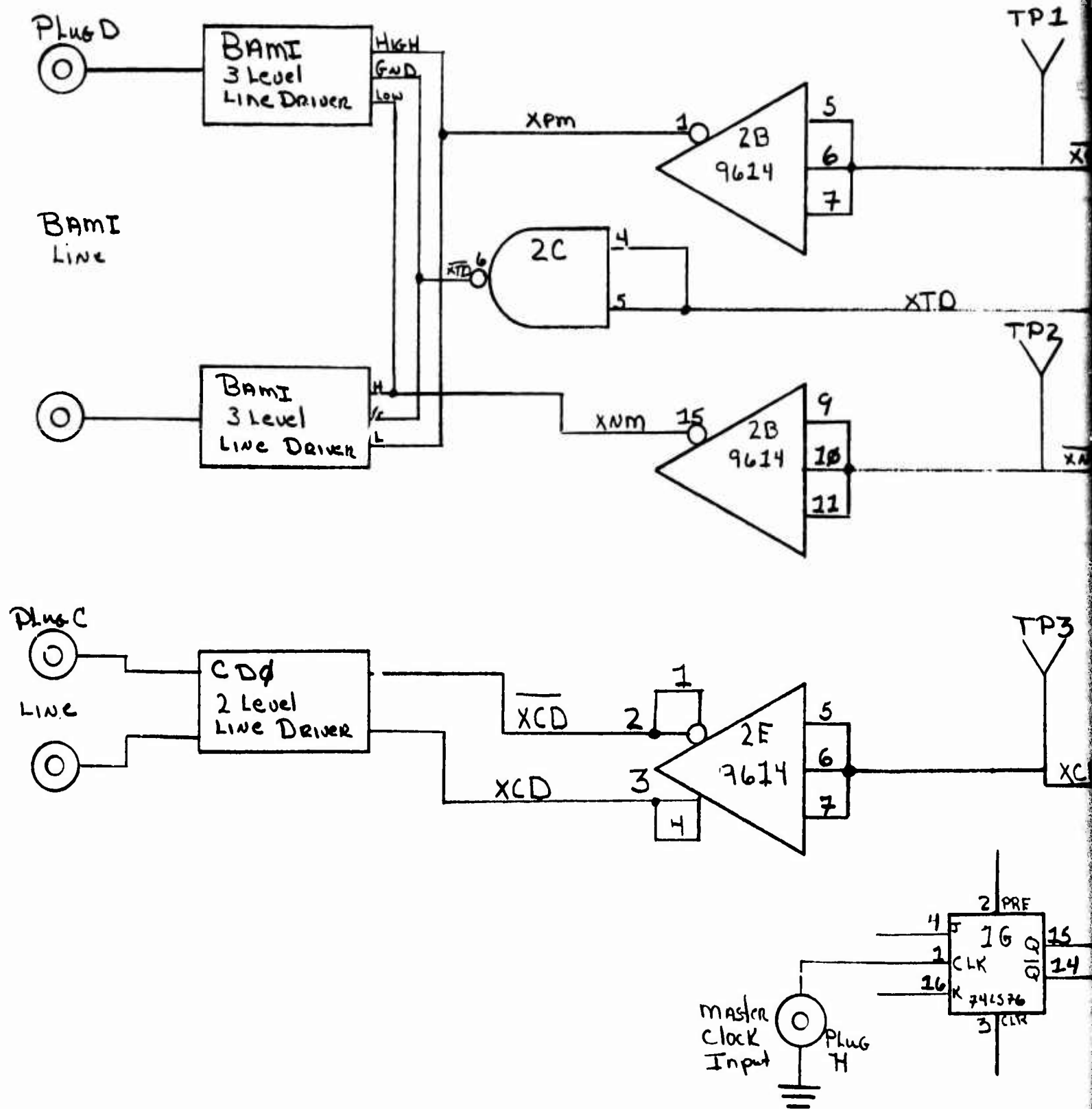
DICEF indicate this is not a serious problem since the base cable setup here had the transmitted and received signals as adjacent pairs in the same cable bundle. The NEXT loss was measured at 69 db for BAMI, 68 db for CDØ.

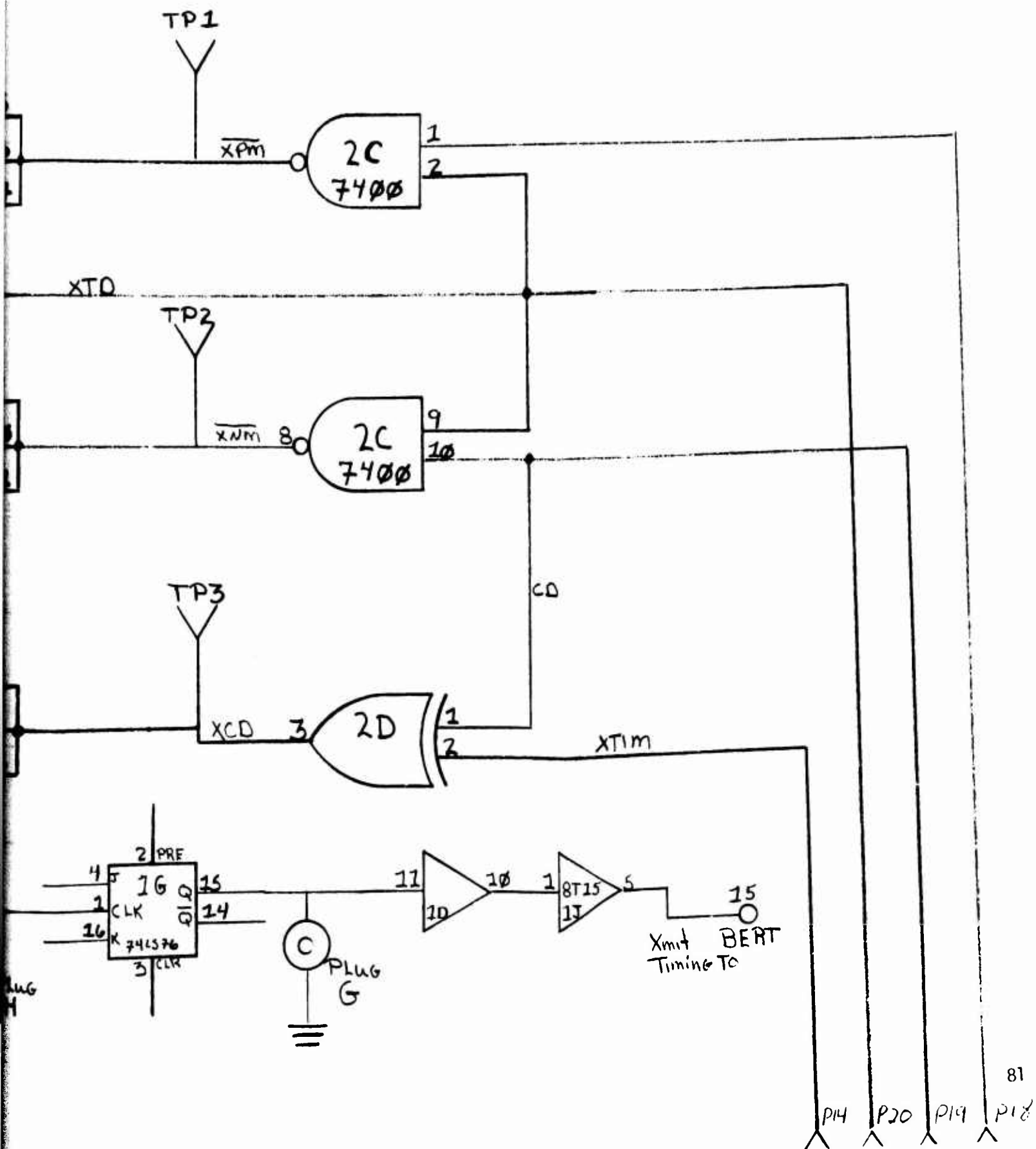
The limiting parameter for the hardware tested at Griffiss AFB was impulse noise. The wideband noise present on the cable was on the order of 0.8 mv rms while the impulse noise had values in the range of hundreds of millivolts.

Paragraph 4.1.2.1.2 discusses the impulse noise and wideband noise measured on the Griffiss AFB cable plant. The practical loop length limitations for a given level of performance can be estimated. The method would be to determine the amount of attenuation a signal could suffer before the impulse noise causes the specified error rate and then relate that attenuation to a length of cable.

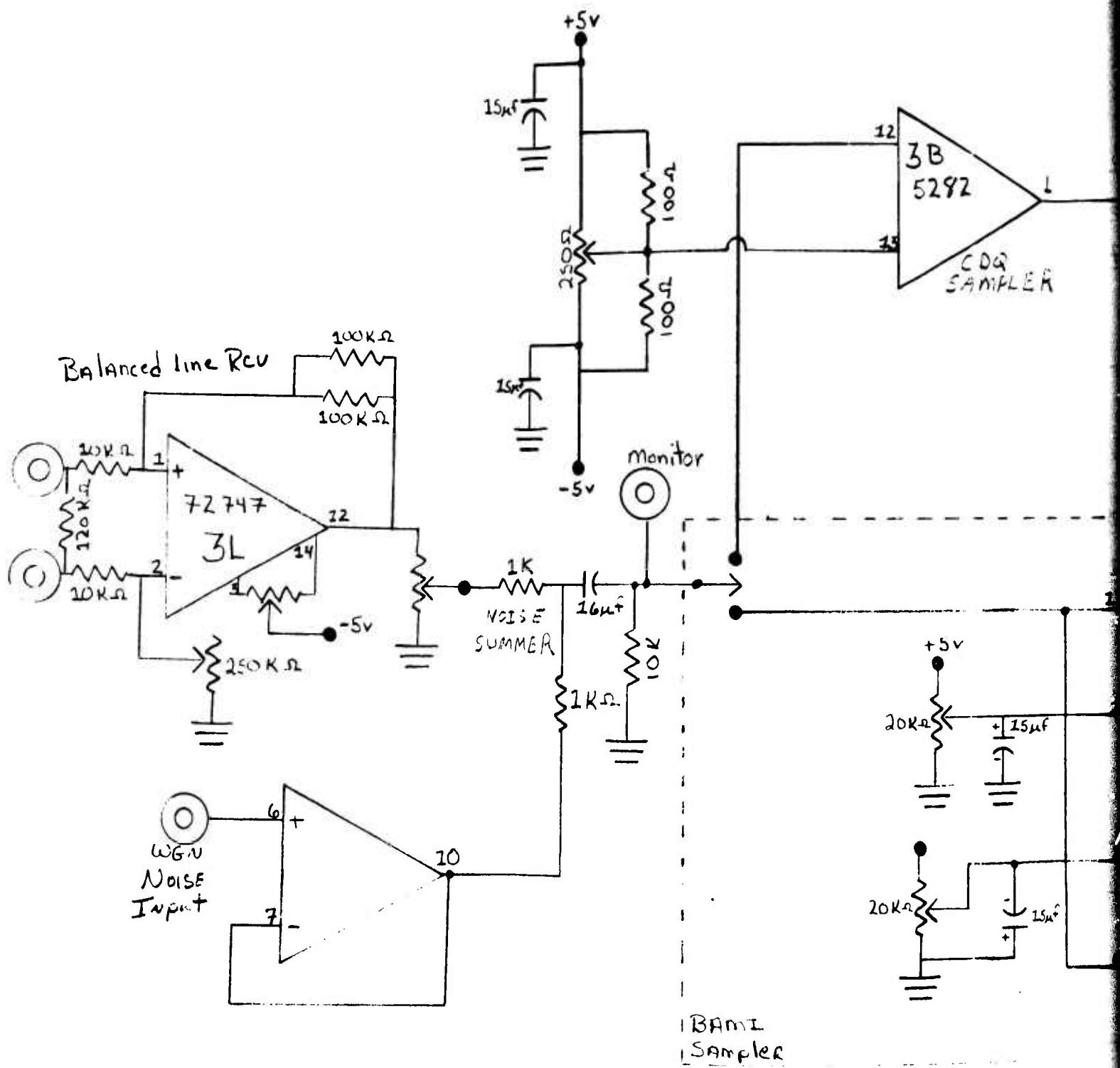
## Appendix 1

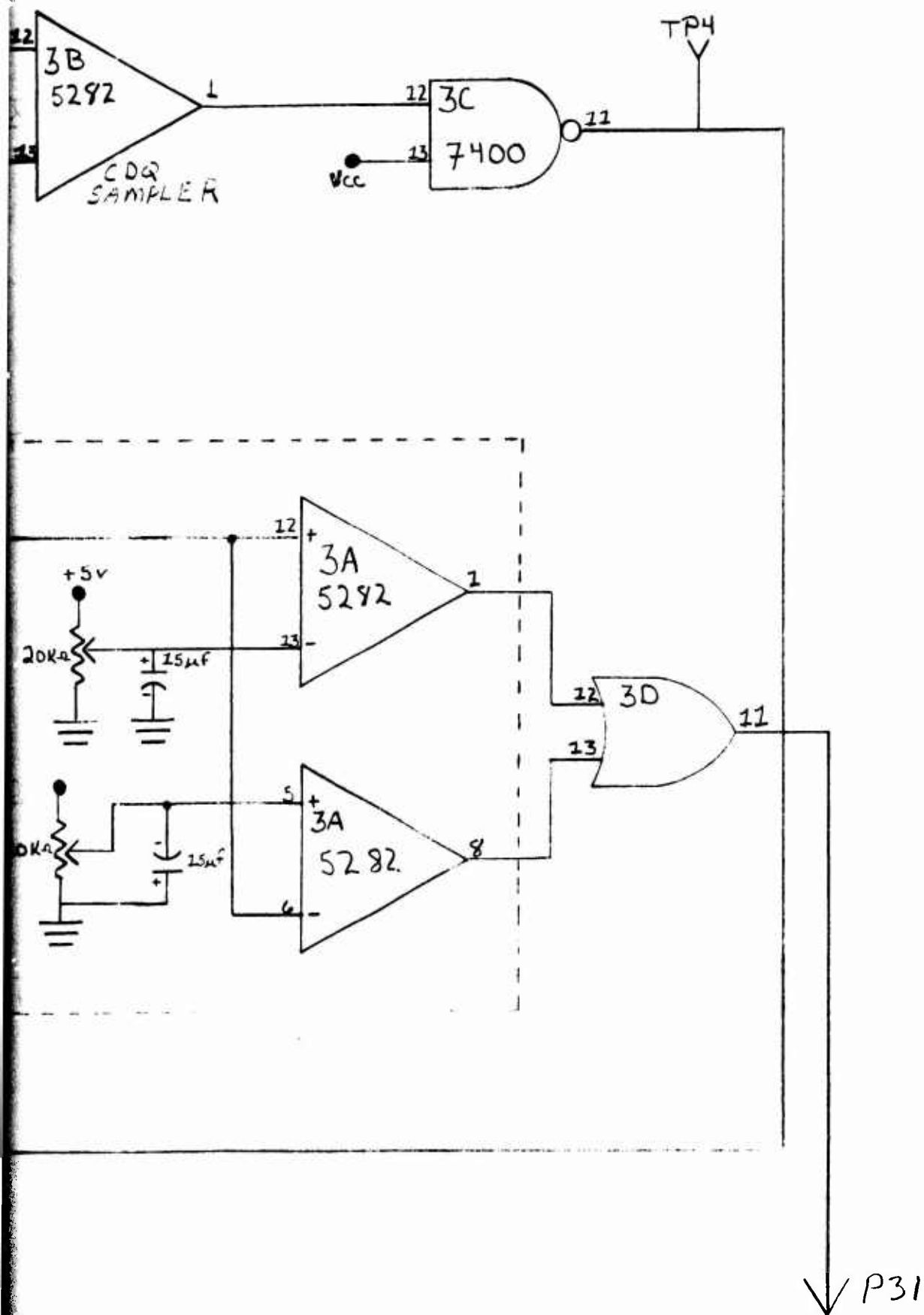
Schematics for CDØ and BAMl Transmitters and Receivers Built at the DICEF

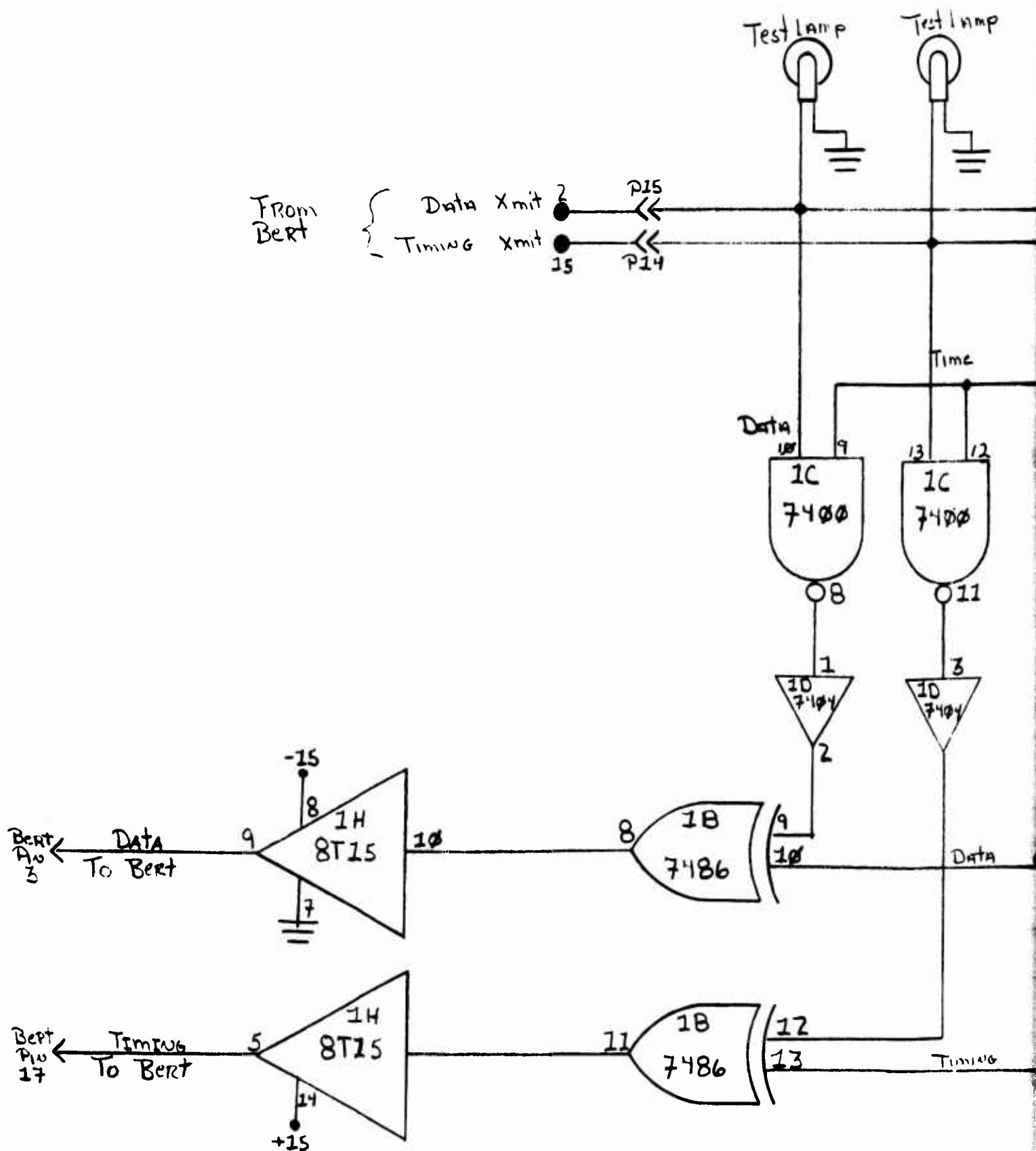




2

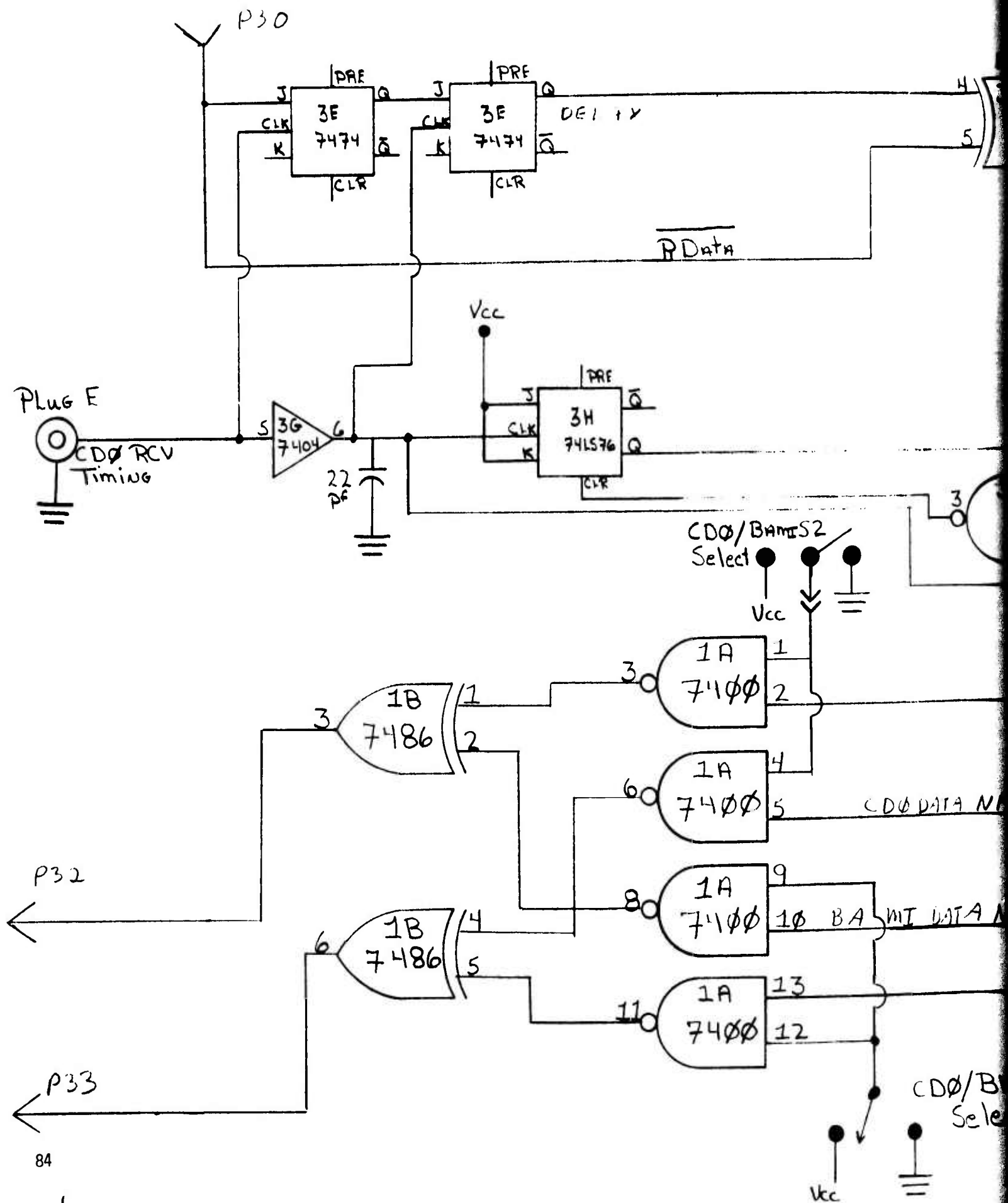


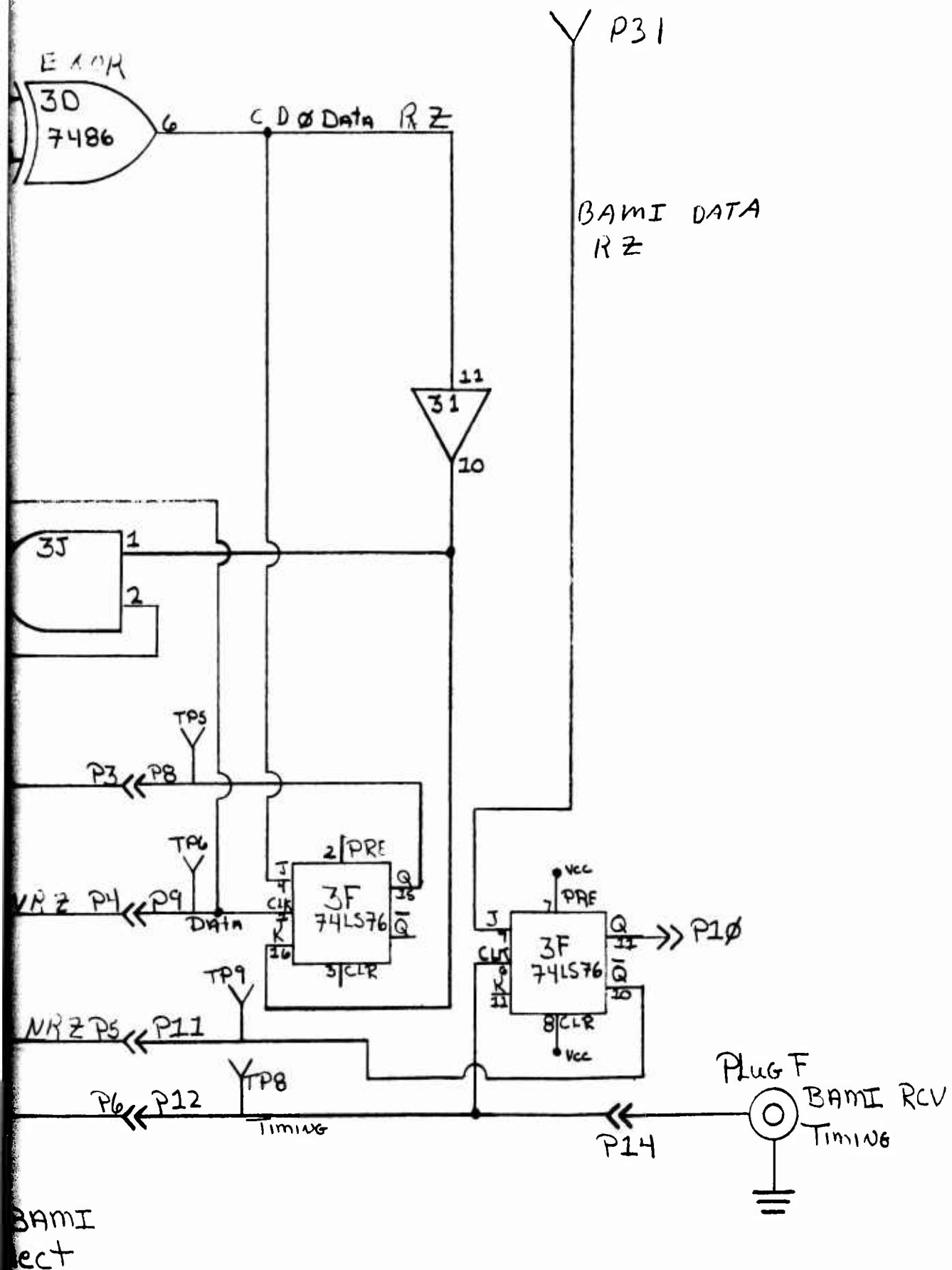












## Appendix 2

### Digital Signal Processor

The Digital Signal Processor (DSP) used in these experiments is the Model SD360 built by Spectral Dynamics Corporation. It is capable of performing 15 functions in real time such as 2048 point FFT, transfer functions of a "block box," cross spectrum Analysis, probability density function, cross and auto correlation, etc. The functions used in this report were the 2048 FFT displayed in logarithmic squared and the transfer function displayed in logarithmic magnitude and linear phase.

The AD 360 DSP performs all functions digitally and has a bandwidth of 150 KHz. The only analog portions of the SD 360 are aliasing filters before the input A/D converters, the A/D converters, and the display output D/A converters. The Kaiser/Bessel window is used on the input data. The aliasing filters have a cut-in frequency which is always  $3/4$  of the maximum frequency displayed. Therefore any data above  $3/4$  of the maximum frequency plotted in the graph is attenuated 66 db/octave which is the filter slope. The only exception to this is the transfer function which is explained below.

The digital FFT transform is implemented in the usual manner where the data is windowed, bit reversal is done, butterfly operation, summing is performed and the averaging of typically 1024 transforms is done to smooth the results. The output is then plotted on a calibrated X-Y recorder.

For the transfer function two channels of the SD 360 are utilized as shown in Figure 1. The source signal is passed through the system to be analyzed and to the A channel of the SD 360. The signal out of the system goes into channel B of the SD 360. The transfer function  $H(j\omega)$  is calculated as follows:

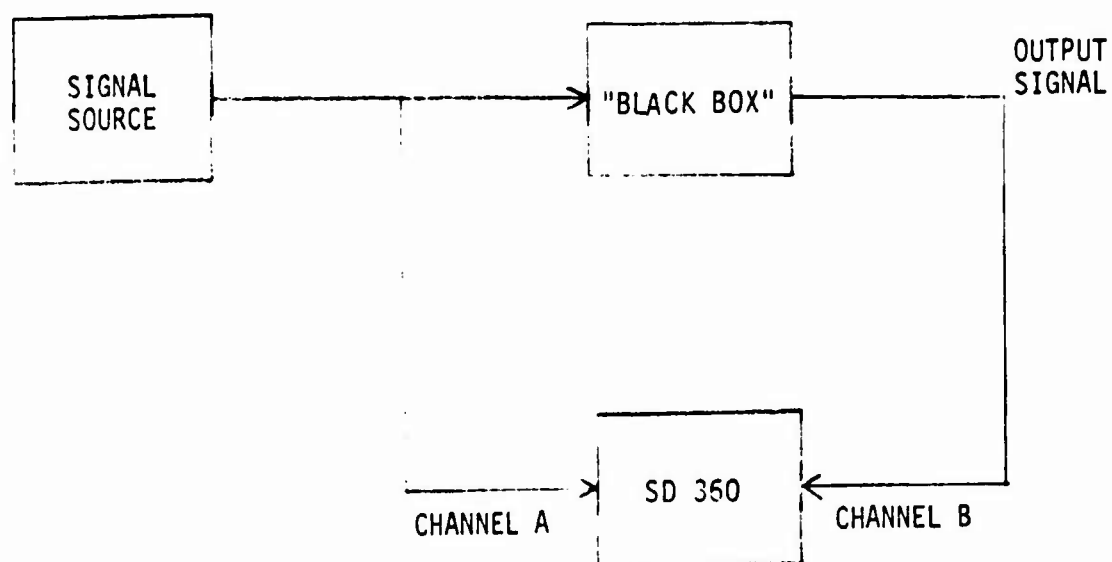


Figure 1  
SD 360 SETUP FOR MEASUREMENT  
OF SYSTEM TRANSFER FUNCTION

$$H(j\omega) = \frac{G_{BA}(j\omega)}{G_{AA}(j\omega)} = \frac{S_B(j\omega)}{S_A(j\omega)}$$

$$H(j\omega) = \frac{S_B(j\omega)}{S_A(j\omega)} = \frac{S_B^*(j\omega)}{S_A^*(j\omega)}$$

where  $G_{BA}$  is the cross spectrum between output and input,  $G_{AA}$  is the input signal cross spectrum with itself.  $S_A$  and  $S_B$  are input and output Fourier transforms respectively, and  $*$  denotes conjugation. Thus the magnitude of the transfer function is calculated as the ratios of the magnitudes of the input and output signal Fourier transforms, and the phase angle of the transfer function is equal to the difference in phase of the two signals.

As mentioned above the aliasing filters do not distort the magnitude of the transfer function because both channel A and channel B signals are attenuated the same amount. However, the resolution of the transfer function is decreased by this attenuation.

## REFERENCES

1. Johnson, W.C., Transmission Lines and Networks. McGraw-Hill Co., New York, NY, 1950.
2. RADC TR-74-258 September 1974, "Air Force Communications Service Digital Transmission Study," Vol II.
3. Bell Telephone Laboratory Staff, Transmission Systems for Communications, Western Electric Co., Winston Salem, N.C., 1970.
4. Davies, O.L. (Ed.), The Design and Analysis of Industrial Experiments, Hafner Publishing Co., New York, NY, 1967.
5. Lucky, R.W., J. Salz, E.J. Weldon, Jr., Principles of Data Communication, McGraw-Hill Book Co., New York, NY, 1968.
6. Jacobsen, B.B., "Cable Crosstalk on Low Capacity Pulse Code Modulation Systems," Electrical Communication, Vol 48, No. 1 and 2, 1973.
7. Williams, H., H.W. Silcock, D. Sibbold, "Social Crosstalk in the Local Area Network," Electrical Communication, Vol 49, No. 4, 1974.
8. Ungerboeck, G., "Nonlinear Equalization of Binary Bipolar Signals in Gaussian Noise," IEE Com Tech, December 1971.
9. "Evaluation of the RCA Modified Diphase Transmission System," Boeing Co., Seattle Washington, CR-61-419-15, January 26, 1962. Contr #AF04(647)-289.
10. Hebbert, C.M., "The Transmission Characteristics of Toll Telephone Cables at Carrier Frequencies," BSTJ Vol 20, June 1941.
11. Stein, S., J.J. Jones, Modern Communication Principles, McGraw Hill, Inc. 1967. Performance of Comm Systems,
12. Sunde, E.S., Communications Systems Engineering Theory, John Wiley & Sons, Inc, 1969. Power Spectral Densities, Timing Recovery, Data Switchline Transmission.
13. Aaron, M.R., "PCM Transmission in the Exchange Plant," BSTJ 41, January 1962. Power Spectral Densities.
14. Bell System Technical Journal, Vol 54, #5, May/June 1975.
15. Fennick, J.H., "Amplitude Distribution of Telephone Channel Noise and a Model for Impulse Noise," GSTJ Vol 48, December 1969.

16. Gresh, P.A., "Physical and Transmission Characteristics of Consumer Loop Plant," BSTJ Vol 48, December 1969.
17. Deleted
18. Carlsen, A.B., "Communication Systems: An Introduction to Signals and Noise in Electrical Communications," 1968, McGraw-Hill, Inc., New York, NY
19. Papoulis, A., "Probability, Random Variables, and Stockastic Processes," 1965, McGraw-Hill, Inc., New York, NY.
20. Millman, J., T. Taub, "Pulse, Digital, and Switching Waveforms," McGraw-Hill, Inc., New York, NY, 1965.



# METRIC SYSTEM

## BASE UNITS:

Quantity	Unit	SI Symbol
length	metre	m
mass	kilogram	kg
time	second	s
electric current	ampere	A
thermodynamic temperature	kelvin	K
amount of substance	mole	mol
luminous intensity	candela	cd

## SUPPLEMENTARY UNITS:

plane angle	radian	rad
solid angle	steradian	sr

## DERIVED UNITS:

Acceleration	metre per second squared	m/s <sup>2</sup>
activity (of a radioactive source)	disintegration per second	(disintegration)/s
angular acceleration	radian per second squared	rad/s <sup>2</sup>
angular velocity	radian per second	rad/s
area	square metre	m <sup>2</sup>
density	kilogram per cubic metre	kg/m <sup>3</sup>
electric capacitance	farad	A·s/V
electrical conductance	siemens	A/V
electric field strength	volt per metre	V/m
electric inductance	henry	V·s/A
electric potential difference	volt	W/A
electric resistance	ohm	V/A
electromotive force	volt	W/A
energy	joule	N·m
entropy	joule per kelvin	J/K
force	newton	kg·m/s <sup>2</sup>
frequency	hertz	(cycle)/s
illuminance	lux	lm/m <sup>2</sup>
luminance	candela per square metre	cd/m <sup>2</sup>
luminous flux	lumen	cd·sr
magnetic field strength	ampere per metre	A/m
magnetic flux	weber	V·s
magnetic flux density	tesla	Wb/m <sup>2</sup>
magnetomotive force	ampere	...
power	watt	J/s
pressure	pascal	N/m <sup>2</sup>
quantity of electricity	coulomb	A·s
quantity of heat	joule	N·m
radiant intensity	watt per steradian	W/sr
specific heat	joule per kilogram-kelvin	J/kg·K
stress	pascal	N/m <sup>2</sup>
thermal conductivity	watt per metre-kelvin	W·m <sup>-1</sup> ·K <sup>-1</sup>
velocity	metre per second	m/s
viscosity, dynamic	pascal-second	Pa·s
viscosity, kinematic	square metre per second	m <sup>2</sup> /s
voltage	volt	W/A
volume	cubic metre	m <sup>3</sup>
wavenumber	reciprocal metre	(wave)/m
work	joule	N·m

## SI PREFIXES:

Multiplication Factors	Prefix	SI Symbol
1 000 000 000 000 = 10 <sup>12</sup>	tera	T
1 000 000 000 = 10 <sup>9</sup>	giga	G
1 000 000 = 10 <sup>6</sup>	mega	M
1 000 = 10 <sup>3</sup>	kilo	k
100 = 10 <sup>2</sup>	hecto*	h
10 = 10 <sup>1</sup>	deka*	da
0.1 = 10 <sup>-1</sup>	deci*	d
0.01 = 10 <sup>-2</sup>	centi*	c
0.001 = 10 <sup>-3</sup>	milli	m
0.000 001 = 10 <sup>-6</sup>	micro	μ
0.000 000 001 = 10 <sup>-9</sup>	nano	n
0.000 000 000 001 = 10 <sup>-12</sup>	pico	p
0.000 000 000 000 001 = 10 <sup>-15</sup>	femto	f
0.000 000 000 000 000 001 = 10 <sup>-18</sup>	atto	a

\* To be avoided where possible.

# **MISSION** **of** **Rome Air Development Center**

**RADC plans and conducts research, exploratory and advanced development programs in command, control, and communications (C<sup>3</sup>) activities, and in the C<sup>3</sup> areas of information sciences and intelligence. The principal technical mission areas are communications, electromagnetic guidance and control, surveillance of ground and aerospace objects, intelligence data collection and handling, information system technology, ionospheric propagation, solid state sciences, microwave physics and electronic reliability, maintainability and compatibility.**

